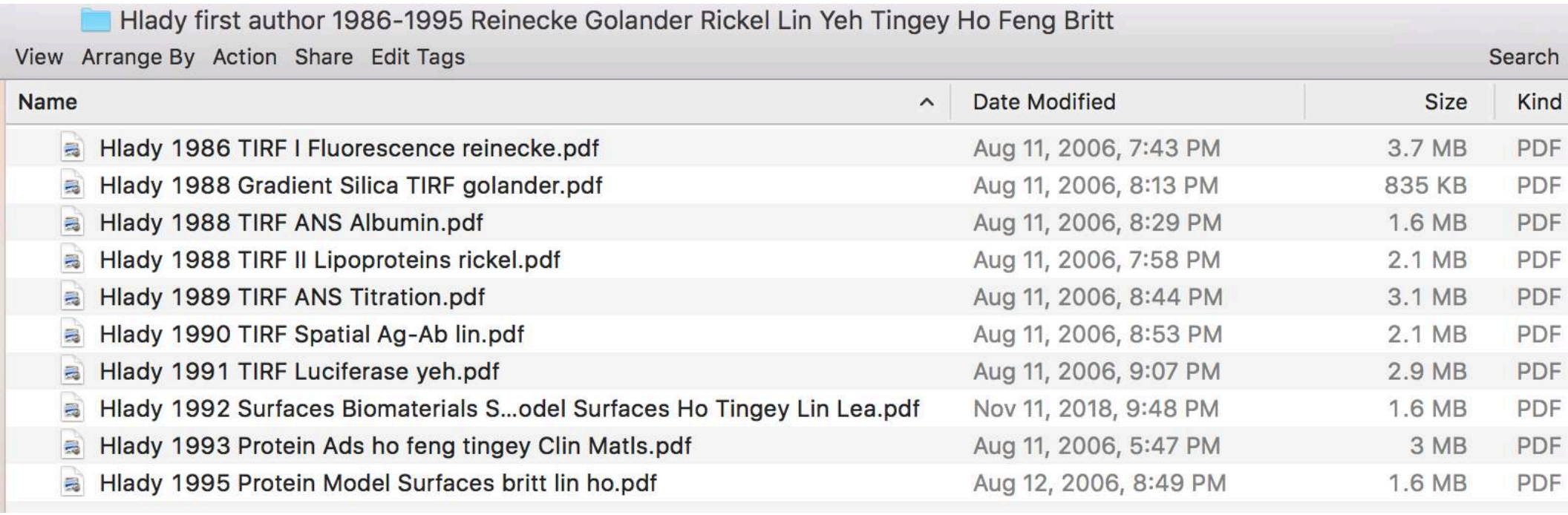
Hlady first author 1986-1995 Reinecke Golander Rickel Lin Yeh Tingey Ho Feng Britt
View Arrange By Action Share Edit Tags Search
Name Date Modified Size Kind
Hlady 1986 TIRF I Fluorescence reinecke.pdf Aug 11, 2006, 7:43 PM 3.7 MB PDF
Hlady 1988 Gradient Silica TIRF golander.pdf Aug 11, 2006, 8:13 PM 835 KB PDF
Hlady 1988 TIRF ANS Albumin.pdf Aug 11, 2006, 8:29 PM 1.6 MB PDF
Hlady 1988 TIRF II Lipoproteins rickel.pdf Aug 11, 2006, 7:58 PM 2.1 MB PDF
Hlady 1989 TIRF ANS Titration.pdf Aug 11, 2006, 8:44 PM 3.1 MB PDF
Hlady 1990 TIRF Spatial Ag-Ab lin.pdf Aug 11, 2006, 8:53 PM 2.1 MB PDF
Hlady 1991 TIRF Luciferase yeh.pdf Aug 11, 2006, 9:07 PM 2.9 MB PDF
Hlady 1992 Surfaces Biomaterials S...odel Surfaces Ho Tingey Lin Lea.pdf Nov 11, 2018, 9:48 PM 1.6 MB PDF
Hlady 1993 Protein Ads ho feng tingey Clin Matls.pdf Aug 11, 2006, 5:47 PM 3 MB PDF
Hlady 1995 Protein Model Surfaces britt lin ho.pdf Aug 12, 2006, 8:49 PM 1.6 MB PDF

LAST COPY
DO NOT SEND
OR REMOVE

Fluorescence of Adsorbed Protein Layers

I. Quantitation of Total Internal Reflection Fluorescence

V. HLADY,[1] D. R. REINECKE,[2] AND J. D. ANDRADE[3]

Department of Bioengineering, College of Engineering, University of Utah, Salt Lake City, Utah 84112

Received October 9, 1985; accepted December 20, 1985

A quantitative total internal reflection intrinsic fluorescence (TIRIF) method for determining the adsorption of proteins at optically suitable solid/liquid interface is presented. Intrinsic protein fluorescence is excited by evanescent part of the standing wave produced by total internal reflection. The TIRIF data are quantified using as an internal standard the fluorescence from nonadsorbed proteins which are present in the evanescent region. In order to account for the fraction of fluorescence excited by scattered light which propagates through and beyond the volume sensed by the evanescent wave, a set of nonadsorbing external standards has to be used. The combination of TIRIF and ^{125}I–protein γ-photon detection system is described and applied to bovine serum albumin (BSA) and human immunoglobulin (IgG) adsorption at silica/electrolyte interfaces. The difference between the results obtained with different adsorption detection systems is discussed. An average fluorescence emission efficiency of adsorbed proteins can be evaluated by combining TIRIF adsorption data with the independent *in situ* quantitation of protein adsorption. It was found that in some cases adsorbed proteins emit fluorescence with significantly lower quantum yield.

INTRODUCTION

The concept of total internal reflection fluorescence (TIRF) at solid/liquid interfaces was introduced by Hirschfeld (1). Although this first use of TIRF was not applied to adsorbed species but to bulk dissolved dye, the advantage over the conventional fluorescence technique was demonstrated: fluorescence intensity vs concentration relation was linear up to a concentration 100-fold higher due to the shallow penetration of the evanescent wave. Applications of TIRF include collection of fluorescence from dansyl-bovine serum albumin molecules by TIRF optics (2), TIRF-based immunoassay for specific dye-labeled antibodies from the solution to an antigen coated surface (3), and "virometer," an optical sensor for viruses treated with a fluorescent probe bound to the virus nucleic acid (4, 5).

The applications of TIRF to the study of interactions between surfaces and proteins have been recently reviewed (6, 7). Two different routes to TIRF protein adsorption results are distinguished: in the first one the emission from those protein amino acids which intrinsically fluoresce upon excitation in ultraviolet, like tryptophan and tyrosine, is monitored; hence the name, total internal reflection *intrinsic* fluorescence (TIRIF), while in the second approach the emission from an *extrinsic* fluorophor covalently bound to the protein, such as fluorescein or rhodamine, is followed.

First approach parallels the protein solution fluorescence studies and allows one to analyze intrinsic protein fluorescence emission and excitation spectra, and other fluorescence phenomena. In principle, TIRIF can thus provide an insight to the conformational

[1] Presented at the 5th International Conference on Surface and Colloid Science, Clarkson University, Potsdam, N.Y., June 24–26, 1985, as part of a symposium entitled Protein and Polyelectrolyte Adsorption.

[2] This work was carried out when V. Hlady was on leave of absence from Institute "Ruđer Bošković," Zagreb, Yugoslavia.

[3] Taken in part from M.Sc. thesis of D. R. Reinecke, submitted to the University of Utah, July 1985.

[4] To whom correspondence should be addressed.

0021-9797/86 $3.00

changes in adsorbed proteins. It was shown recently that with appropriate apparatus based on total internal reflection, intrinsic fluorescence lifetimes of the adsorbed protein could be determined (8). Intrinsic fluorescence was also used in the TIRIF mode to study the adsorption of insulin, a protein molecule with a few tyrosine residues and no tryptophan in its structure (9).

The extrinsic fluor approach is more suitable to competitive protein adsorption studies and to protein adsorption kinetic studies, provided that the protein labeling by an extrinsic fluor does not cause different protein adsorbability. The uptake of fluorescein-labeled albumin, γ-globulin, and fibrinogen onto silicone rubber coated surfaces has been followed as a function of time (10). The adsorption of the same proteins was followed also as a function of flow rate of protein solution; it was demonstrated that adsorption is diffusion-limited (11). A combination of total internal reflection with fluorescence photobleaching recovery and fluorescence correlation spectroscopy was described and applied to the study of protein surface diffusion and exchange rates (12, 15).

In all TIRF protein adsorption experiments it is desirable to correlate the intensity of fluorescence with the excess protein concentration at the interface. The adsorbed layer is often in equilibrium with nonadsorbed protein molecules which are also situated inside the "evanescent volume" and contribute to overall fluorescence. Various methods have been proposed to calibrate TIRF data: (a) external nonadsorbing standards were used (13, 14); (b) some type of evanescent energy distribution calculation was preformed while solution proteins in the evanescent region were used as internal standards (14); and, (c) protein surface excess was measured independently (15).

However, inconsistent results often emerged and TIRF was considered to be only semiquantitative. It will be shown here that TIRIF can be made quantitative by using both external and internal fluorescence standards and by appropriate accounting for the part of fluorescence which is excited by scattered light propagating through and beyond the region sensed by the evanescent surface wave.

Quantitation Scheme of TIRIF

A full account of evanescent wave theory has been presented elsewhere (6, 14, 16). Only those parts pertinent to the present quantitation scheme will be given here. The TIRIF quantitation of protein adsorption is based on the distribution of evanescent electromagnetic radiation intensity beyond the reflecting solid/liquid interface. The superposition of incident and reflected waves in total internal reflection forms a standing wave in the optically more dense medium. The nature of the standing wave is a function of both the optically more dense medium (medium 1; here, a hydrophilic amorphous silica) and the less optically dense medium (medium 2; here, an aqueous protein solution). The electric field amplitude right at the interface in the denser medium has a nonzero value in the case of two dielectrics. Solution of Maxwell's wave equation for total internal reflection shows the existence of a surface wave which propagates along the interface (17). Since the boundary conditions for electromagnetic wave reflection do not allow any discontinuity of the tangential field across the interface, the electric field amplitude at the interface in medium 2 will be equal to the electric field amplitude at the interface in medium 1. The electric field amplitude of the evanescent wave, $E_\perp^e$, will decay exponentially with distance z normal to the interface in medium 2:

$$E_\perp^e(z) = (E_\perp^{t,0}/E_\perp^{i,0})\exp(-z/d_p)$$
$$= (2\cos\theta_1)/\{[1-(n_2/n_1)^2]^{1/2}\} \times \exp(-z/d_p), \quad [1]$$

$$d_p = \lambda \cdot 1/[2\pi(n_1^2\sin^2\theta_1 - n_2^2)^{1/2}] \quad [2]$$

where $E_\perp^{t,0}$ is electric field amplitude right at the interface in less dense medium 2; $E_\perp^{i,0}$ is electric field amplitude of incident, perpendiculary polarized light; n_1 and n_2 are refractive

indices of the two media, θ_1 is the angle of incidence of electromagnetic wave measured from the interfacial normal, and d_p is defined as a distance from the interface where the electric field amplitude decrease to e^{-1} of its interfacial value. The parameter d_p is often called "depth of penetration of the evanescent wave." From the experimental point of view it is important to recognize that $[E^e_\perp(z)]^2$ is proportional to the profile of electromagnetic radiation intensity present in medium 2. Such profile determines the "surface sensitivity" of the particular evanescent wave.

In general, the observed fluorescence intensity is proportional to the product of incident light, and the probabilities of absorption and emission. When the evanescent region is populated with proteins, the fluorescence intensity N is given by

$$N = 2.303ab \int_0^\infty \Phi(z)[f(\lambda)](z) \times \epsilon(z)c(z)[E^e(z)]^2\, dz \quad [3]$$

where Φ is quantum yield. The extinction coefficient at excitation wavelengths ϵ, the protein concentration c, and the fraction of total fluorescence emitted at wavelength λ, $f(\lambda)$, are all given as a function of distance from the interface. The constant a accounts for the fraction of total fluorescence collected by the detector and $b \int [E^e(z)]^2\, dz$ is a term equivalent to the product of light path distance and incident light intensity, $d \cdot I_0$, in conventional spectrofluorometry (this makes $b = I_0 n_2/2.303 n_1 \cos\theta_1$). If the adsorbed protein layer has a thickness Δ, the ratio between the observed fluorescence intensities of adsorbed proteins N_a and nonadsorbed proteins N_b is given by

$$\frac{N_a}{N_b} = \frac{2.303ab \int_0^\Delta \Phi(z)[f(\lambda)](z)\epsilon(z)c(z)[E^e(z)]^2\, dz}{2.303ab \int_\Delta^\infty \Phi(z)[f(\lambda)](z)\epsilon(z)c(z)[E^e(z)]^2\, dz}. \quad [4]$$

Equation [4] can be simplified by assuming a step distribution of protein molecules in the evanescent region; for $0 < z < \Delta$ protein concentration c equals Γ_{vol}, and for $\Delta < z < d$, c equals c_p (d is thickness of TIRIF cell). It can be further assumed that ϵ, $f(\lambda)$, and $[E^e(z)]$ remain unchanged by the adsorption. Then

$$\frac{N_a}{N_b} = \frac{\Phi_a \Gamma_{vol} \int_0^\Delta [(E^{t,0}_\perp/E^{i,0}_\perp)e^{-z/d_p}]^2\, dz}{\Phi_b c_p \int_\Delta^\infty [(E^{t,0}_\perp/E^{i,0}_\perp)e^{-z/d_p}]^2\, dz}. \quad [5]$$

Figure 1a shows a typical TIRIF data output; introduction of protein into the TIRIF cell causes an increase of fluorescence intensity due to the protein adsorption. After a given period of protein interfacial residence time, nonadsorbed proteins in the cell are replaced with buffer solution and an immediate decrease of fluorescence intensity follows. Both N_a and N_b are thus experimentally accessible and Eq. [5] can be used to calculate Γ_{vol}. As a first approximation it can be assumed that the emission probability does not change by adsorption, i.e., that $\Phi_a/\Phi_b \approx 1$. The thickness of the adsorbed layer can be estimated from protein molecular dimensions. The implication of these assumptions will be discussed later.

Preliminary studies showed that the changes in fluorescence intensity after protein solution flush-out, N_b, varied considerably between repeated experiments, while N_a remained relatively constant. This indicated that beside the excitation by evanescent surface wave there was some other source of excitation which induced the fluorescence from nonadsorbed protein. It was found that the light scattered by imperfections in optical components of the TIRIF cell propagated through and beyond the evanescent region. Nonadsorbed protein molecules in the whole volume of TIRIF cell were excited by this scattered light and their fluo-

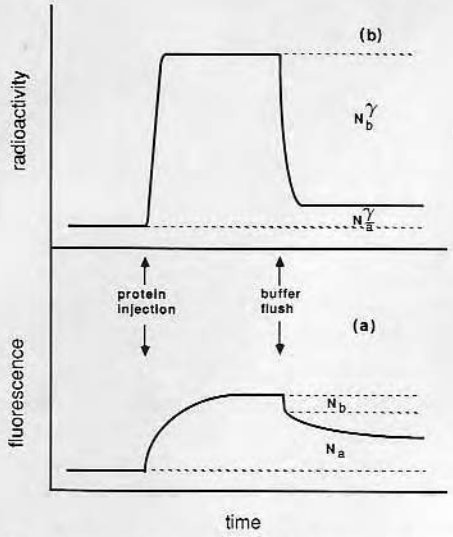

FIG. 1. An illustration of TIRIF data output (a) combined with the output of the parallel γ-photon detection (b) in a typical protein adsorption experiment. See text for explanation of symbols used.

rescence contributed to overall N_b signal. Different extent of scattering which varied from one optical interface to the other caused nonreproducible adsorption results. The same propagating nature of the scattered excitation light was used to correct N_b for its scatter-originated part. By increasing the concentration of a particular nonadsorbing standard which has the same fluorescence characteristics as the protein used (they will be referred to as external standard, subscripted by s), a condition can be attained at which the incident intensity of the propagated scattered excitation light is completely attenuated in the TIRIF cell volume, i.e., where $\epsilon_s c_s d > 2$. Since the fluorescence from the TIRIF cell is collected at the front face, any further increase of either d or c_s will not result in any further increase of fluorescence. The scatter-originated contribution to overall fluorescence will remain constant. On the contrary, fluorescence excited by the evanescent surface wave will, in this case, still increase linearly with increasing c_s due to the shallow penetration depth of the evanescent wave. The contributions of scatter-originated and evanescently excited fluorescence of nonadsorbing standards to overall fluorescence are given in Fig. 2. At the higher ϵc, the scatter-originated part becomes constant while the evanescently excited part increases linearly with concentration. The overall fluorescence intensity is the sum of both parts and depends on the thickness of TIRIF cell only at $\epsilon c < d/2$. The fluorescence excited by the evanescent surface wave can be resolved from the total fluorescence by translating the linear part of total fluorescence vs ϵc curve along the y axis until it passes through the origin. It represents the evanescent part of the total TIRIF signal, while the rest is the contribution excited by scattered propagating light. The ratio between the evanescent component N_s^e and the total fluorescence N_s^{tot} is unique for given ϵcd, wavelength of excitation, and experimental geometry. When the protein solution is in the TIRIF cell, it will absorb both the evanescent and the propagating excitation radiation in the same *relative* proportions as the external standards do at the same ϵc. Here, eventual rescattering of propagating light by protein molecules in the TIRIF cell is neglected. It is also assumed that the scattered propagating light in the TIRIF cell does not produce a significant fluorescence contribution from the adsorbed protein layer, since the thickness of this layer is much smaller than the TIRIF cell thickness.

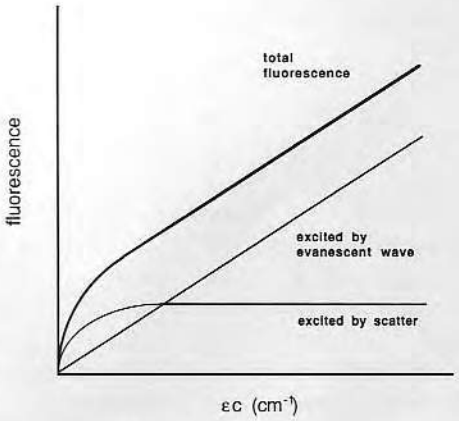

FIG. 2. Contributions of scatter-originated and evanescent wave excited fluorescence of nonadsorbed molecules to the total fluorescence collected from the TIRIF cell.

The absorbed radiation will be then reemitted as bulk protein fluorescence N_b^{tot} with an appropriate quantum yield. The evanescent part of N_b^{tot}, N_b^e, which should be used in Eq. [5] can be calculated as

$$N_b^e = N_b^{tot} \cdot N_s^e / N_s^{tot}|_{ecd=const} \cdot \quad [6]$$

Note that N_b^{tot} is obtained in the presence of the adsorbed layer of thickness Δ, while the ratio N_s^e/N_s^{tot} is determined using the external standards in the absence of this layer. Due to this difference, N_b^e has to be corrected by a factor

$$\frac{\int_0^\infty [(E_\perp^{t,0}/E_\perp^{i,0}) \cdot e^{-z/d_p}]^2 \, dz}{\int_\Delta^\infty [(E_\perp^{t,0}/E_\perp^{i,0}) \cdot e^{-z/d_p}]^2 \, dz}$$

or Eq. [5] has to be rewritten as

$$\frac{N_a}{N_b^e} = \frac{\Phi_a \Gamma_{vol} \int_0^\Delta [(E_\perp^{t,0}/E_\perp^{i,0}) e^{-z/d_p}]^2 \, dz}{\Phi_b c_p \int_0^\infty [(E_\perp^{t,0}/E_\perp^{i,0}) e^{-z/d_p}]^2 \, dz} \quad [7]$$

which simplifies to

$$\frac{N_a}{N_b^e} = \frac{\Phi_a \Gamma_p}{\Phi_b c_p \Delta} (1 - e^{-2\Delta/d_p}) \quad [8]$$

where protein surface concentration Γ_p (mass/area) equals $\Gamma_p = \Delta \cdot \Gamma_{vol}$. Although the thickness of adsorbed protein layer is largely an unknown, it can be shown that the calculated amount of adsorbed protein Γ_p does not depend critically on the choice of Δ. As long as Δ is small, $(1 - e^{-2\Delta/d_p}) \approx 2\Delta/d_p$. Most protein dimensions are of the right order of magnitude. Furthermore, an average fluorescence quantum yield of adsorbed proteins can be evaluated by Eq. [8], provided that Γ_p is determined by an independent method, preferably *in situ*. Such information can provide an additional insight into the conformational changes of the adsorbed protein molecules.

EXPERIMENTAL

Materials

Fluorescence standard, 5-hydroxytryptophan methyl ester hydrochloride (TrpOH), was purchased from Calbiochem. Human immunoglobulin (IgG), fraction II (No. 64-145-1, lots 44 and 45) and bovine serum albumin (BSA) (monomer standard protein powder, No. 81-028, lot P341) were products of Miles Laboratories. Carrier free (100 mCi/ml) ^{125}I was purchased from New England Nuclear. Proteins were labeled with ^{125}I using a modified chloramine-T method (18) and separation procedure developed by Tuszinsky (19). Labeled proteins were stored at 4°C and used within 1 week. All solutions were made from analytical grade reagents and low conductivity water. All buffer solutions were tested for presence of fluorescence impurities. Both BSA and IgG were used without further purification. Unlabeled protein solution was prepared fresh prior to each experiment. Fluorescence of labeled and unlabeled proteins in solution was compared for evidence of ^{125}I-induced quenching. Protein stock solution concentration were determined using BSA and IgG extinction coefficients at 280 nm ($\epsilon_{BSA} = 0.667$, $\epsilon_{IgG} = 1.38$ liters $\cdot g^{-1} \cdot cm^{-1}$, respectively). Absorbances of internal and external standard solutions were always determined at particular excitation wavelengths prior to their use.

The hydrophilic amorphous silica microscope slides (ESCO Products) served as the adsorbing surfaces. Each surface for protein adsorption were cleaned as described earlier (20). The clean hydrophilic silica surface exhibited complete wetting and absence of contact angle hysteresis.

Methods

The TIRIF apparatus combined with γ-photon detection system has been described in details elsewhere (6, 21). The heart of this system was the dovetail quartz prism coupled with glycerol to the silica plate, as shown in Fig. 3. A Silastic (Dow Corning) gasket, at least 0.5 mm thick, formed a TIRIF flow field. Second silica plate with ports for solution injection was supported by a black-anodized aluminium support. The excitation source was a 150-W Xe high-pressure lamp. The excitation

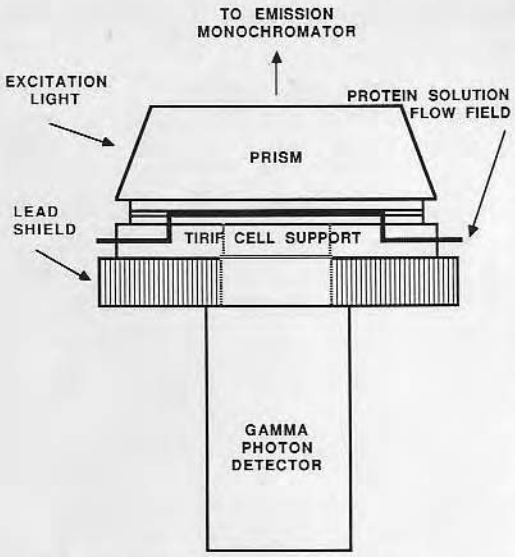

FIG. 3. Design of the TIRIF cell combined with γ-photon detector. The protein flow field is indicated.

monochromator with scan controller (H10-UV, Instrument, SA) was used to select the appropriate excitation wavelengths. A digital shutter, UV-polarizer and quartz optics delivered a perpendiculary polarized, collimated beam of UV light normal to the one face of the dovetail prism. Light impinged at the reflecting interface at the angle of 70°, exceeding the critical angle for total internal reflection at silica/water interface ($\theta_{crit} = 64.7°$). Fluorescence was collected through the dovetail prism at normal incidence to the interface, focused on the slit of the emission monochromator (HR-640, Instrument SA, 300 gr/mm grating), and detected by a photomultiplier tube. Preamplified signals were counted by Ortec photon-counting equipment and recorded both in analog and digital form.

The γ-photon detection system consisted of NaI(Tl) scintillation crystal (2.5-cm diameter, 1.25-cm thick) joined to the face of second photomultiplier tube by a quartz light pipe, all enclosed in a light-tight steel jacket (custom designed, Bicron). A 2.5-cm-diameter sensing window covered by thin aluminum foil was situated directly behind the second silica plate with a circular detecting area defined by a lead shield. The signal from the second photomultiplier tube was preamplified and discriminated against a preset threshold before multiplexing with the TIRIF signal into the time-shared Ortec photon counting unit.

Quantitation of Protein Adsorption by γ-Photon Detection

A schematic of the γ-photon signals from a protein adsorption experiment is given in Fig. 1b. As in the case of TIRIF two distinct signal levels can be distinguished: N_a^γ and N_b^γ. Unlike TIRIF, γ-photon detection is not surface sensitive and detects γ-photon emission from the whole TIRIF volume. In the absence of preferential binding the detected signal was proportional to the mass of protein m in the sensing volume V (determined by radius r of the lead shield aperture and thickness of TIRIF cell, d):

$$N_b^\gamma = km_b; \quad m_b = c_p V = c_p \pi r^2 d, \qquad [9]$$

$$N_a^\gamma = km_a; \quad m_a = \Gamma_p^\gamma \cdot 2\pi r^2, \qquad [10]$$

and from N_b^γ and N_a^γ the adsorbed amount of protein can be calculated as

$$\Gamma_p^\gamma = (N_a^\gamma c_p d)/(2N_b^\gamma). \qquad [11]$$

Experimental Protocols

In situ TIRIF and γ-photon detected protein adsorption. All experiments were done at room temperature. For *in situ* protein adsorption experiments the TIRIF flow cell was primed with buffer solution after necessary optical alignments. Fluorescence emission was generated by exciting at 285 nm and collected at 335 nm (330 nm in the case of IgG adsorption). Slits of 16-nm half-bandwidth were used both in excitation and in emission monochromators. Background fluorescence and γ-photon counts were taken and buffer solution was replaced with the external standard (TrpOH) solutions in increasing order of concentration. The fluorescence intensity was recorded and between each standard sample the buffer solution was used to return the fluorescence signal to the background level. When both TIRIF

and γ-photon detection measurements were combined 3 ml of labeled protein solution were injected, the TIRIF cell was sealed and both signals were recorded. Adsorption was allowed to proceed for 30 min. The fluorescence counting time was 1 s for single measurements while the γ-photon counting system required at least 10 s of counting time. A digital shutter was used to prevent overexposure of adsorbed proteins to UV light. After 30 min, 20 ml of buffer solution was injected manually into the TIRIF cell to remove nonadsorbed proteins and both signals were recorded. The procedure was then repeated by injecting the next protein solution. An increasing order of protein concentration was used. In this way a step-adsorption experiment was performed as opposed to single-shot adsorption experiments where the clean silica surface was exposed only once to each protein solution. At the end of the adsorption experiment, a protein solution of the highest concentration used was injected into and flushed out of the TIRIF cell several times to obtain a reliable internal standard fluorescence signal.

Initial BSA adsorption kinetics were followed only by TIRIF; the cell was primed by 10 ml BSA solution at a flow rate of 16 ml/min after which the flow was stopped and the TIRIF cell sealed.

Ex situ protein adsorption on silica chips. Parallel to the *in situ* measurement of protein adsorption via the γ-photon detection system, similar *ex situ* measurements were performed using smaller rectangular chips of silica (total area of ≈ 5 cm^2) and a commercial γ-photon well counter. The experimental protocol simulated the *in situ* protocol, excluding the formation of any air-adsorbed protein interface. All *ex situ* and preferential binding experiments were performed in a single-shot manner. Details of *ex situ* measurements are given elsewhere (21).

Results

Fluorescence of external TIRIF standard. The fluorescence emission of TrpOH standard solutions (phosphate buffer, 0.145 *M* NaCl, pH 7.4) was centered at 340 nm. A typical background-subtracted fluorescence of external standards measured as a function of ϵc at different TIRIF cell thicknesses is shown in Fig. 4. The same silica plate was used while

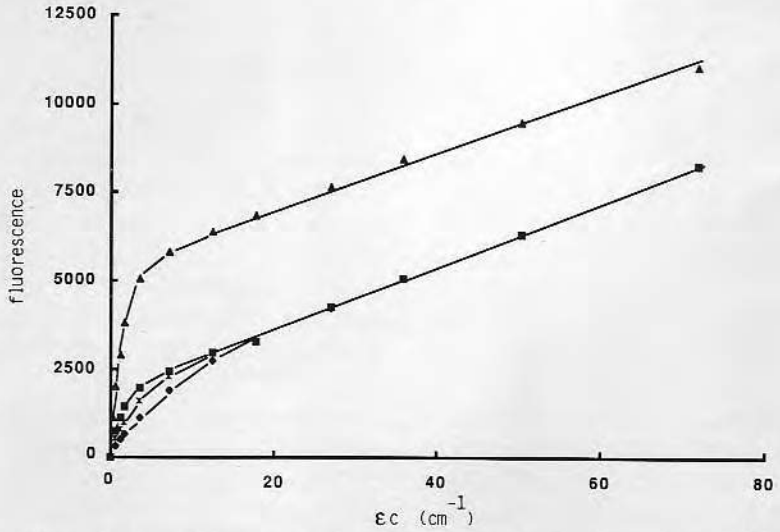

FIG. 4. Background subtracted fluorescence of (TrpOH) as a function of ϵc. Excitation at 285 nm, emission collected at 335 nm. TIRIF cell thickness: ♦, 0.7 mm; ∗, 1.4 mm; ■, 2.4 mm; ▲, 2.4 mm + silica dust mixed with optical matching fluid, glycerol.

cell thickness was increased from 0.7 to 1.4 and 2.4 mm, respectively (lower three curves). The upper curve was obtained with a 2.4-mm-thick TIRIF cell gasket after the scattering of the excitation light was greatly increased by mixing the optical matching fluid with crushed silica dust. In all four cases a linear increase of fluorescence was found at high ϵc. As one would expect, by reducing the cell thickness the linear part appears at higher values of ϵc. Before each protein adsorption experiment similar TrpOH calibration plot was generated for particular silica plate and cell gasket used. These plots were used in the quantitation procedure as previously described.

BSA adsorption on hydrophilic silica. The adsorption of BSA on hydrophilic silica from 0.01 *M* acetate buffer solutions of pH 4.8 and 4.0 was determined by the TIRIF and γ-photon (*in situ* and *ex situ*) detection system. The emission of BSA fluorescence is found to be centered at 342 nm (solution) and at 333 nm (adsorbed layer) at both pH. The fluorescence intensity of the internal BSA standard solution (0.5 mg/ml) was corrected for its scatter-originated part using the external (TrpOH) standard calibration plot determined in the beginning of the experiment. The TIRIF adsorption data were calculated using Eq. [8], assuming that $\Phi_a/\Phi_b = 1$. The thickness of the BSA layer was taken to be equal to 4 nm. The isotherms of BSA adsorption are combined in Figs. 5 and 6. One adsorption isotherm (Fig. 5, dashed line) was calculated from raw TIRIF fluorescence data without the external standard calibration plot. Preferential binding of ^{125}I–BSA molecules to the hydrophilic silica was not investigated.

Initial BSA adsorption kinetic from dilute protein solutions (c_p = 0.0193 mg/ml at pH 4.8, and c_p = 0.0259 mg/ml at pH 4.0, respectively), was followed on clean hydrophilic silica surfaces. At these low BSA concentrations the fluorescence contribution from nonadsorbed BSA was not significant. Moreover, diffusion of BSA to the surface was slow enough so that the process of the adsorption was followed in real time with TIRIF resolution of 1 s. The TIRIF adsorption kinetic data are given in Fig. 7 as a function of (time)$^{1/2}$. The diffusion-limited adsorption data for two BSA concentrations used (given as straight lines in Fig. 7) were calculated from Eq. [12]. They were shifted along x axis to match the start of the adsorption.

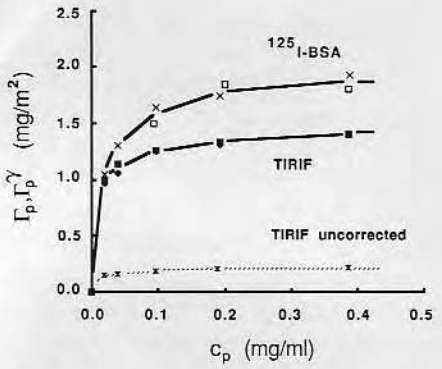

FIG. 5. TIRIF- and ^{125}I–BSA detected adsorption isotherms of BSA onto hydrophilic silica at room temperature, 0.01 M acetate buffer, pH 4.8. ♦, ■, TIRIF; □, ^{125}I–BSA *in situ* step-adsorption mode; ×, *ex situ* adsorption; *, TIRIF, uncorrected for scattering.

IgG adsorption on hydrophilic silica. Adsorption of IgG was followed from phosphate buffer solution (phosphate buffer, 0.145 *M* NaCl, pH 7.2). Preferential binding of ^{125}I–IgG to hydrophilic silica surface was investigated using IgG solutions of identical concentrations (0.18 mg/ml) which had different IgG radioactivities. The *in situ* γ-photon detection system was used. The results indicated that no preferential binding of ^{125}I–IgG has taken place. The fluorescence emission of IgG in the buffer solution was found to be centered at 340 nm. The adsorption of IgG on hydrophilic silica was measured by TIRIF and γ-photon detection (*in* and *ex situ*). The fluorescence of the internal IgG standard solution (0.8 mg/ml) was corrected for its scatter-originated part using an external (TrpOH) standard calibration plots. Both single-shot and step-adsorption experiments were performed. The results are summarized in Fig. 8. The TIRIF adsorption data have been calculated assuming that $\Phi_a/\Phi_b = 1$. The thickness of the IgG layer was

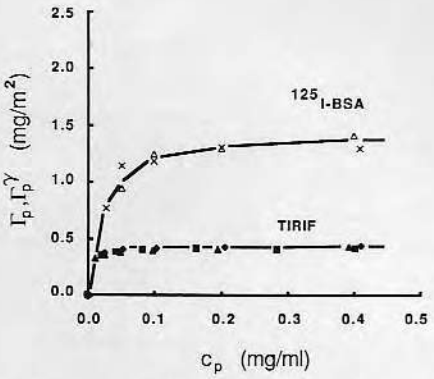

FIG. 6. TIRIF- and ^{125}I–BSA detected adsorption isotherms of BSA onto hydrophilic silica at room temperature, 0.01 *M* acetate buffer, pH 4.0. ♦, ■, ▲, TIRIF; △, ^{125}I–BSA *in situ* step-adsorption mode; ×, *ex situ* adsorption.

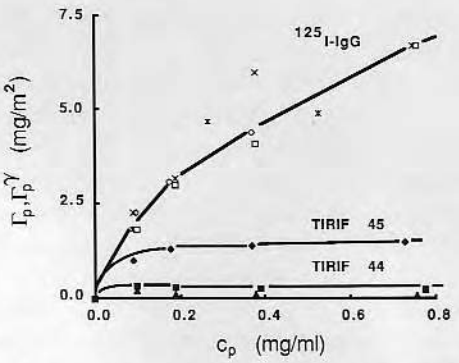

FIG. 8. TIRIF- and ^{125}I–IgG detected adsorption isotherms of IgG onto hydrophilic silica at room temperature, phosphate buffer, 0.145 *M* NaCl, pH 7.2. ♦, TIRIF, IgG lot 45; ▲, ■, TIRIF, IgG lot 45; ◇, □, ^{125}I–IgG *in situ* step-adsorption mode, lots 45 and 44, respectively; ∗, *in situ* single-shot adsorption mode; ×, *ex situ* adsorption.

assumed to be equal to 10 nm which roughly corresponds to the height of the "T"-shaped IgG molecule (22). Two TIRIF adsorption isotherms coded 44 and 45 represent two different IgG lots, respectively. No significant difference in the adsorption of two IgG lots was found in the case of γ-photon detected adsorption. Initial adsorption kinetics of IgG were not investigated.

Fluorescence emission efficiency of adsorbed proteins. In order to analyze the influence of adsorption on the fluorescence emission efficiency of BSA and IgG, the ratio of protein fluorescence quantum yields in the adsorbed layer and in the solution, Φ_a/Φ_b, was calculated. Equation [8] was used together with experimentally determined Γ_p^γ. The ratio Φ_a/Φ_b is given in Fig. 9 as a function of maximum adsorption fraction, $\Gamma_p^\gamma/\max \Gamma_p^\gamma$.

DISCUSSION

Most studies of protein adsorption by total internal reflection methods have focused on

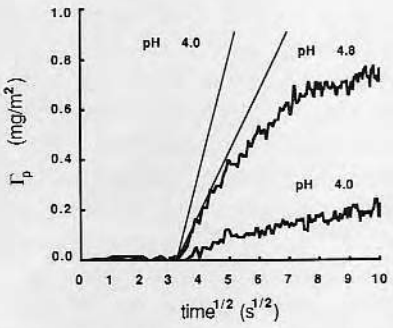

FIG. 7. Initial kinetics of BSA adsorption on hydrophilic silica at room temperature, 0.01 *M* acetate buffer. The straight lines represent diffusion limited rate of adsorption calculated from Eq. [12] for c_p = 0.0193 mg BSA/ml (pH 4.8) and 0.0259 mg BSA/ml (pH 4.0), respectively.

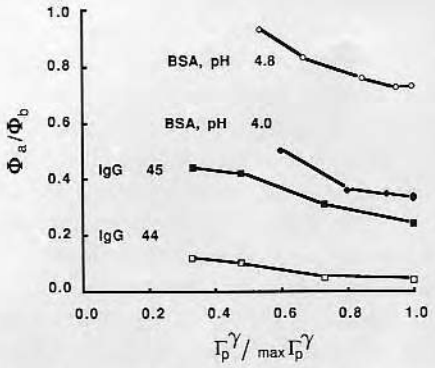

FIG. 9. The ratio of protein fluorescence quantum yields in the adsorbed layer and in the solution, Φ_a/Φ_b, given as a function of maximum adsorption fraction (as determined by γ-photon detection system), $\Gamma_p^\gamma/\max \Gamma_p^\gamma$.

the question: *how much* protein is adsorbed at a particular interface? To this end various quantitation schemes were proposed (13–15, 20). More often than not, they agreed that protein surface concentration had to be determined independently. Consequently, total internal reflection methods applied to protein adsorption were considered to be semiquantitative at best; the final adsorbed amount was determined by some independent method and all intermediate adsorption values were derived by scaling up or down measured fluorescence or absorbance in the case of attenuated total reflection methods. Such an approach was particularly successful in TIRF adsorption studies where proteins were labeled with an extrinsic fluorophore (10–13, 15).

The use of the fluorescence emitted by nonadsorbed proteins in solution as an internal standard in TIRIF experiments was initially proposed by Van Wagenen *et al.* (20). Later, Rockhold *et al.* proposed both graphical and numerical TIRIF quantitation schemes (14) but failed to recognize importance of scattered propagating excitation light. Present quantitation scheme is based on a similar concept; nonadsorbed proteins in the *evanescent* region are used as an internal fluorescence standard. However, in order to account fully for the extent of nonadsorbed bulk protein fluorescence excited by propagating scattered light, a number of external fluorescence standards of relatively large concentration range have to be used. It is also necessary to use such external standard whose excitation and emission characteristics are similar to the protein under study since the extent of scattering is related to $1/\lambda^4$ of excitation wavelength. As an external standard TrpOH was chosen; it has greater solubility than other tryptophan derivatives and its fluorescence emission is centered at 340 nm when excited at 285 nm.

The fluorescence from the standard solution should be dependent both on the TIRIF cell thickness and on the scattered light intensity due to the propagating nature of scattered light. Both effects were indeed found using solutions of TrpOH (Fig. 4). By increasing the thickness of the TIRIF cell the fluorescence intensity vs ϵc plots differed, but only at $\epsilon c < d/2$. This justifies the concept of calibration plots in TIRIF protein adsorption. From the experimental data at $\epsilon c < d/2$ it can be inferred that the scattered light in the TIRIF cell traveled a distance greater than the actual cell thickness. This was due to the wide range of angles at which the scattered light propagated in the TIRIF cell as well as due to the possible back-reflection from the second silica surface and TIRIF cell support.

Any rescattering of the excitation light by macromolecules in the TIRIF cell was examined by comparing the standard calibration plots of tryptophan (Trp) and tryptophan-labeled dextran (*N*-acetyl-tryptophanyl-dextran, $M_w = 70{,}000$). No significant increase of fluorescence was noticed; at given ϵc both Trp and Trp-dextran derivates fluoresced according to their respective quantum yields.

The TIRIF data of BSA adsorption on hydrophilic silica at pH 4.8 and the *in situ* and *ex situ* measured ^{125}I–BSA adsorption are of the same order of magnitude (Fig. 5). If the scatter-originated contribution to the fluorescence would be completely neglected, the TIRIF adsorption would amount to much lower values, as indicated by the adsorption isotherm given in dashed line (Fig. 5). By accounting for this part of the internal standard fluorescence sets the fluorescence-detected BSA adsorption is in reasonable agreement with both *in situ* and *ex situ* measured ^{125}I–BSA adsorption. However, the TIRIF adsorption experiments resulted in somewhat lower Γ_p which is particularly evident at higher BSA concentration. Possible reasons for this difference which may originate in some experimental artifacts or from the assumptions used, have to be considered in more detail.

Preferential binding of either ^{125}I-labeled or nonlabeled-BSA was ruled out since it was not detected in the case of BSA adsorption on a variety of surfaces (23). The fluorescence of ^{125}I-labeled and nonlabeled BSA in solution

was identical, with no evidence of ^{125}I-induced quenching.

The BSA molecules in the adsorbed layer may themself become scattering sources for the evanescent surface wave, which would induce a larger N_b. Since the calibration plots were generated with the external standards in the absence of adsorbed layers, this effect will result in smaller Γ_p. Use of the external standards with the adsorbed protein layer in place was not possible. The 285-nm excitation peak intensity in the fluorescence emission spectra which were taken prior to and after the BSA adsorption was not significantly increased. The question is whether this peak fully reflects the extent of scattering in the TIRIF cell? No scattering of the evanescent wave by adsorbed cells at glass/water interface was detected (7), although the scattering of the evanescent wave is predicted and analyzed in electromagnetic theory (24).

Second possible reason for the adsorption isotherm difference may be due to the different refractive indices of the protein solution and the adsorbed protein layer. There is little doubt that such difference exists; a 30% BSA solution has a refractive index of 1.41 at 285 nm (25), as compared with the dilute protein solution where the refractive index was taken to be equal to that of buffer solution (n_2 = 1.353). The quantitation scheme used here does not recognize the adsorbed proteins as a separate optical layer. The influence of an increased refractive index of adsorbed protein layer on electromagnetic energy distribution in the evanescent region is, however, smaller than intuitively expected. Due to the continuity requirement of the electric field amplitudes at the interface, any increase of $E_\perp^e$ in the part of evanescent region occupied by adsorbed protein will be followed by an increased $E_\perp^e$ outside the adsorbed layer. Hence, the ratio of integrals in Eq. [5] will not significantly change in value. For example, an increase of refractive index of the adsorbed layer from 1.353 (n_2 of aqueous phase) to 1.496 (n_1 of silica) will change the ratio of integrated evanescent intensities by a factor of 0.95. This would result as 5% higher adsorption! Hence, these two effects just compensate each other.

The most probable reason for the adsorption isotherm differences is a decreased fluorescence quantum yield of the adsorbed BSA molecules. Namely, the adsorption of protein at the interface may result in fluorescence surface quenching and shorter fluorescence lifetimes. It is also expected that a degree of protein unfolding at the interface could decrease the fluorescence emission efficiency.

The difference between two types of BSA adsorption isotherms is much larger at pH 4.0 (Fig. 6). Repeated TIRIF experiments on different silica plates showed excellent reproducibility of the adsorption results (Fig. 6). Yet, the BSA surface concentration detected by γ-photon detection was almost 3 times larger even when the scatter-originated fluorescence contribution was taken into account. No evidence of significantly increased scattering by the adsorbed BSA layer at pH 4.0, as compared with pH 4.8, was found. Also, no increase of refractive index of adsorbed BSA layer could possibly account for this large difference in the adsorption. Hence, the difference is largely determined by a decreased fluorescence efficiency of the adsorbed BSA molecules at the interface.

It is plausible that at its isoelectric point (pH_{iep} 4.8) BSA molecule does not experience the same conformational changes during the adsorption as it does when the adsorption is carried out from the more acidic solutions. The decrease of BSA quantum yield in acidic solution in which BSA molecule undergoes so-called "N–F transition" is well documented (26). However, this decrease has already been taken into the account in the present quantitation scheme by using BSA solution of pH 4.0 as the internal standard. At pH 4.0 BSA molecules are positively charged, while silica surface carries the negative charges. The attraction forces between opposite charges can contribute to BSA unfolding, if any, at the interface; this may induce a decreased fluores-

cence efficiency. Recently, similar conclusion has been reached from the TIRIF lifetime measurements of intrinsic BSA fluorescence from the adsorbed layer (8). The fluorescence lifetimes of adsorbed BSA molecules were found to be shorter than the lifetimes in solution.

The initial kinetics of BSA adsorption supports the conclusion about decreased fluorescence quantum yields. At pH 4.8 there is a good agreement between the initial TIRIF adsorption vs $(\text{time})^{1/2}$ data and the adsorption data calculated from the diffusion-limited rate of arrival of BSA molecules to the surface (Fig. 7). The latter rate, often called "diffusion-limited rate of adsorption," was calculated using (23)

$$d\Gamma_p = 2c_p(D/\pi)^{1/2}\, dt^{1/2} \qquad [12]$$

where D is BSA diffusion coefficient (7×10^{-7} $cm^2\ sec^{-1}$) (27). The coincidence between the initial TIRIF adsorption data and the calculated diffusion-limited adsorption indicates that at the beginning of the adsorption, $\Phi_a/\Phi_b = 1$. In the case of BSA adsorption at pH 4.0 the diffusion-limited adsorption exceeded TIRIF adsorption data. Similar difference between the experimental adsorption data and the diffusion-limited adsorption was found in BSA adsorption on glass and negatively charged polystyrene surfaces. It was explained by an energy barrier of adsorption (23). Namely, not all BSA molecules diffusing to the surface are "ready" to become adsorbed; only those with enough energy needed to overcome the adsorption energy barrier will "stick" to the surface.

Initial adsorption kinetics could not be followed with the *in situ* γ-photon detection system. This was due to low time resolution and relatively high bulk BSA contribution to overall γ-signal even at low BSA concentration. The following analysis could be done: TIRIF-detected adsorption at pH 4.0 was proportionally increased using as a reference point the final surface concentration of ^{125}I–BSA, Γ_p^γ, at the same c_p. In this way TIRIF adsorption data were corrected for the quantum yield decrease. They were compared with calculated diffusion-limited adsorption rate. The latter was still exceeding the experimental rate by a factor of 0.3. Such an adsorption rate decrease by a factor of $e^{-A/kT}$ would be due to an adsorption energy barrier A of $1.2kT$ units.

Interestingly, initial BSA adsorption at pH 4.0 reveals that the first contact between the protein and the silica surface immediately results in decreased fluorescence emission efficiency. It indicates that some conformational changes are taking place at very short interfacial residence times and at very low surface coverages. The picture is different at pH 4.8; the TIRIF adsorption data deviate from the diffusion limited adsorption data only at $\Gamma_p > 0.4$ mg m^{-2}. This may also be due to the limitation of Eq. [12] which is derived using the assumption that the surface acts as a protein sink. When there is more protein accommodated on the surface, however, less chance a new diffusing BSA molecule has to find an unoccupied adsorption site and adsorption slows down.

Possible conformational changes due to the adsorption are best illustrated by the ratio of protein fluorescence quantum yields in the adsorbed layer and in the solution, Φ_a/Φ_b, which is given in Fig. 9. It amounted to an average of 0.9 at pH 4.8 and to 0.5 at pH 4.0, respectively, as measured at the half maximum adsorption (at $\Gamma_p^\gamma/\max \Gamma_p^\gamma = 0.5$). Unfortunately, there is no direct relation between a degree of conformational BSA change and decreased fluorescence efficiency. The intrinsic fluorophors in proteins report their environment seen at the time of the emission. The BSA fluorescence is largely determined by two tryptophan residues although the energy available to their emission can be transferred to them from several tyrosines residues along the polypeptide chain. Overall photophysical "sensitivity" of BSA fluorophors to the conformational alterations in various parts of BSA molecule is not yet known. Before this information is available, a decrease of Φ_a/Φ_b at pH

4.0 may only serve as an indication that adsorbed BSA is conformationally changed.

The situation is even less clear in the case of IgG adsorption. Different isotherms of IgG adsorption on hydrophilic silica from phosphate buffer were determined depending on the method of detection used; TIRIF-detected adsorption depended on the particular IgG lot used, while ^{125}I–IgG-detected adsorption was almost independent on IgG lot used but it was an order of magnitude larger (Fig. 8). No difference between the fluorescence quantum yields of two different IgG lots could be detected in solution. Preferential adsorption of ^{125}I-labeled or unlabeled IgG on hydrophilic silica was excluded. Also, there was no evidence of ^{125}I-induced quenching of IgG fluorescence in the solution. It may be concluded that the labeling of IgG was not the cause of difference between the TIRIF and ^{125}I-labeled IgG adsorption isotherms.

The extent of scattering due to IgG molecules at the interface was considerably larger than in the case of BSA; the excitation peak maximum increased approx 30% for both lots. Increased intensity of scattered excitation light was also evident in the fluorescence of nonadsorbed IgG molecules in TIRIF cell. It was compared with TrpOH standards at given ϵc. The ratio of TrpOH/nonadsorbed IgG fluorescence intensities decreased as the surface concentration of IgG increased in the step-adsorption experiments. The fluorescence quantum yield of nonadsorbed IgG molecules in the TIRIF cell should not depend on the adsorption. Since the depletion of IgG was excluded an alternative explanation was that the intensity of excitation light increased due to the adsorption. Such an increase was estimated to amount up to 45%; it would decrease TIRIF adsorption results in the same proportions.

Two other factors may also influence the TIRIF-detected adsorption; a larger thickness of the adsorbed IgG layer and/or an increase of its refractive index. The influence of adsorbed layer thickness can be estimated: at constant Γ_p, an increase of Δ from 10 to 20 nm alone would increase calculated adsorption by 10%. Similar result would be found if the difference between the refractive indices was taken into the account. Again, all these effects compensate each other. Therefore, such a large difference between two types of the adsorption results may only originate in significantly decreased fluorescence efficiency of IgG molecules in the adsorbed state.

Not all tryptophan side chains contribute equally to IgG fluorescence; predominant contributors are tryptophans in hypervariable region (28). Because of that, ligand-binding to IgG often results in a decrease of fluorescence. In the present case IgG fluorescence may be quenched upon the binding to the surface. The surface-induced fluorescence quenching is currently studied by TIRIF using monoclonal IgG antibodies. The intrinsic IgG fluorescence is found to be a sensitive indication of subtle changes in this protein upon binding to various surfaces (29). An increased interest in TIRF-based immunosensors warrants further research in this area (29–31).

Difference between the two types of IgG adsorption detection is also reflected in the ratio of protein fluorescence quantum yields, Φ_a/Φ_b, given in Fig. 9. The fluorescence efficiency of adsorbed IgG has apparently decreased by a factor of 3 and 10 for lots 45 and 44, respectively. Both IgG lots were heterogenous populations of proteins commonly defined as fraction II. It is therefore possible that an IgG subpopulation with a higher affinity toward silica surface is also characterized with a smaller quantum yield of fluorescence.

It has to be noted that decreased fluorescence quantum yield of adsorbed proteins also reflects some possible changes of adsorption parameters, particularly of ϵ, which were assumed not to change upon the adsorption. The extents of change of ϵ are unknown. One would, however, expect that in the case of multitryptophan proteins such as IgG, the changes of ϵ due to the adsorption would be too small to account for observed difference.

Figure 9 shows that Φ_a/Φ_b decreases as

$I_p^{\gamma}/\max I_p^{\gamma}$ increases. Possible reasons for this were already discussed: (a) an increase of scattering due to the formation of an adsorbed layer at the interface; (b) the adsorbed protein layer may become physically different, i.e., thicker and optically more dense as the adsorption proceeds; and also (c) lateral interactions may also play an important role in determining the fluorescence emission efficiency of adsorbed proteins.

The optical changes of adsorbed protein layer were recently confirmed by ellipsometric measurements (32, 33).

CONCLUSION

It has been shown that total internal reflection fluorescence applied to protein adsorption can be quantitated using two types of standards; with external standards one can account for the fluorescence of internal standards excited by nonevanescent scattered radiation propagating beyond the depth of evanescent wave penetration. We believe that this quantitation scheme is neither restricted to *intrinsic* protein fluorescence nor to the TIRIF method in particular. It can be applied to adsorption studies which generally use evanescent surface wave. Combined with an independent quantitation of protein adsorption, quantitative TIRIF also allows an average fluorescence emission efficiency of adsorbed proteins to be calculated. To do so *in situ* ^{125}I γ-photon detection system was developed. The adsorption of two model proteins, BSA and IgG, were measured simultaneously by both TIRIF and ^{125}I γ-photon detection. The results showed that the assumption of a constant fluorescence quantum yield of proteins in the adsorbed layer and in the bulk solution should be used with caution. While for BSA at iep relatively small difference between the quantum yields was determined, much larger difference seen at IgG adsorption, and in the case of BSA adsorption at pH 4.0, could only be explained by a greatly diminished fluorescence efficiency.

ACKNOWLEDGMENTS

Discussions with P. Suci, W. M. Reichert, and R. A. Van Wagenen are gratefully acknowledged. The assistance from H. Chuang with protein iodination is appreciated. One of us (V.H.) acknowledges with appreciation a Fulbright Program Grant awarded for academic year 83/84. Part of this work was supported by financial help from a University of Utah Faculty Research Grant and NIH Grant HL 18519.

REFERENCES

1. Hirschfeld, T., *Canad. Spectrosc.* **10,** 128 (1965).
2. Harrick, N. J., and Loeb, G. I., *Anal. Chem.* **45,** 687 (1975).
3. Kronick, M. N., and Little, W. A., *J. Immunol. Meth.* **8,** 235 (1975).
4. Hirschfeld, T., and Block, M. J., *Opt. Eng.* **16,** 406 (1977).
5. Hirschfeld, T., Block, M. J., and Mueller, W., *J. Histochem. Cytochem.* **25,** 719 (1977).
6. Hlady, V., Van Wagenen, R. A., and Andrade, J. D., *in* "Surface and Interfacial Aspects of Biomedical Polymers, Vol. 2. Protein Adsorption" (J. D. Andrade, Ed.), Chap. 2. Plenum, New York, 1985.
7. Axelrod, D., Burghardt, T. P., and Thompson, N. L., *Ann. Rev. Biophys. Bioeng.* **13,** 247 (1984).
8. Rainbow, M. R., Atherton, S., and Eberhard, R. C., *J. Biomed. Mater. Res.*, submitted, 1985.
9. Iwamoto, G. K., Van Wagenen, R. A., and Andrade, J. D., *J. Colloid Interface Sci.* **86,** 581 (1984).
10. Watkins, R. W., and Robertson, C. R., *J. Biomed. Mater. Res.* **11,** 915 (1977).
11. Lok, B. K., Cheng, Y.-L., and Robertson, C. R., *J. Colloid Interface Sci.* **91,** 104 (1983).
12. Thompson, N. L., and Axelrod, D., *Biophys. J.* **43,** 103 (1983).
13. Lok, B. K., Cheng, Y.-L., and Robertson, C. R., *J. Colloid Interface Sci.* **91,** 87 (1983).
14. Rockhold, S. A., Quinn, R. D., Van Wagenen, R. A., Andrade, J. D., and Reichert, W. M., *J. Electroanal. Chem.* **150,** 261 (1983).
15. Burghardt, T. P., and Axelrod, D., *Biophys. J.* **33,** 455 (1981).
16. Hansen, W. N., *Advan. Electrochem. Electrochem. Eng.* **9,** 1 (1973).
17. Born, M., and Wolf, E., "Principles of Optics," 5th ed., Pergamon, New York, 1975.
18. Chuang, H. Y. K., King, W. F., and Mason, R. G., *J. Lab. Clin. Med.* **92,** 483 (1978).
19. Tuszynski, G. P., Knight, L., Piperno, J. R., and Walsh, P. N., *Anal. Biochem.* **106,** 118 (1980).
20. Van Wagenen, R. A., Rockhold, S. A., and Andrade, J. D., *Advan. Chem. Ser.* **199,** 351 (1982).
21. Reinecke, D. R., M.Sc. thesis, Univ. of Utah, 1985.

22. Bagchi, P., and Birnbaum, S. M., *J. Colloid Interface Sci.* **83,** 460 (1981).
23. Van Dulm, P., and Norde, W., *J. Colloid Interface Sci.* **91,** 248 (1983).
24. Chew, H., Wang, D.-S., and Kerker, M., *Appl. Opt.* **18,** 2679 (1979).
25. Andersen, M., and Painter, L. R., *Biopolymer* **13,** 1261 (1974).
26. Sogami, M., Itoh, K. B., and Nemoto, Y., *Biochim. Biophys. Acta* **393,** 446 (1975).
27. Keller, K. H., Canales, E. R., and Yum, S. I., *J. Phys. Chem.* **75,** 379 (1971).
28. Schreiber, A. D., Strosberg, A. D., and Pecht, I., *Immunochemistry* **15,** 207 (1978).
29. Lin, J-N., Hlady, V., Reichert, W. M., and Andrade, J. D., to be published.
30. Newby, K., Andrade, J. D., Benner, R. E., and Reichert, W. M., *J. Colloid Interface Sci.* **111,** 000 (1986).
31. Sutherland, R. M., Dähne, C., Place, J. F., and Ringose, A. R., *J. Immunol. Meth.* **74,** 253 (1984).
32. Cuypers, P. A., Corsel, J. W., Janssen, M. P., Kop, J. M. M., Hermens, W. Th., and Hemker, H. C., *J. Biol. Chem.* **258,** 2426 (1983).
33. Cuypers, P. A., Corsel, J. W., Janssen, M. P., Kop, J. M. M., Hermens, W. Th., and Hemker, H. C., *in* "Surfactants in Solution" (K. L. Mittal and B. Lindman, Eds.), Vol. 2, p. 1301. Plenum, New York, 1984.

last page

8) D. V. Turner and L. Brandt, Biochemistry, 7 (1968) 3381.
9) L. Stryer, J. Mol. Biol., 13 (1965) 482.
10) P. Van Dulm and W. Norde, J. Colloid Interface Sci., 91 (1983) 248.
11) S. D. Dowling and W. R. Seitz, Anal. Chem., 57 (1985) 605.

LAST COPY
DO NOT REMOVE

33

Colloids and Surfaces, 26 (1988) 185–190
Elsevier Science Publishers B.V., Amsterdam — Printed in The Netherlands

HYDROPHOBICITY GRADIENT ON SILICA SURFACES: A STUDY USING TOTAL INTERNAL REFLECTION FLUORESCENCE SPECTROSCOPY

V. HLADY*, C. GÖLANDER and J. D. ANDRADE
Center for Biopolymers at Interfaces, University of Utah, Salt Lake City, Utah 84112, USA
and *"Ruđer Bošković" Institute, POB 1016, 41000, Zagreb, Croatia, Yugoslavia

(Received 22 February 1988; accepted in final form 21 April 1988)

ABSTRACT

A silica surface with hydrophobicity gradient was characterized using total internal reflection fluorescence spectroscopy and ANS, 1-anilinonaphthalene-8-sulfonate, as a surface probe. The probe responded to the hydrophobicity gradient of the surface. Strong enhancement of ANS fluorescence was found at the hydrophobic side of the gradient and no fluorescence enhancement at the hydrophilic side. Similar results were obtained with ANS binding to bovine serum albumin adsorbed on the gradient surface.

INTRODUCTION

Detailed analysis of surface-induced changes of an adsorbed protein requires a set of well-characterized surfaces, each having a constant chemical composition. A large number of time-consuming experiments, by which each surface is prepared and characterized, was often needed. It was shown recently that surfaces with a hydrophobicity gradient can be prepared (1). An example is the dichlorodimethylsilane (DDS)-modified, hydrophilic silicon dioxide surface, which carries an excess of methyl groups at one side of the sample, making it hydrophobic, while the other side has an excess of hydroxyl groups, making it hydrophilic. Such a surface was shown to be an excellent tool in the analysis of surface-induced changes of adsorbed protein amount (1,2).

It is the purpose of this study to demonstrate that total internal reflection fluorescence (TIRF) spectroscopy can be used to characterize the hydrophobicity of gradient silica surfaces. In our previous work the TIRF method was used in protein adsorption studies exclusively with non-gradient silica surfaces (3,4). Here, we report on

he characterization of a hydrophobicity gradient on a DDS-modified silica surface with -anilinonaphthalene-8-sulfonate, (ANS).

EXPERIMENTAL

All chemicals used were of analytical grade. BSA, a monomer standard protein owder (Miles) and ANS, bis-ANS free (Molecular Probes), were used as received. heir solution concentration was determined using respective extinction coefficients (5). he TIRF method and apparatus have been described elsewhere (4,6). The silica urface with the hydrophobicity gradient was prepared using the procedure of Elwing et l. (1). A full account of silica surface gradient characterization will be published (J.D ndrade et al. in preparation). Selective illumination of the silica/buffer interface was chieved with a 325 nm cw laser beam (Lexonic). The TIRF cell was set on a icrometer-driven stage which allowed movements perpendicular to the optical axis of he emission monochromator. While the excitation and emission optical light-paths were ept constant these lateral movements brought different positions along the gradient into he excitation and emission light-path cross-section (Fig. 1). The distance between lateral

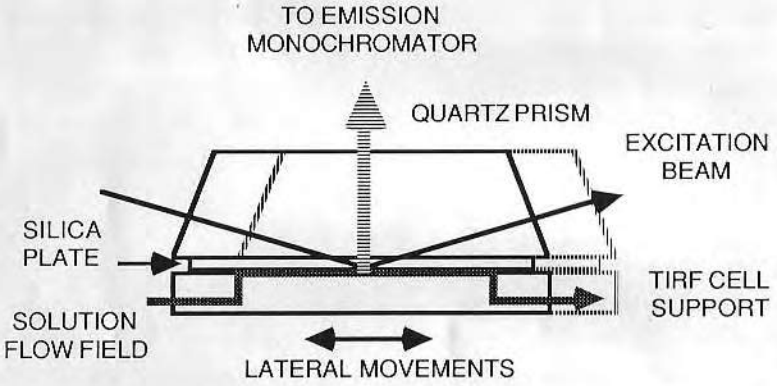

igure 1. Schematics of TIRF cell with lateral scanning resolution.

easurement positions was 1 mm; fluorescence was measured from the area which was .5 mm wide. In this study the hydrophobic gradient was checked with the capillary rise ethod (1); the midpoint of the gradient was placed approximately at the median position f the TIRF cell stage. Fluorescence was measured at 470 nm using 8 nm slit halfwidths. he TIRF cell was filled with working solutions in the following order: 1) buffer, 2) ANS olution, 3) buffer, 4) BSA solution, 5) buffer, 6) ANS solution 7) buffer. Solutions of ANS nd BSA were prepared in a buffer (0.07 mol/l phosphate, pH 5.3). BSA was allowed to dsorb for 1 hour from 1 mg/ml solution after which non-adsorbed BSA was flushed-out ith the buffer solution and ANS solution was injected again (steps 5 and 6).

RESULTS AND DISCUSSION

Fluorescence intensities measured along the hydrophobicity gradient are shown in Fig. 2. The hydrophobicity of the surface is decreasing with the increase in position number. Three sets of data are given:

a) - fluorescence of buffer solution ,

b) - fluorescence of $4.96 \cdot 10^{-5}$ mol/l ANS solution, and

c) - fluorescence of $4.96 \cdot 10^{-5}$ mol/l ANS solution added to the irreversibly adsorbed BSA layer.

Fluorescence from the buffer solution was constant along the gradient (a, Fig 2). This background signal was due to the fluorescence of the quartz prism which has a broad

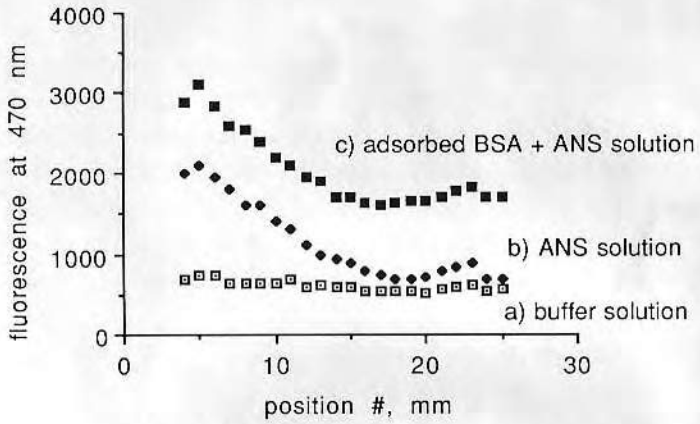

Figure 2. Fluorescence intensity at 470 nm measured along the hydrophobicity gradient.

maximum at 390 nm. Once the buffer solution was replaced with the ANS solution, the fluorescence increased on the hydrophobic side of gradient, while at the hydrophilic side it was similar to the buffer background. It is known that in water ANS does not fluoresce (7,8). Its fluorescence is sensitive to the polarity of its environments: a decrease in polarity of the ANS environment leads to both an increase in the fluorescence quantum yield and a blue-shifted fluorescence maximum (9). Hence, it seems that the interfacial ANS fluorescence originated from adsorbed ANS molecules which interacted with a non-polar environment on the hydrophobicity gradient surface. ANS molecules were excited by the evanescent surface wave which was created by total internal reflection of a 325 nm laser beam at the silica/solution interface (3). By replacing the ANS solution with the buffer the fluorescence returned to the background signal level indicating that the interaction between the surface and ANS is reversible. Absence of ANS fluorescence enhancement at hydrophilic silica surfaces has been observed before (3). An explanation is thatthe hydrophobic DDS gradient on silica surface used here is also an

ectric charge gradient. Negatively charged hydrophilic side of gradient surface ectrostatically repels the ANS anion away from the surface. Consequently its orescence is excited by the less intense evanescent surface wave and strongly enched by the surrounding water molecules.

In this study the layer of BSA was adsorbed at the gradient surface. The BSA ncentration of 1 mg/ml ensured that the plateau of the adsorption isotherm is reached 1 mg/m^2 in the case of hydrophilic silica at pH 4.8) (4). Non-adsorbed protein olecules were removed by buffer flush-out and only irreversibly adsorbed BSA was left the surface. The fluorescence of irreversibly adsorbed BSA layer in the absence of NS did not differ from the buffer background fluorescence. Once the ANS solution was ected into the TIRF cell a further enhancement of ANS fluorescence was found; the me ANS concentration ($4.96 \cdot 10^{-5}$ mol/l) showed larger fluorescence in the presence adsorbed BSA (c, Fig 2). The fluorescence intensity profile was similar to that obtained the absence of adsorbed BSA layer (b, Fig. 2) with one exception due to the adsorbed otein: the hydrophilic side of the gradient showed a much larger fluorescence than in e absence of BSA. Fig. 3 shows the background-subtracted and smoothed orescence emission spectra taken at each side of the gradient (position#5 and #20). e fluorescence maximum of the quartz prism served as an internal normalization andard in the subtraction of spectra. A difference in ANS emission maxima was found: the hydrophobic side of gradient the ANS fluorescence maximum was at 465 nm.

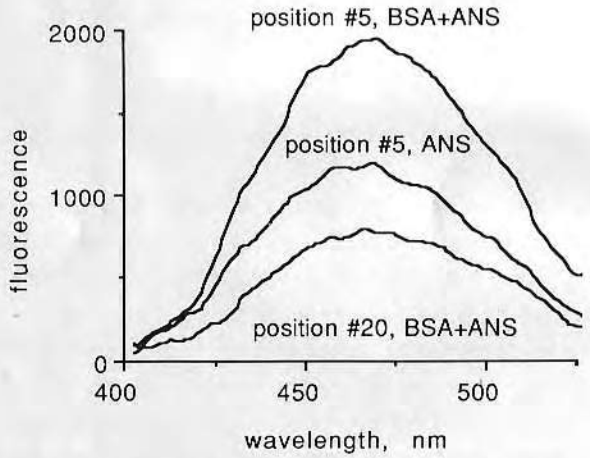

gure 3. Background subtracted and smoothed fluorescence emission spectra at two sitions along the hydrophobicity gradient.

the case of DDS-modified chromatographic silica particles, fluorescence of adsorbed NS indicated a more polar environment; the emission maximum was found at 470 nm 1). This difference probably arises from different silanization procedures. Due to the

very low signal at the hydrophilic side of the gradient, no information about the maximum could be obtained. Spectra taken in the middle of similar gradients (not shown here) showed maxima at 465 nm. The ANS interactions along the gradient did not cause a red shift in fluorescence emission due to the overall polarity increase. This indicates that there is one predominant mode of the ANS-hydrophobic surface interaction. The present results were inconclusive with respect to the molecular distribution of methyl groups on the gradient surface.

In the presence of adsorbed BSA the emission maxima wavelengths at the hydrophobic and hydrophilic sides of the gradient were found to be equal at 470 nm. This maximum position was also found earlier for BSA-bound ANS at a hydrophilic silica surface (3). No changes in emission wavelengths indicated that the polarity of ANS binding sites was not changed by adsorption onto surfaces of different hydrophobicity. In the favorable case, if the ANS-adsorbed BSA binding affinity remains unchanged along the gradient, ANS fluorescence could be used as a quantitative measure of BSA adsorption. A higher BSA adsorption onto the DDS-modified glass surface than onto unmodified glass is known from literature (10). Whether the same holds for DDS hydrophobicity gradient on silica needs to confirmed by independent BSA adsorption measurements.

In conclusion, TIRF spectroscopy can be used to characterize surfaces with a hydrophobicity gradient by direct spectroscopic characterization with a fluorescence probe, like 1-anilinonaphthalene-8-sulfonate.

ACKNOWLEDGEMENT

V. Hlady and C. Gölander wish to thank the Center for Biopolymers at Interfaces for providing support for their stay at the University of Utah. This work was also supported by the Authority for Scientific Research of Croatia (Yugoslavia).

REFERENCES

1) H. Elwing, S. Welin, A. Askendahl, U. Nilsson, and I. Lundström,J. Colloid Interface Sci., 119 (1987) 203
2) H. Elwing, A. Askendahl,B. Ivarsson, U. Nilsson, S. Welin and I. Lundström, in J. L. Brash and T. A. Horbett (Eds.), Proteins at Interfaces, ACS Symp. Ser., 343 (1987) 468.
3) V. Hlady and J. D. Andrade, Colloids and Surfaces, 32 (1988) 359.
4) V. Hlady, D. Reinecke, J.D. Andrade, J. Colloid Interface Sci., 111 (1986) 565.
5) D. A. Kolb and G. Weber, Biochemistry, 14 (1975) 4476.
6) V. Hlady, R. A. Van Wagenen and J. D. Andrade, in J. D. Andrade (Ed.), Surface and Interfacial Aspects of Biomedical Polymers. Vol. 2. Protein Adsorption. Plenum Press, N.Y., 1985, pp. 81-119.
7) E. M. Kosower and H. Kanethy, J. Am. Chem. Soc., 100 (1978) 4179.

Head-7

Colloids and Surfaces, 32 (1988) 359–369
Elsevier Science Publishers B.V., Amsterdam — Printed in The Netherlands

Fluorescence Emission from Adsorbed Bovine Serum Albumin and Albumin-bound 1-Anilinonaphthalene-8-sulfonate Studied by TIRF

V. HLADY[1,2*] and J.D. ANDRADE[2]

[1]*Institute "Ruder Bošković" Bijenička 54, 41000 Zagreb (Yugoslavia)*
[2]*Center for Biopolymers at Interfaces, and Department of Bioengineering, University of Utah, Salt Lake City, UT 84112 (U.S.A.)*

(Received 22 September 1987; accepted in final form 31 December 1987)

ABSTRACT

Total internal reflection fluorescence (TIRF) spectroscopy was used to analyse the conformational changes of bovine serum albumin (BSA) upon adsorption to silica surfaces. The intrinsic fluorescence emitted by BSA tryptophans and the fluorescence of BSA-bound ligand 1-anilinonaphthalene-8-sulfonate (ANS) were analysed prior to and after the removal of nonadsorbed protein. It was found that the irreversibly adsorbed BSA emits a blue-shifted intrinsic fluorescence (11 nm) and that the surface-adsorbed BSA-bound ANS fluorescence emission is red-shifted (12 nm). It was concluded that the conformational change in adsorbed BSA involves the whole BSA molecule: tryptophans become exposed to a less polar environment while the binding site polarity is increased. The conformation of irreversibly adsorbed BSA is not similar to the unfolded conformation of heat-denatured BSA. The red-edge excitation of adsorbed BSA-bound ANS indicates a slower spectral relaxation in the adsorbed protein as compared with the protein in solution. The fluorescence intensity contributions from irreversibly adsorbed species (BSA with and without bound ANS) suggest some changes in either ANS-BSA binding affinity and/or ANS fluorescence enhancement.

INTRODUCTION

The adsorption of proteins at solid/liquid interfaces remains a subject of considerable interest [1,2]. The applications of protein adsorption can be found in different areas such as biotechnology, biosensing, food processing and drug-release pharmaceutics. In the field of biomedical engineering protein adsorption from body fluids is a major concern [1,3]. Protein–surface interactions play important roles in material blood-compatibility, soft contact lenses, and bacterial adhesion on prosthetic devices. Protein contact with artificially-made surfaces is considered to determine the biocompatibility and in vivo applica-

*To whom correspondence should be adressed.

0166-6622/88/$03.50

tions [4]. The adsorption of protein onto a surface is thought to induce conformational alterations in protein structure which produces biochemical interactions which are often undesirable. Due to the complexity of protein structure these conformational alterations remain the most elusive part of the adsorption process [5–8]. Are these changes large? Do they involve the protein tertiary structure or are they restricted to protein secondary structure? Proteins in solution are highly dynamic entities sampling constantly through a number of conformations, a characteristic which often makes particular protein function possible. Can adsorption of protein onto a surface constrain these dynamic fluctuations and thus change the protein's average conformation?

At the present time, different spectroscopic methods can be applied to protein adsorption at solid/liquid interfaces by using total internal reflection optics. In the case of two optically different phases (i.e. silica/aqueous solution) this optical effect produces an evanescent electromagnetic field in the optically less dense phase (aqueous solution). A total internal reflection counterpart of fluoresence spectroscopy, called TIRF (Total Internal Reflection Fluorescence), is becoming increasingly applied to biologically important processes at interfaces [1,4,9].

In this study the intrinsic fluorescence emission characteristics of silica-adsorbed bovine serum albumin (BSA), obtained by using TIRF, will be compared with BSA fluorescence emission from bulk solution. Furthermore, the fluorescence emission of the albumin-bound 1-anilinonaphthalene-8-sulfonate (ANS) will be used to probe binding sites changes in BSA upon its adsorption at silica surfaces. Intrinsic protein fluorescence is known to be sensitive to alterations in protein conformation [10,11]. ANS exhibits a large difference in this spectral characteristics depending on the local polarity of its environment [12]. By comparing the intrinsic BSA fluorescence with the fluorescence of BSA-bound ANS the conformational alterations of BSA upon adsorption will be correlated. In addition, red-edge excitation of the BSA-bound ANS in solution and at the interface is used to gain information about the relaxational changes of the ANS microenvironment upon BSA adsorption.

MATERIALS AND METHODS

Bovine serum albumin (monomer standard protein powder) was purchased from Miles Laboratories. 1-Anilinonaphthalene-8-sulfonate (bis-ANS free) was a product of Molecular Probes (Junction City, Oregon). All other chemicals were of analytical grade. Only freshly prepared solutions were used. The fluorescence emission spectra of adsorbed species were taken by a custom-built TIRF apparatus described previously [7,9]. The new TIRF cell is comprised of a truncated quartz hemicylinder (Harrick) coupled with a fused silica rectangular fluorescence cell equipped with flow lines (Fig. 1). In this way one of the fluorescence cell inner surfaces was used as the adsorbing surface. The

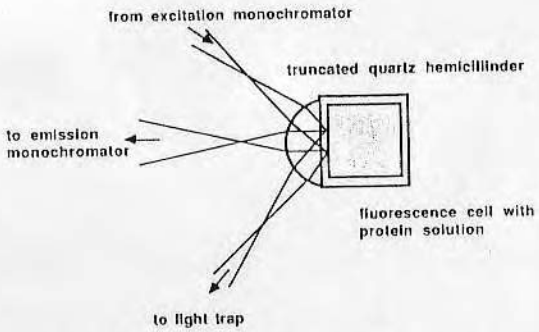

Fig. 1. Schematic illustration of TIRF cell geometry.

selective illumination of this interface was achieved by totally reflecting incident ultraviolet light (285 nm). Fluorescence emission was collected normal to the interface through the quartz hemicylinder. The TIRF cell set-up is given schematically in Fig. 1. Prior to each experiment all inner surfaces of the TIRF cell were rigorously cleaned according to the established procedure [13]. All experiments were carried out at room temperature (approximately 20°C).

The experimental procedures were as follows: the TIRF cell was primed with a buffer (0.01 *M* acetate, pH 5.0) and background emission was recorded. The buffer was replaced with buffered BSA solution which was allowed to contact the silica surface for one hour. At that time a second fluorescence spectrum was recorded. Nonadsorbed protein was than slowly flushed out of the cell with 40 ml of buffer solution (about 10 times the volume of the TIRF cell) under conditions which excluded the formation of a silica–air interface. Once the protein solution was replaced with the buffer, final emission spectra were taken. All spectra were recorded with 8 nm slit halfwidths in the excitation and emission monochromators. The incident light was perpendiculary polarized with respect to the incident plane; no polarizer was used in the emission light path. Spectra were not corrected for spectral sensitivity of the TIRF instrument. In the experiments where ANS was used, the experimental procedure was the same but all solutions contained $1 \cdot 10^{-5}$ *M* ANS. The red-edge excitation of the BSA-ANS complex in the solution was performed by use of front face geometry ($c_{ANS} = 5 \cdot 10^{-6}$ *M*, $c_{BSA} = 0.1$ mg ml^{-1}) and at the silica/aqueous solution interface by using TIRF. Vertical polarizers (perpendicular in the case of TIRF geometry) and 4 nm slit halfwidths were used in excitation and emission light paths. The incident light wavelength varied from 350 to 420 nm. The emission maxima were found after background fluorescence subtraction.

RESULTS

The fluoresence emission spectra of BSA adsorbed onto silica surface from

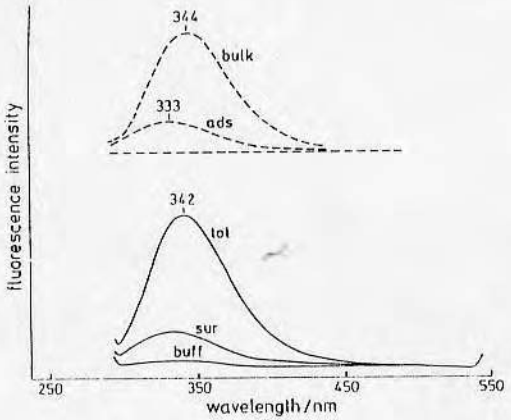

Fig. 2. Fluorescence emission spectra for the adsorption of 0.1 mg ml^{-1} BSA solution (in 0.01 *M* acetate buffer, pH 5.0). See text for explanation of spectra.

acetate buffer, without and with bound ANS, are given in Figs 2 and 3, respectively. Only the emission spectra from the experiments obtained with 0.1 mg ml^{-1} BSA are given. The spectra obtained with 0.05 and 1.0 mg ml^{-1} BSA showed essentially the same features. Each figure displays: (a) background fluorescence emission spectrum from the buffer-filled TIRF cell, marked buff (Fig. 3 also displays an additional spectrum obtained after the $1 \cdot 10^{-5}$ *M* ANS

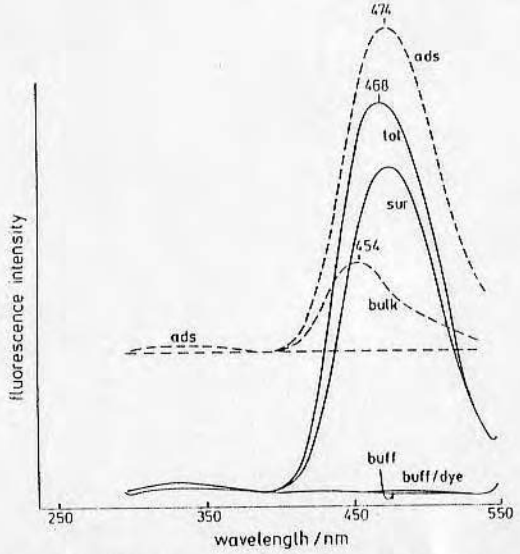

Fig. 3. The fluorecence emission spectra for the adsorption of 0.1 mg ml^{-1} BSA + $1 \cdot 10^{-5}$ *M* ANS solution (in 0.01 *M* acetate buffer, pH 5.0). See text for explanation of spectra.

solution in acetate buffer was injected into the clean TIRF cell, marked buff/dye), (b) fluorescence spectrum recorded after 1 h of protein–surface contact prior to the buffer flush-out, marked tot for total, (c) fluorescence spectrum taken approximately 10 min after the initiation of the solution protein flush-out, marked sur for surface, and (d) spectra given in dashed lines, marked bulk and ads obtained as difference between tot and sur, and sur and buff (in Fig. 3 buff-dye) spectra, respectively.

Intrinsic BSA fluorescence

The fluorescence spectra taken after 1 h contact between silica surface and BSA solution showed the intrinsic BSA fluorescence centered at 342 nm (tot, Fig. 2). After the nonadsorbed BSA has been removed from the cell the intensity of fluorescence decreased by 75% leaving a blue-shifted emission from irreversibly adsorbed BSA (sur, Fig. 2). The spectra ads and bulk show the contributions from irreversibly adsorbed BSA and BSA removed in the course of the flush-out process, respectively. Although there may be some loosely adsorbed BSA which was removed during the flush-out process, it is very likely that the spectrum bulk is largely due to nonadsorbed BSA. Its fluorescence emission is centered at 344 nm as is typical for BSA dissolved in aqueous solution. The emission maxima of fluorescence spectrum ads emitted by irreversibly adsorbed BSA is centered at 333 nm.

Albumin-bound ANS fluorescence

Figure 3 shows the emission spectra of BSA-bound ANS during the adsorption at silica surface. The background spectra buff and buff-dye coincided. The small difference in the region between 470 and 530 nm is probably contributed by free ANS molecules in solution which are exposed to the strong evanescent surface field. It is known that water is an excellent collisional quencher of ANS fluorescence [12]. No enhancement of ANS fluorescence, due to its contact with the negatively charged hydrophilic silica surface, was found as in the case of ANS interaction with hydrocarbon silane-modified silica surfaces [14].

The fluorescence spectra taken after 1 h contact between the silica surface and BSA with bound ANS showed two distinct regions: a shallow maximum in the ultraviolet (at ~330 nm) and a large peak in the visible part of the spectrum (at 468 nm) (tot, Fig. 3). The residual BSA fluorescence in the ultraviolet is very weak compared with the fluorescence of BSA-bound ANS in the visible. After the nonadsorbed material has been removed from the cell and replaced with the dye-buffer solution the fluorescence decreased in the visible region by ~10%, displaying a red-shifted emission from the irreversibly adsorbed BSA-ANS complex (sur, Fig. 3). Weak fluorescence in the ultraviolet remained unchanged by the flush-out. The subtracted spectra ads and bulk

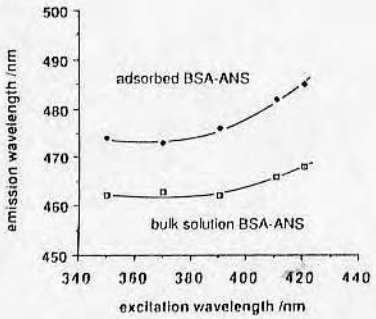

Fig. 4. The excitation red shifts for BSA-bound ANS in the buffer solution and at the silica/electrolyte interface.

in Fig. 3 show contributions from irreversibly adsorbed BSA-ANS and BSA-ANS molecules removed in the course of the flush-out process, respectively. Emission from the irreversibly adsorbed protein is centered at 474 nm as compared with the bulk contribution maximum found at 454 nm.

Emission maxima of BSA-bound ANS observed at various excitation wavelengths are shown in Fig. 4. The maxima in ANS fluorescence from the BSA-ANS complex in the solution shift from 462 to 468 nm as the excitation wavelength is increased from 350 to 420 nm. Upon BSA adsorption onto the silica surface, the ANS emission maxima emitted from the irreversibly adsorbed BSA-ANS complex shifts from 474 to 485 nm in the same excitation range.

DISCUSSION

A comparison of the spectra obtained by using BSA without and with bound ANS (Figs 2 and 3) and BSA-ANS red-edge excitation data (Fig. 4) shows: (a) different fluorescence spectral characteristics of BSA and BSA-bound ANS upon adsorption. (b) different fluorescence red-edge shifts of BSA-bound ANS upon adsorption, and (c) different fluorescence intensity ratios between the contributions from removed versus adsorbed protein in the case of intrinsic BSA fluorescence and BSA-bound ANS fluorescence, respectively.

These differences will be discussed in the same order.

Spectral characteristics

The emission maxima of BSA fluorescence spectrum bulk (Fig. 2) was found at 344 nm as typical for BSA in solution, while the spectrum ads emitted by irreversibly adsorbed BSA was centered at 333 nm. These spectral characteristics of bulk and ads spectra are similar to the typical class II protein fluorescence emission (with maximum at 340–342 nm and a band width of 53–55 nm) from tryptophan surface residues surrounded by bonded water dipoles with low

mobility and to the class I emission (with maximum at 330–332 nm and a band width of 48–50 nm) from tryptophan residues in a nonpolar environment, respectively [10]. Consequently, the emission maxima change of −11 nm in Fig. 2 is an evidence of some conformational changes in BSA molecules upon the adsorption. Adsorption onto a hydrophilic silica surface causes the BSA molecules to "hide" their tryptophans in the nonpolar pocket opposite to heat-denatured BSA in solution, where the fluorescence maximum shifts to 350 nm upon disruption of the secondary and tertiary structure. Thus the protein at the interface is far from being completely unfolded. Conformational changes of silica-adsorbed BSA, which involve the environments of BSA tryptophans, were deduced from a decrease in BSA fluorescence quantum yield [7] and from shorter fluorescence lifetimes [8]. It is quite possible that the blue-shifted emission found in this study and the latter two effects are interconnected. Often, the longer-lived fluorescence is found on the red side of emission, as in human serum albumin [15,16]. If the silica surface affects primarily longer-lived fluorescence it may effectively shift the emission towards shorter wavelength and decrease the quantum yield. The fluorescence of BSA is emitted by two tryptophans situated in positions 134 and 212 in the polypeptide chain in subdomains 1-C and 2-AB, respectively. Their exposure to solvent was a topic of controversy. On the basis of fluorescence quenching it was concluded that one tryptophan is within 1.4 nm from the BSA surface while the other is at the center of the BSA interior [17]. However, other authors concluded that both tryptophans are at the BSA surface but have only limited contact with the solvent [18]. In other proteins with two tryptophans, like 3-phosphoglycerate kinase, their spectral contributions and lifetimes have been separated and assigned to a particular residue [19]. In the case of BSA such information was not available so that the possibility of long-wave tryptophan emission being quenched upon adsorption remains hypothetical. The possible changes due to energy transfer from tyrosine residues to tryptophans upon BSA adsorption was ruled out since the blue-shifted fluorescence of the adsorbed BSA was also found at excitation wavelength of 295 nm [9].

The emission of adsorbed BSA-bound ANS showed a red-shift of +12 nm (Fig. 4)*. In the terms of polarity change this is equivalent to a change of solvent polarity from butanol to ethanol [12]. The red-shift of bound-ANS emission is in contrast to the blue-shifted intrinsic emission from the two BSA tryptophans (Fig. 3). Different spectral shift directions indicate different local conformational changes taking place in the close vicinity of the tryptophans and the bound ANS molecules, respectively. At the concentrations used here (0.1 mg ml^{-1} BSA, $1 \cdot 10^{-5}$ *M* ANS), the bulk solution BSA-ANS complex

*As compared with the 454 nm bulk contribution maximum in Fig. 3 the maximum of BSA-ANS complex in the solution was found to be at 462 nm (excited with 285 nm) which was taken as a more reliable value in agreement with the literature [21].

contribution to the fluorescence from the adsorbed layer because the thickness of the adsorbed layer is negligible compared with the thickness of the TIRF cell.

It was found that the contribution from intrinsic fluorescence emitted by irreversibly adsorbed protein is only a small fraction (0.25) of the bulk contribution (Fig. 2), while the fluorescence intensity of the adsorbed protein/dye complex exceeds the bulk contribution almost by factor of 4 (Fig. 3). This brings the intensity ratio between the fluorescence contributions from removed versus adsorbed species to a range from 4 (intrinsic BSA fluorescence) to 0.27 (bound-ANS fluorescence). Different extent of parasitic scattering can provide only a partial explanation for this difference (i.e. more scattered light will increase the contribution to the bulk spectra but will not influence the ads spectra). No rigorous quantitation of scatter has been performed in this study. In 0.1 mg ml^{-1} BSA solution, the free ANS concentration will decrease by some 50% due to its binding to BSA. In this case, by putting the adsorbed BSA (which is only a tiny fraction of total BSA) in contact with a new $1 \cdot 10^{-5}$ *M* ANS solution in buffer will induce more ANS binding to the adsorbed BSA. Although this can also account for a part of the fluorescence ratio mismatch, the experiments done with smaller BSA concentration showed a similar effect. Assuming that the binding of ANS to the BSA does not increase the adsorbed amount of BSA there are several possible explanations for the ratio mismatch: (1) affinity for ANS increases upon BSA adsorption leading to the additional ANS binding to the adsorbed BSA; and/or (2) more than four bound ANS molecules become strongly fluorescent upon BSA adsorption, (3) adsorbed BSA fluorescence quantum yield has been overestimated. Which of these possible effects is responsible for the different fluorescence intensity ratio remains to be determined by future quantitative ANS-adsorbed BSA binding experiments.

CONCLUSION

The adsorption of BSA onto the hydrophilic silica surface produces conformational changes in the protein molecule as evidenced from a blue-shifted intrinsic emission of adsorbed BSA and red-shifted emission of BSA-bound fluorescent probe ANS. Different spectral shifts indicate that different conformational alterations are taking place in the close vicinity of tryptophans and bound ANS molecules upon the adsorption. While the microenvironment of the two BSA tryptophans becomes less polar, the ANS fluorophore emission indicates an increase in their binding site polarity. Less efficient quenching of tryptophan fluorescence by bound ANS also indicates conformational alterations. It is concluded that the conformational changes caused by the irreversible adsorption of BSA onto hydrophilic silica surface involve the whole BSA molecule. These conformational changes are not similar to the unfolding of the

BSA polypeptide chain caused by heating. The red-edge excitation indicates a slower spectral relaxation of the ANS binding site portions of irreversible adsorbed BSA. Possibly, the constrained dynamics is experienced by the whole adsorbed protein due to the influence of the adsorption forces. The fluorescence intensity contribution from adsorbed species (BSA versus BSA-ANS) suggest some changes in either binding affinity and/or ANS fluorescence enhancement.

ACKNOWLEDGEMENTS

The financial help from Center for Biopolymers at Interfaces, University of Utah and Selfmanagement Council for Scientific Research of Croatia is gratefully acknowledged.

REFERENCES

1 J.D. Andrade (Ed.), Surface and Interfacial Aspects of Biomedical Polymers, Vol. 2, Protein Adsorption, Plenum, New York, 1986.
2 W. Norde, Adv. Colloid Interface Sci., 24 (1986) 267-340.
3 S.L. Cooper and N.A. Peppas (Eds), Biomaterials: Interfacial Phenomena and Applications, American Chemical Society, Washington, 1982.
4 J.D. Andrade and V. Hlady, Adv. Polym. Sci., 79 (1986) 1-65.
5 A.G. Walton and F.C. Maenpa, J. Colloid Interface. Sci., 72 (1979) 265-278.
6 C.H. Lochmüller and S.S. Saavedra, Langmuir, 3 (1987) 435-437.
7 V. Hlady, D.R. Reinecke and J.D. Andrade, J. Colloid Interface Sci., 111 (1986) 555-569.
8 M.R. Rainbow, S. Atherton, R.C. Eberhart, J. Biomed. Mat. Res., 21 (1987) 539-555.
9 V. Hlady, R.A. Van Wagenen and J.D. Andrade, in J.D. Andrade (Ed.), Surface and Interfacial Aspects of Biomedical Polymers, Vol. 2, Protein Adsorption, Plenum, New York, 1985, pp. 81-119.
10 A.P. Demchenko, Ultraviolet Spectroscopy of Proteins, Springer-Verlag, Berlin, 1986.
11 J.R. Lakowicz, Principles of Fluorescence Spectroscopy, Plenum, New York, 1983.
12 L.S. Stryer, J. Mol. Biol., 13 (1965) 432-445.
13 R.A. Van Wagenen, S.A. Rockhold and J.D. Andrade, Adv. Chem. Ser., 199 (1982) 351-369.
14 S.D. Dowling and W.R. Seitz, Anal. Chem., 57 (1985) 602-605.
15 J.R. Lakowicz and H. Cherek, J. Biol. Chem., 255 (1980) 831-834.
16 A. Greenwald and I.Z. Steinberg, Biochemistry, 13 (1974) 5170-5178.
17 C.K. Luk, Biopolymers, 10 (1971) 1229-1241.
18 E.A. Burstein, N.S. Vedenkina and M.N. Ivkova, Photochem. Photobiol., 18 (1973) 263-279.
19 J.P. Privat, P. Wahl, J.C. Auchet and R.H. Pain, Biophys. Chem., 11 (1980) 239-248.
20 H. Terada, K. Hiramatsu and K. Aoki, Biochim. Biophys. Acta, 622 (1980) 161-170.
21 E. Daniel and G. Weber, Biochemistry, 5 (1966) 1893-1900.
22 S.R. Anderson and G. Weber, Biochemistry, 8 (1969) 371-377.
23 E. Daniel and G. Weber. Biochemistry, 5 (1966) 1900-1907.
24 D.A. Kolb and G. Weber, Biochemistry, 14 (1975) 4476-4481.
25 J.R. Lakowicz and S. Keating-Nakamoto, Biochemistry, 23 (1984) 3013-3021.

Hlady – 3

Colloids and Surfaces, 34 (1988/89) 171–183
Elsevier Science Publishers B.V., Amsterdam — Printed in The Netherlands

Fluorescence of Adsorbed Protein Layers. II. Adsorption of Human Lipoproteins Studied by Total Internal Reflection Intrinsic Fluorescence

V. HLADY[1,2,*], J. RICKEL[1] and J.D. ANDRADE[1]

[1]*Department of Bioengineering, University of Utah, Salt Lake City, UT 84112 (U.S.A.)*
[2]*"Ruder Bošković" Institute, P.O. Box 1016, 41000, Zagreb, Croatia (Yugoslavia)*

(Received 2 February 1988; accepted in final form 27 June 1988)

ABSTRACT

The total internal reflection intrinsic fluorescence (TIRIF) method was applied to the study of adsorption of intact human lipoproteins. High (HDL) and low (LDL) density lipoproteins were adsorbed separately on two model surfaces: hydrophilic and hydrophobic silica. The adsorption of the two lipoproteins on the two surfaces was different. The lipoprotein adsorption on the hydrophilic surface can be described quantitatively using the transport-limited adsorption model and assuming that the lipoprotein fluorescence quantum yield decrease upon adsorption is constant. The latter was caused by the interactions between the exposed lipoprotein tryptophanyl residues and the surface. The fluorescence emission maximum shift supported this conclusion. The hydrophobic silica surface induced different and probably larger changes in lipoprotein conformation than the hydrophilic silica surface. In the case of HDL adsorption onto the hydrophobic silica surface the adsorption maximum and the subsequent adsorption decrease found in the mid-course of the adsorption indicate preferential surface accumulation of the HDL apo A-II protein.

INTRODUCTION

Plasma lipoproteins are lipid–protein complexes responsible for the transport of water-insoluble lipids in the circulation. The presently accepted structure of these complex aggregates pictures them as an apolar core surrounded by polar and amphiphilic components [1–3]. Triglycerides and cholesterol esters are the major components of the lipophilic core, while free cholesterol, phospholipids, and proteins (known as apolipoproteins) provide a barrier between the aqueous medium and the hydrophobic region [3,4]. Two of the main classes of lipoproteins, low density lipoprotein (LDL) and high density lipoprotein (HDL), have been implicated in atherogenesis. HDL has been found to play a protective role while LDL, as the major vehicle for the transport of

*To whom correspondence should be addressed.

0166-6622/88/$03.50

plasma cholesterol in man [5], is thought to contribute to atherosclerotic plaque formation [6].

Lipoproteins can form deposits on man-made surfaces [7–11]. HDL adsorbs preferentially from plasma onto polyvinyl chloride and polystyrene surfaces; its adsorption causes lower adsorption of albumin, fibrinogen and immunoglobulin from plasma [7]. Adsorption of LDL produced less inhibition of other plasma protein adsorption in comparison to HDL [8]. ^{125}I-labeled LDL binds with high affinity to glass beads at physiologic pH and ionic strength [9,10]. ^{125}I-LDL adsorption is lower on silicone-treated glass than on untreated glass [9]. It was shown that ^{125}I-LDL adsorption on glass is not influenced greatly with temperature [11]. Biomer (a commercial polyetherurethane) and poly(dimethylsiloxane) adsorb less ^{125}I-LDL than glass at 25°C; however, at 37°C the situation is reversed [11]. Apo A-II, one of the two major apolipoproteins in HDL, is lost from a solution of intact HDL upon contact with the surface of hydrophobic glass beads [12].

In this study we compare the adsorption of human HDL and LDL on hydrophilic and hydrophobic silica surfaces, respectively. Particular attention is directed towards the initial stage of adsorption. The analysis of the initial part of protein adsorption poses practical problems, as the analytical methods for detection of surface protein often disturb the adsorption process. A surface-sensitive spectroscopic method like total internal reflection fluorescence (TIRF) [13] is suitable for the study of protein adsorption. In the present adsorption study we chose to follow the intrinsic protein fluorescence (hence, the name of the method: total internal reflection intrinsic fluorescence [TIRIF]). A general quantitation method for the TIRIF protein adsorption experiments, which gives the amount of adsorbed protein, is available [14,15]. However, the method does not account for eventual fluorescence quantum yield change upon adsorption. The TIRIF-measured protein surface concentration will be identical to actual protein surface concentration only if the fluorescence quantum yield remains unchanged. This is an apparent disadvantage of the TIRIF method as compared to the straightforward determination of the amount of adsorbed protein. However, it should be noted that intrinsic protein fluorescence is a sensitive probe for examining protein conformation. Therefore, any difference between the TIRIF-measured adsorbed amount and actual adsorbed amount, which can be determined by other methods, is a measure of protein conformational change which takes place upon adsorption [15]. Essentially the same conclusions can be derived from the difference between the TIRIF-measured initial adsorption rate and the initial adsorption rate as predicted by appropriate model calculations. The latter approach is used in this work: the initial lipoprotein adsorption rate onto two types of surfaces is compared with the initial adsorption rate predicted by the transport-limited case of a convection/diffusion protein adsorption model [16]. On the basis of this comparison the lipoprotein conformation on the two surfaces is inferred.

EXPERIMENTAL

Materials

5-Hydroxytryptophan methyl ester hydrochloride (TrpOH, Calbiochem) was used as an external fluorescence standard. Lipoproteins were isolated by sequential flotation [17,18] with the density adjusted to 1.030–1.063 g ml^{-1} for LDL and 1.063–1.230 g ml^{-1} for HDL, respectively. Protein content of the lipoprotein fractions was determined by the Lowry method modified to reduce interfering lipid cloudiness [19]. All lipoprotein concentrations were recalculated from the protein content into mass of intact lipoprotein per volume or per surface area assuming 20% apoprotein in LDL and 50% apoprotein in HDL, respectively [3]. Hydrophilic silica slides were prepared as described elsewhere [20]. Silanized hydrophobic surfaces were prepared by immersion of clean silica slides in a freshly prepared dry toluene solution containing 10% dimethyldichlorosilane (DDS) for 10 min. Surfaces were then rinsed three times in ethanol followed by a distilled water rinse and a final ethanol rinse. After drying in air, DDS slides were cured for 3 hours at 80°C under nitrogen. All surfaces were used within 48 hours.

Methods

A typical TIRIF data profile is shown in Fig. 1: the introduction of protein solution into the TIRIF cell causes an increase of fluorescence intensity due to protein adsorption. After a given period of protein interfacial residence time, the protein solution of concentration c_p is replaced with the buffer solution. An immediate decrease of fluorescence intensity follows because the nonadsorbed proteins present in the volume penetrated by the evanescent surface wave are flushed out of the cell. Thus, in principle, both the fluorescence intensity emitted from adsorbed proteins, N_a, and from nonadsorbed proteins in the volume penetrated by the evanescent surface wave, N_b, (the subscripts a and b denote the adsorbed state and the bulk solution state, respectively) are

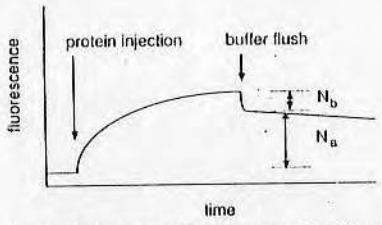

Fig. 1. Typical TIRIF data output in a lipoprotein adsorption experiment. The fluorescence was excited at 280 nm and collected at 335 nm. See text for explanation of symbols used.

experimentally accessible. Both parameters can be used to find the volume concentration of protein, A_{vol}, in the adsorbed layer of thickness Δ:

$$N_a/N_b = (A_{vol}/c_p)\cdot(F_a/F_b)\cdot(1-e^{-2\Delta/d_p}) \quad (1)$$

where F's are respective protein fluorescence quantum yields and d_p is the depth of penetration of the evanescent wave [14,15]. The unknown thickness of the adsorbed layer, Δ, can be estimated from protein molecular dimensions. The protein surface concentration, A (mass/area) equals $A_{vol}\cdot\Delta$, and does not depend critically on the choice of Δ, as long as Δ is small, since for small Δ, $(1-e^{-2\Delta/d_p}) \approx 2\Delta/d_p$. The experimental parameter c_p/N_b can be used as an internal fluorescence standard so that the TIRIF-measured adsorption, $A\cdot(F_a/F_b)$, (in mass per area units) equals:

$$A\cdot(F_a/F_b) = (c_p/N_b)\cdot N_a\cdot(d_p/2) \quad (2)$$

Although the reflection in TIRIF experiments is total, there is always a fraction of excitation light generated by scattering from imperfections in the optical components of the TIRIF cell. This light propagates through the TIRIF cell far beyond the interface and excites the fluorescence from protein molecules outside the evanescent wave volume. Experimentally, fluorescence is observed from the whole depth of the TIRIF cell so that the "scatter"-excited fluorescence contributes mainly to measured N_b due to the fact that $A_{vol}\cdot\Delta \ll c_p\cdot b$ (b is the thickness of the flow cell). In this work the "scatter"-excited contribution to N_b was accounted for by using a series of external standards in situ prior to the protein adsorption experiment, as described previously [15].

Experimental adsorption procedure

The lipoprotein adsorption experiments were performed using a custom-built TIRIF apparatus and TIRIF flow cell described elsewhere [14,15]. An elliptical TIRIF flow chamber was used (0.05×2×7 cm). All TIRIF experiments were carried out at room temperature, approximately 18°C. Adsorption was followed from phosphate buffers; either from 0.05 *M* phosphate buffer (PBS, 0.05 *M* phosphate, 0.145 *M* NaCl, pH 7.4) or from Dulbecco phosphate buffer (DPBS, 0.05 *M* phosphate, 0.147 *M* NaCl, 0.90 m*M* $CaCl_2$, 0.88 m*M* $MgCl_2$, 2.7 m*M* KCl, pH 7.4). Fluorescence was excited at 280 nm and collected at 335 nm from a 2 mm by 8 mm area situated in the middle of the flow cell. The half-bandwidth of the monochromators was 16 nm.

Adsorption was followed in a "single-shot" manner, i.e. each surface was exposed to a lipoprotein solution only once. Before any contact between the lipoprotein and the surface took place, a range of TrpOH solutions was sequentially injected into the TIRIF flow cell and the fluorescence intensity was measured. The calibration plots thus generated for each surface provided necessary normalization data for the adsorption results. A typical calibration plot

is shown in Fig. 2 (upper panel). After the cell had been washed with buffer and fluorescence had returned to its background level, a lipoprotein sample was injected into the TIRIF cell at a flow rate of approximately 0.5 ml min^{-1} and allowed to adsorb under constant flow conditions. After 30 minutes of adsorption, N_b was determined by flushing out nonadsorbed material from the TIRIF cell with 20 ml of buffer (within 10 s) and the fluorescence emission maximum was located. The parameter N_b was corrected for its "scatter"-excited part* (Fig. 2). In the same TIRIF cell the ratio between the "scatter"-excited and the evanescent wave-excited fluorescence is equal at given solution absorbances of internal and external standards [15]. $A\cdot(F_a/F_b)$ was then calculated from Eqn (2). Although repeated adsorption experiments often showed different levels of fluorescence signals, this quantitation procedure resulted in reproducible adsorption values.

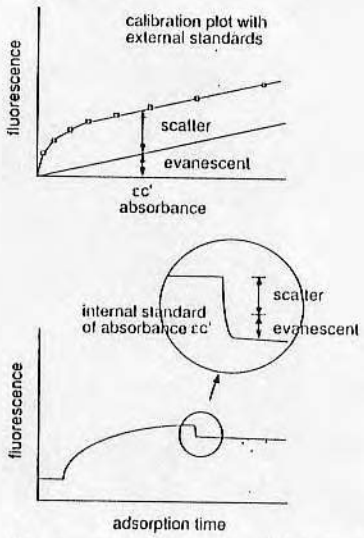

Fig. 2. Procedure used in the quantitation of TIRIF data: a calibration plot generated with external standards (upper panel); TIRIF adsorption data (lower panel) including an internal standard: a lipoprotein solution flush-out (magnified). The internal standard has the absorbance, $\varepsilon c'$, which is also indicated in the upper panel.

*Each calibration plot also contains information about the relative efficiency of illumination of the interface by the evanescent surface wave and collection of the fluorescence from the interface, so-called overall TIRIF sensitivity. The latter can be estimated from the slope of the straight line named "evanescent" in Fig. 2. Generally, overall TIRIF sensitivity was found to be dependent on various experimental parameters such as optical alignment of the TIRIF cell, the particular silica plate used, and UV-lamp output.

RESULTS

The course of lipoprotein adsorption with time is summarized in Figs 3 and 4. The time zero of the adsorption kinetics was defined as the moment when the flow of lipoprotein solution into the TIRIF cell was initiated. The initial flat part corresponds to the time needed for the lipoprotein solution to flow through the connecting tubing to the observation spot in the TIRIF flow cell. When the lipoprotein solution reaches this spot, the adsorption becomes apparent; the increase in the adsorbed amount is faster in the case of the higher lipoprotein concentrations. In the case of adsorption on hydrophilic silica the

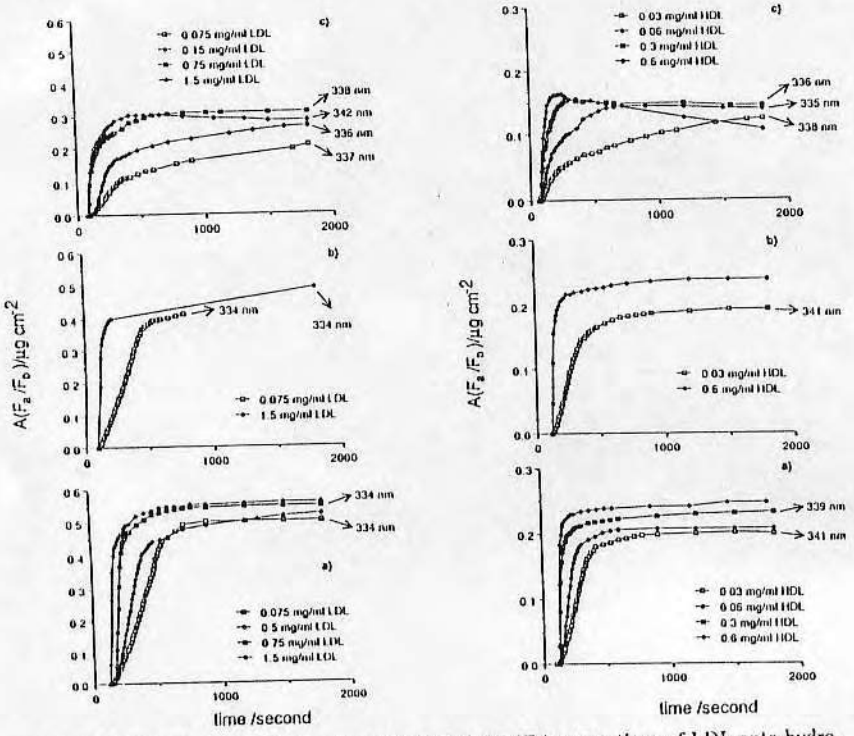

Fig. 3. (left) TIRIF-measured adsorption kinetics, $A\cdot(F_a/F_b)$ versus time, of LDL onto hydrophilic silica from PBS (a) and from DPBS (b), and onto hydrophobic silica from PBS (c). The numbers indicate the location of the fluorescence spectra maximum.

Fig. 4. (right) TIRIF-measured adsorption kinetics, $A\cdot(F_a/F_b)$ versus time, of HDL onto hydrophilic silica from PBS (a) and from DPBS (b), and onto hydrophilic silica from PBS (c). The numbers indicate the location of the fluorescence spectra maximum.

increase is followed by a leveling-off of the adsorption curve. The initial lipoprotein adsorption from DPBS buffer (Figs 3b and 4b) fully coincided with the adsorption from PBS. The lipoprotein adsorption kinetics onto hydrophobic silica showed different characteristics: the adsorption from 0.06 mg ml^{-1} HDL solution showed a flat maximum after 13 minutes of adsorption time while the adsorption from 0.3 and 0.6 mg ml^{-1} HDL solution passed through a maximum in the 5th and 2nd minute of adsorption time, respectively (Fig. 4c). The LDL adsorption on the hydrophobic silica showed a flat maximum only at $c_{LDL}=1.5$ mg ml^{-1} (5th minute) (Fig. 3c). The maxima of fluorescence emission where available are indicated in Figs 3 and 4. The corresponding values measured in the bulk PBS solution were 337 nm (LDL) and 339 nm (HDL), respectively.

The highest 30-minute TIRIF-measured lipoprotein adsorption values, $A\cdot(F_a/F_b)$, are given in Table 1. The TIRIF-measured adsorption of LDL exceeded the adsorption of HDL on both surfaces and from both buffers by a factor of two. Table 1 also gives the adsorbed mass of LDL and HDL monolayer adsorption calculated on the basis of their respective molecular dimensions.

Figures 5 and 6 give a magnified view of initial lipoprotein adsorption from the solution of 0.075 mg ml^{-1} LDL and 0.03 mg ml^{-1} HDL, respectively. The same figures also show the lipoprotein adsorption, A_f, as a function of time (in straight lines) as predicted by the transport-limited case of a convection/diffusion model [16]:

$$dA_f/dt = (\Gamma(4/3))^{-1}\, 9^{-1/3}\, (6q/b^2wlD)^{1/3}\, Dc_p \qquad (3)$$

where dA_f/dt is the protein flux to the surface, Γ is the gamma function, q is the experimental volumetric flow rate, b is the thickness of the TIRIF flow cell

TABLE 1

The highest 30-minute TIRIF-measured lipoprotein adsorption values, $A\cdot(F_a/F_b)$. The numbers given in parenthesis refer to the equivalent mass of apolipoprotein; all values are given in $\mu g\ cm^{-2}$ units. Monolayer adsorption refers to the mass of lipoprotein molecules which can be packed in one layer on the unit surface. Monolayer adsorption was calculated from the lipoprotein average molecular weights ($M.W._{LDL}=2.5\cdot10^6$, $M.W._{HDL}=2.0\cdot10^5$), the lipoprotein radii ($r_{LDL}=11$ nm, $r_{HDL}=4.5$ nm) [3,25] assuming that the surface packing efficiency is 0.7

		PBS	DPBS
Hydrophilic silica	LDL	0.56(0.11)	0.49(0.09)
	HDL	0.25(0.12)	0.24(0.12)
DDS silica	LDL	0.31(0.06)	–
	HDL	0.14(0.07)	–
Monolayer adsorption	LDL	0.76(0.15)	
	HDL	0.36(0.18)	

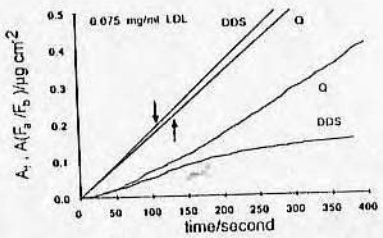

Fig. 5. (left) TIRIF-measured initial lipoprotein adsorption kinetics from 0.075 mg ml^{-1} LDL solution on the hydrophilic and hydrophobic silica surfaces (Q and DDS, respectively). The model LDL adsorption is given by straight lines. The arrows indicate the completion of the development of a steady-state LDL concentration boundary layer.

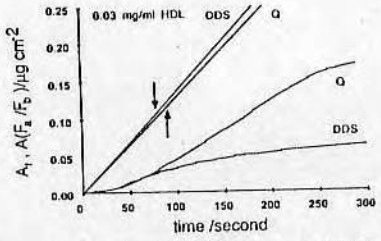

Fig. 6. (right) TIRIF-measured initial lipoprotein adsorption kinetics from 0.03 mg ml^{-1} HDL solution on the hydrophilic and hydrophobic silica surfaces (Q and DDS, respectively). The model HDL adsorption is given by straight lines. The arrows indicate the completion of the development of a steady-state HDL concentration boundary layer.

(b=0.05 cm), w is the width of the cell (w=2 cm), l is the distance from the entrance of the flow chamber to the slit-like observation spot (l=3.5 cm) and D is the lipoprotein diffusion coefficient ($D_{LDL}=1.8\cdot10^{-7}$ cm^2 s^{-1}, $D_{HDL}=4.7\cdot10^{-7}$ cm^2 s^{-1}). The small differences in the A_f versus time slopes are due to differences between the experimental flow rates. Actual rates (in cm^3 min^{-1}) were as follows: 0.48 (HDL/Q), 0.57 (HDL/DDS and LDL/DDS), 0.46 (LDL/Q). Experimental adsorption data in Figs 5 and 6 are time-shifted to match the first apparent adsorption with the time zero. The time needed for development of a steady-state lipoprotein concentration boundary layer at the interface [16] is indicated by the arrows in Figs 5 and 6.

DISCUSSION

In this work the quantitative TIRIF method was applied to the study of lipoprotein adsorption onto two model surfaces. Lipoproteins fluoresce in the ultraviolet due to the presence of tyrosine and tryptophan amino acids in their structure. Tryptophan is the most efficient protein fluorophor and its emission is dependent on the polarity of its environment. A change in protein fluorescence characteristics is, therefore, a sensitive measure of protein conformational change which involves a tryptophanyl residue(s) environment. In this discussion we will compare the initial TIRIF-measured adsorption rate of lipoproteins with the adsorption rates calculated by the appropriate model [16] and assume that the experimental and the model adsorption differ as a result of the change in the fluorescence quantum yield. Together with the analysis of

fluorescence emission maxima, such a comparison will indicate the extent of lipoprotein conformational change on each of the two model surfaces.

Figures 3 and 4 show that as the lipoprotein solution concentration is increased, the initial adsorption rate is higher. Also, at higher lipoprotein solution concentrations the adsorption levels off earlier. In the case of hydrophobic silica the adsorption kinetics curves sometimes display a maximum after which the adsorption decreases.

Figures 5 and 6 show that the initial adsorption rate increases gradually as the steady-state concentration boundary layer develops*. Two different characteristics of initial adsorption can be recognized:

(a) In the case of hydrophilic silica; after the steady-state concentration boundary layer is completely formed (indicated by the arrows in Figs 5 and 6) the experimental adsorption curves are linear with time, as predicted [16].

(b) In the case of hydrophobic silica; the linear parts are not well-resolved and the TIRIF-measured adsorption starts to level off even before the steady-state transport conditions are reached.

Hydrophilic silica surface

The experimental adsorption rates from 0.075 mg ml^{-1} LDL and 0.03 mg ml^{-1} HDL PBS solutions (as determined from the slope of the linear parts of the experimental adsorption curves in Figs 5 and 6) amount to 0.75 and 0.63 of the respective adsorption rates calculated by Eqn (3). In the case of adsorption from 0.15 mg ml^{-1} LDL and 0.06 mg ml^{-1} HDL PBS solutions (data not shown here) the same comparison gives the similar results. We conclude that because of the contact with the hydrophilic silica surface the lipoprotein fluorescence quantum yield has decreased by approximately 25% (LDL) and 37% (HDL), respectively. Lipoprotein quenching experiments in solution have shown that the tryptophanyl residues in lipoproteins are more embedded in the hydrophobic core in LDL than in HDL [21]. Hence, less overall quenching of LDL (as compared with HDL) can be expected upon contact with the surface. The lipoprotein fluorescence quantum yield decrease is further supported by the experimentally determined lipoprotein adsorption maxima which were measured after 30 minutes of adsorption (Table 1). They amount to 0.74 (LDL from PBS) and 0.69 (HDL from PBS) of the respective monolayer adsorption values. If the corrected quantum yield, i.e. $F_a/F_b=0.75$ (LDL), $F_a/F_b=0.63$ (HDL), is used in Eqn (2) to calculate lipoprotein adsorption, the initial adsorption rates determined by TIRIF experiments (both from PBS and DPBS

*Another possible cause for the gradual increase may be the elliptical shape of the TIRIF chamber, in which case there would be an initial concentration delay at the upper and lower side of the slit-like observation spot resulting in a lower overall adsorption. No allowances were made for this effect.

buffer) will coincide with the model calculated by Eqn (3). Note, that the experimental and the model adsorption rate do not match beyond the initial stage of the adsorption process. This is because Eqn (3), when applied to the adsorption process, implies that the surface acts as a protein sink, which is valid only in the early adsorption times. The corrected quantum yields will also make an exact match between the lipoprotein adsorption plateaus (measured from PBS) and the monolayer adsorption. The same is valid in the case of HDL adsorption from DPBS. Only in the case of LDL adsorption from DPBS buffer will the lipoprotein adsorption plateau be lower then the monolayer adsorption. Apparently, divalent ions from DPBS only influence the fully formed LDL adsorption layer and not the initial LDL surface deposition.

The fluorescence emission maximum of LDL shifts from 337 (solution) to 334 nm (hydrophilic silica), which indicates that the majority of the tryptophanyl residues emit from a less polar environment (Fig. 3a, b). Apparently, the emission from the LDL tryptophanyl residues buried in the hydrophobic LDL core is not influenced by the adsorption and only the exposed tryptophanyl residues are quenched. The net result is 25% less fluorescence intensity with the emission shifted toward the shorter wavelengths; an indication that conformational change is not too large and involves only the outer parts of the LDL molecule. A combination of decreased fluorescence quantum yield and blue-shifted fluorescence of adsorbed protein is not uncommon [22]. Since the HDL tryptophanyl residues are less buried in the hydrophobic core than in the case of LDL, the HDL adsorption should lead to somewhat larger but uniform quenching of the whole HDL fluorophore population. Indeed, this is found experimentally (Fig. 4a, b): the fluorescence efficiency decrease by 37% and the HDL emission maxima increase slightly, or do not change significantly, upon adsorption on the hydrophilic surface.

Hydrophobic silica surface

The TIRIF-measured adsorption of LDL and HDL on the hydrophobic silica surface is more complex to interpret. The adsorption kinetics curves display maxima (Figs 3c and 4c), which are more pronounced in the case of higher HDL concentrations. Also, the initial adsorption data do not show well-resolved linear parts. The initial rates are well below the model calculations (Figs 5 and 6). It can be seen that the fluorescence quantum yield decrease is not constant during the early adsorption period. Adsorption of lipoproteins on hydrophobic surface may proceed via hydrophobic interactions. They are known to be involved in many protein–surface interactions [23] and could cause a larger lipoprotein conformational change. The apolipoprotein amphipathic helix, for example, is oriented with its hydrophilic face towards the solution and with its hydrophobic face towards the lipid core [24]. Interactions with the hydrophobic surface may reorient the helix and smear the lipoprotein aggregate over the surface. In this case the lipoprotein molecule will occupy a larger area and overall adsorption will be lower.

There is some evidence of a possible change in the composition of adsorbed HDL. The maximum found in the case of HDL adsorption and the subsequent adsorption decrease (Fig. 4c) suggest a preferential accumulation of some less fluorescent HDL component on the surface. It is known that one of the HDL apolipoproteins, apo A-II, is lost from a solution intact HDL upon contact with the surface of hydrophobic glass beads. The remaining lipoprotein particles in the solution had a higher molecular mass and a smaller density than the intact HDL [12]. Apo A-II has no tryptophans in its polypeptide chain [3]. Hence, it will not be detected by methods based on intrinsic protein fluorescence. However, its preferential accumulation on the surface will be indirectly "seen" by the TIRIF method as an adsorption decrease (Fig. 4c). The preferential apo A-II adsorption should be dependent on its solution concentration, i.e. on the HDL concentration in solution. This is, indeed, found: in the case of the lowest HDL concentration no maximum is reached and the adsorption is still increasing after 30 minutes. At higher HDL concentration the maximum does become apparent and in the case of the highest HDL concentrations the adsorption decrease following the maximum is at its largest (Fig. 4c). The fluorescence maximum of adsorbed HDL decreases with increasing HDL solution concentration: from 339 (bulk solution) to 338, 336 and 335 nm in the case of adsorption from 0.03, 0.06 and 0.3 mg ml^{-1} HDL solutions, respectively (Fig. 4c). With respect to the uniformly exposed HDL tryptophanyl residues it appears that the residues become less exposed to polar surroundings as the surface apo A-II concentration increases.

The position of the LDL fluorescence maximum (337 nm) is not sensitive to the hydrophobic surface adsorption (Fig. 3c), because the majority of tryptophanyl LDL residues are buried. The exception is in the case where LDL is adsorbed from the solution of 1.5 mg ml^{-1} LDL: the fluorescence is red-shifted (342 nm) and, moreover, a flat maximum is found at the 5th minute of adsorption time (Fig. 3c').

The quantitation of TIRIF protein adsorption allows only for a change in fluorescence efficiency and assumes that the same species are present in the bulk solution and at the interface. Any changes in the adsorbed lipoprotein composition will result in an error in the TIRIF quantitation. Therefore, the lipoprotein adsorption measured by TIRIF on hydrophobic silica may differ from the actual adsorption more than in the case of the adsorption on hydrophilic silica. The larger difference also indicates that the hydrophobic surface leads to much larger changes of lipoprotein conformation/aggregation. This indication is not without importance in the future design of blood-contacting materials. A detailed analysis of lipoprotein interactions with surfaces requires additional in-situ measurements of the adsorbed layer composition and a knowledge of the adsorbed lipoprotein fluorescence lifetime.

CONCLUSIONS

The total internal reflection intrinsic fluorescence (TIRIF) method was applied to the study of the adsorption of human lipoproteins. These are large macromolecular aggregates, in which only one part, the apolipoprotein contains fluorophores. High and low density lipoprotein fractions of human serum were adsorbed separately on two model surfaces: hydrophilic and hydrophobic silica. The adsorption of two lipoproteins on the two surfaces is different. The initial lipoprotein adsorption on the hydrophilic surface can be quantitatively described with the transport-limited adsorption model assuming a constant decrease of the lipoprotein fluorescence quantum yield by 25% (LDL) and 37% (HDL). The comparison between the lipoprotein adsorption plateau and the calculated monolayer adsorption, and the fluorescence emission maximum shifts, support the quantum yield decrease. The latter is caused by the interactions between the exposed lipoprotein tryptophanyl residues and the surface. The hydrophobic silica surface induces different and probably larger changes in lipoprotein conformation and, in the case of HDL, also in lipoprotein composition. The HDL adsorption maximum and the subsequent adsorption decrease found in the mid-course of the adsorption are indicative of preferential surface accumulation of the fluorescence-"invisible" HDL apo A-II protein.

ACKNOWLEDGEMENTS

The authors acknowledge a Fulbright Program Grant awarded to V. Hlady for his stay at the University of Utah and financial support from the Authority for Scientific Research of Croatia (Yugoslavia). This work was supported by a University of Utah Faculty Research Grant and NIH grant HL18519.

REFERENCES

1 R.M.S. Smellie, Plasma Lipoproteins, Academic Press, New York, 1971.
2 P. Alaupovic, Atherosclerosis, 13 (1971) 141.
3 W.W. Mantulin and H.J. Pownall, in R.F. Steiner (Ed.), Excited States of Biopolymers, Plenum Press, New York, 1983, pp. 163–202.
4 R.E. Counsell and R.C. Pohland, J. Med. Chem., 25 (1982) 141.
5 J.D. Morrissett, R.L. Jackson and A.M. Gotto Jr, Ann. Rev. Biochem., 44 (1977) 183.
6 R.L. Levy, Clin. Chem., 27 (1982) 653.
7 A. Bantjes, W. Breemhaar, T. Beugeling, E. Brinkman and D.J. Ellens, Macromol. Chem. Suppl., 9 (1985) 99.
8 W. Breemhaar, E. Brinkman, D.J. Ellens, T. Beugeling and A. Bantjes, Biomaterials, 5 (1984) 269.
9 S.D. Dana, M.S. Brown and J.L. Goldstein, Biochem. Biophys. Res. Commun., 74 (1977) 1369.

10 M.S. Brown, Y.K. Ho and J.L. Goldstein, Ann. N.Y. Acad. Sci., 276 (1976) 244.
11 D.E. Dong, Ph.D. Dissertation, University of Utah, Salt Lake City, UT, 1983; and D.E. Dong, J.D. Andrade and D.L. Coleman, J. Biomed. Mater. Res., 21 (1987) 683.
12 B.W. Shen, P. Lagocki and A.M. Scanu, Circulation, Suppl. II, (1979) II-55.
13 T. Hirschfield, Can. Spectrosc., 10 (1965) 128.
14 V. Hlady, R.A. Van Wagenen and J.D. Andrade, in J.D. Andrade (Ed.), Surface and Interfacial Aspects of Biomedical Polymers, Vol. 2, Protein Adsorption, Plenum Press, New York, 1985, pp. 81–119.
15 V. Hlady, D.R. Reinecke and J.D. Andrade, J. Colloid Interface Sci., 111 (1986) 555.
16 B.K. Lok, Y-K. Cheng and C.R. Robertson, J. Colloid Interface Sci., 91 (1983) 87, 104.
17 D.M. Lee and P. Alaupovic, Biochem. J., 137 (1974) 155.
18 A. Suenram, W.J. McConathy and P. Alaupovic, Lipids, 14 (1979) 505.
19 M.K. Markwell, S.M. Haas, L.L. Bieber and N.E. Tolbert, Anal. Biochem., 87 (1978) 206.
20 R.A. Van Wagenen, S.A. Rockhold and J.D. Andrade, Adv. Chem. Ser., 199 (1982) 351.
21 R.A. Badley, Biochim. Biophys. Acta, 379 (1975) 517.
22 V. Hlady and J.D. Andrade, Colloids Surfaces, 32 (1988) 359.
23 J.D. Andrade, in J.D. Andrade (Ed.), Surface and Interfacial Aspects of Biomedical Polymers, Vol. 2, Protein Adsorption, Plenum Press, New York, 1985, pp. 1–80.
24 J.P. Segrest, R.L. Jackson, J.D. Morrissett and A.M. Gotto, FEBS Lett., 38 (1974) 247.
25 A.M. Scanu, Biochim. Biophys. Acta, 265 (1972) 471.

Colloids and Surfaces, 42 (1989) 85–96
Elsevier Science Publishers B.V., Amsterdam — Printed in The Netherlands

A TIRF Titration Study of 1-Anilinonaphthalene-8-sulfonate Binding to Silica-Adsorbed Bovine Serum Albumin

V. HLADY[1,2,*] and J.D. ANDRADE[2]

[1]*Ruđer Bošković Institute, 41000 Zagreb (Yugoslavia)*
[2]*Center for Biopolymers at Interfaces, Department of Bioengineering, University of Utah, Salt Lake City, UT 84112 (U.S.A.)*

(Received 15 March 1989; accepted 2 June 1989)

ABSTRACT

A novel fluorescence titration method was applied to the qualitative study of conformational characteristics of a surface-adsorbed bovine serum albumin (BSA) layer. The probe, 1-anilinonaphthalene-8-sulfonate (ANS), was used as a fluorescent ligand. The selective excitation of a bound dye in the adsorbed protein layer was achieved using the evanescent surface wave created by total internal reflection at the solid/liquid interface. The same protein/ligand pair dissolved in the bulk solution was used as a reference. The apparent affinity of the ligand towards the surface-adsorbed protein is lower as compared with the dissolved protein. The results of the solution and the surface titration experiments were quantitatively compared after the titration results were normalized with respect to the intrinsic BSA fluorescence in the absence of the ligand. It was found that the protein adsorption leads to fluorescence enhancement of those bound ANS molecules which are otherwise nonfluorescent when bound to BSA in the solution. It is shown that ANS molecules, which are bound to the outer binding sites on the protein surface, can serve as a probe of protein–protein and protein–surface contacts in the adsorbed layer.

INTRODUCTION

The adsorption of proteins at solid/liquid interfaces attracts considerable interest [1,2]. In the field of biomedical engineering protein adsorption from body fluids onto surfaces remains a major concern [1,3]. Interactions between proteins and man-made surfaces are particularly important in the field of material–blood compatibility [4]. It is generally accepted that adsorption onto a solid surface can induce a conformational change of the protein and, consequently, an undesirable biological response may be started. The conformational change of a protein during adsorption is the most elusive part of the adsorption process because the structure of adsorbed protein cannot be determined directly. Consequently, the extent of the conformational change of a protein is often inferred by indirect methods. Physico-chemical events at in-

*To whom correspondence should be addressed.

0166-6622/89/$03.50

terfaces, like adsorption, can be studied by different spectroscopic techniques using total internal reflection (TIR) [1,5,6]. A TIR counterpart of fluorescence spectroscopy, called total internal reflection fluorescence (TIRF), is a particularly suitable technique for the study of protein adsorption [1,4,7].

Many methods of fluorescence spectroscopy are successfully applied to the study of proteins in solution and in membranes [8,9]. A typical example is a fluorescence titration method which is often used to determine the number of fluorescent protein-bound ligands and the respective binding constants. In this paper a new TIRF titration method is applied to the study of ligand binding to protein which is adsorbed at the solid/liquid interface. The binding affinity of an adsorbed protein for a particular ligand may not be the same as the corresponding affinity in the bulk solution. In such a case, changes of binding affinity and number of ligands bound to the adsorbed protein might be used to examine the conformational protein change using the solution environment as a reference. In a preceding publication the fluorescence emission spectra of adsorbed bovine serum albumin (BSA) and BSA-bound 1-anilinonaphthalene-8-sulfonate (ANS) were obtained using the TIRF method [10]. It was found that the change of BSA conformation as a result of adsorption involves the microenvironment of tryptophan residues, as well as the ANS binding sites, respectively. Here, we extend the previous study by titrating irreversibly adsorbed BSA with ANS. The fluorescence quantum yield of ANS in aqueous solutions is very low but increases strongly upon binding to a hydrophobic binding site [11–14]. This characteristic of ANS is particularly suitable for the TIRF titration of surface-adsorbed protein since no fluorescence contribution from the dissolved ANS molecules is to be expected. The binding of ANS to BSA in solution can be quantitated by measuring the fluorescence of fully bound ANS in the presence of an excess of BSA. It has been found that eight to ten molecules of ANS can bind to one BSA molecule but that binding to a limited number of inner, more hydrophobic binding sites leads to the enhancement of ANS fluorescence [15].

MATERIALS AND METHODS

BSA (monomer standard protein powder, Miles Laboratories) and ANS (bis-ANS free, Molecular Probes) were used without further purification. Other chemicals were analytical grade. Only freshly prepared solutions were used. Acetate buffer solutions (0.01 M acetate, pH 5.0) were used throughout the experiments. The concentrations of ANS and BSA stock solutions were determined from the solution absorbances and the respective extinction coefficients (BSA; $4.4 \cdot 10^4\ M^{-1}\,cm^{-1}$ at 279 nm, ANS; $6.3 \cdot 10^3\ M^{-1}\,cm^{-1}$ at 350 nm [15]). The fluorescence titration experiments were performed using the custom-built TIRF apparatus described earlier [7,16]. In this study a TIRF cell was made of a quartz hemi-cylinder which was optically coupled with a rectangular flu-

orescence cell made of fused silica [10]. The cell was closed with a stopper which had two flow lines for removing and adding solution from and to the cell. One of the inner surfaces of the fluorescence cell was used as the adsorbing surface [10]. The adsorbed molecules were selectively excited with an evanescent surface wave which was created by a totally reflected ultraviolet light beam at the cell wall/solution interface. 4 nm excitation halfwidths and 16 nm emission halfwidths were used in the case of surface titrations (8 nm halfwidths in the case of the solution titration). The incident light was perpendicularly polarized with respect to the plane of incidence. No polarizer was used in the emission light path. Fluorescence emission was collected normal to the interface through the quartz hemi-cylinder. All experiments were done at room temperature.

The experimental procedure was as follows: all inner surfaces of the TIRF cell were rigorously cleaned prior to each experiment [17]. The TIRF cell was primed with BSA buffer solution which was left to contact the inner cell surfaces for one hour. Three different BSA concentrations were used: $7 \cdot 10^{-7}$, $1.4 \cdot 10^{-6}$ and $1.4 \cdot 10^{-5}$ *M*, respectively. Nonadsorbed BSA was flushed out of the cell with 40 ml of buffer solution without allowing air to enter the cell. Following the flush-out, the interface was illuminated by the evanescent surface wave ($\lambda_{ex} = 360$ nm), the ANS concentration in the cell was increased by sequential injection of ANS solution and the fluorescence was recorded ($\lambda_{em} = 470$ nm). After each addition a 15 min equilibration was allowed while, at the same time, the incident light was blocked by a shutter in order to prevent overexposure of the bound dye. The surface cleanliness was a major factor influencing eventual displacement of adsorbed BSA by ANS. When clean surfaces were used no displacement of BSA was detected in the range of ANS concentrations used. The titrations were also checked for reversibility; as a rule, very small or no titration hysteresis was detected when the ANS sample was not contaminated with impurities. Preliminary experiments showed that some impurity in the ANS sample caused a strong hysteresis of the titration curve. In such a case the probe bound to adsorbed BSA fluoresced with a red-shifted emission maximum, $\lambda_{em} = 495$ nm, as compared with the pure ANS sample (bulk solution BSA–ANS $\lambda_{em} = 465$ nm, adsorbed BSA–ANS $\lambda_{em} = 475$ nm, respectively [10]), and the TIRF excitation spectra was similar to the spectra of BSA-bound ANS dimer, 1,1′-bi(4-anilino)naphthalene-5,5′-disulfonic acid (bis-ANS) ($\lambda_{ex} = 405$ nm with a shoulder at 370 nm [18]). Bis-ANS is known to have a much stronger affinity towards BSA than ANS [18].

The blank titration experiments without protein showed no enhancement of ANS fluorescence due to its binding at the silica/buffer interface. The surface concentrations of irreversibly adsorbed BSA were determined by using I^{125}-labeled BSA in separate experiments [7]. The fluorescence emission efficiency of adsorbed BSA (relative to the fluorescence quantum yield of BSA in the bulk solution) was determined by quantitative TIRF experiments in which a 5-hydroxytryptophan methyl ester solution was used as an external

fluorescence standard [7]. Titration of BSA with ANS in the bulk solution was performed using a front face geometry and the same fluorescence apparatus as the one used in TIRF titrations ($\lambda_{ex}=360$ nm, $\lambda_{em}=470$ nm). The binding of ANS to the BSA molecule in the bulk solution was quantitated by measuring the fluorescence of fully bound ANS in the presence of an excess of BSA ($1.4\cdot10^{-4}$ M) [14]. A similar procedure was not applied to the surface titration of adsorbed BSA since the BSA surface concentration could not be increased at will. In order to circumvent this experimental difficulty and to compare the surface and the solution titration results, a second set of titration experiments was performed using the intrinsic fluorescence of BSA as a normalization factor. The intrinsic fluorescence of BSA was measured ($\lambda_{ex}=285$ nm, $\lambda_{em}=340$ nm) in the absence of ANS, after which the titration experiment was executed by exciting at 285 nm with emission monitored at $\lambda_{em}=475$ nm. The same procedure was also applied to the titration of BSA in the bulk solution. The surface and the solution titration results were both normalized with respect to the intrinsic BSA fluorescence measured in the absence of the ligand so that both sets of results could be compared with each other.

RESULTS AND DISCUSSION

Table 1 shows the surface concentration of irreversibly adsorbed BSA at the silica/buffer interface and the fluorescence emission efficiency of adsorbed BSA (relative to the quantum yield of BSA in the bulk solution) as determined by measuring the adsorption of I^{125}-labeled BSA in combination with the quantitative TIRF experiments [7]. It was found that the increase of solution BSA

TABLE 1

Comparison of the surface and solution parameters which are relevant to the fluorescence titration of BSA with ANS. The silica surface BSA concentration as determined by I^{125}-labeled BSA adsorption from the $7\cdot10^{-7}$, $1.4\cdot10^{-6}$ and $1.4\cdot10^{-5}$ M BSA solutions, respectively [7]. The adsorbed BSA fluorescence efficiency relative to the fluorescence quantum yield of BSA in the bulk solution as calculated from the surface BSA concentrations and the quantitative TIRF adsorption measurements [7]. The apparent dissociation constant (in $pK_{0.5}=-\log K_{0.5}$) determined from Fig. 1 as [ANS] at half of maximum fluorescence intensity

	Silica surface			Solution
BSA concentration (mg m^{-2})	1.32	1.64	2.1	$3\cdot10^{-6}$ (M)
Adsorbed BSA fluorescence efficiency (relative to BSA in the bulk solution)	0.84	0.78	0.74	1.0
Apparent dissociation constant (in $pK_{0.5}=-\log K_{0.5}$)	5.0	5.0	4.45	5.8

concentration leads to a higher amount of adsorbed BSA, which, nevertheless fluoresces with a lower fluorescence efficiency.

Figure 1 shows the results of the first set of the fluorescence titration experiments in which λ_{ex} was 360 nm and no normalization with respect to the intrinsic BSA fluorescence was used. The comparison between the binding curves shows that the apparent dissociation constants of ANS from BSA, $K_{0.5}$, (defined as [ANS] at the half of maximum fluorescence intensity), were larger for the surface-adsorbed BSA than for the dissolved protein. The values of $pK_{0.5}$, ($pK_{0.5} = -\log K_{0.5}$) (Table 1) indicate that the binding of ANS to surface-adsorbed BSA is weaker as compared with the binding of the same ligand to BSA in solution.

Quantitative fluorescence titration of dissolved BSA with ANS showed that approximately four molecules of ANS bind to one BSA molecule in the solution. The number of bound ANS molecules ($n=3.6$) and the dissociation constant ($pK_{0.5}=5.8$), were in good agreement with the literature [14,19]. The quantitative ANS titration of adsorbed BSA could not be performed using the same methodology which was employed in the solution studies since the surface BSA concentration was fixed by the BSA adsorption isotherm [7]. Because of that, the second set of titration experiments was designed in such a way that allowed the comparison between the solution and the surface titration results, i.e. by using. $\lambda_{ex}=285$ nm and the normalization of measured ANS fluorescence with respect to the intrinsic BSA fluorescence. The intrinsic fluorescence of the adsorbed BSA, which was used as a normalization factor, was corrected for its decreased fluorescence efficiency (see Table 1). The comparison between the surface and solution titration results is given in Fig. 2 showing the normalized fluorescence as a function of free ANS concentration. It was

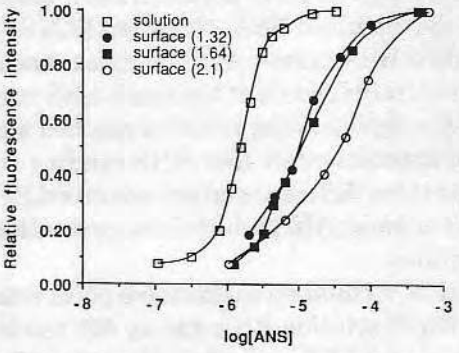

Fig. 1. The fluorescence intensity change upon the surface and the solution titrations of BSA with ANS as a function of ANS concentration in solution. The BSA concentration in the solution, $[BSA]=3\cdot10^{-6}$ M, the surface BSA concentrations at the interface as indicated (in mg m^{-2}). The fluorescence intensity maximum was set to unity for all titration experiments. $\lambda_{ex}=360$ nm, $\lambda_{em}=470$ nm.

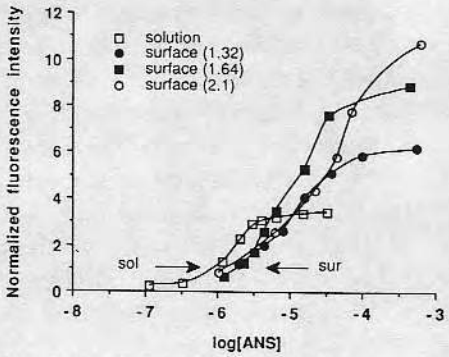

Fig. 2. The fluorescence intensity change upon the surface and the solution titrations of BSA with ANS as a function of ANS concentration in solution. The BSA concentration in the solution, $[BSA]=3\cdot10^{-6}\ M$, the surface BSA concentrations at the interface as indicated (in mg m^{-2}). The fluorescence intensity was normalized with respect to the intrinsic fluorescence of BSA at 340 nm in the absence of ANS. $\lambda_{ex}=285$ nm, $\lambda_{em}=475$ nm.

assumed throughout the TIRF titration experiments that the total ANS concentrations in the TIRF cell equal the free ANS concentrations in the system. This assumption was only invalid at conditions not encountered in this work; at extremely low ANS concentration and at very high BSA surface concentration*. The normalized fluorescence intensity at the saturation binding of ANS by the solution BSA was scaled to match the number of bound ANS molecules per one BSA molecule, i.e. to 3.6, and, correspondingly the normalized fluorescence intensity of the surface titration was scaled by the same factor.

Several features in Fig. 2 which present the greatest interest are: (a) when $[ANS]<1\cdot10^{-5}\ M$, the adsorbed BSA-bound ANS complex showed less fluorescence at a given ANS concentration than in the case of ANS molecules bound to the dissolved BSA, (b) when $[ANS]>1\cdot10^{-5}\ M$, the fluorescence of the adsorbed BSA-bound ANS complex was still increasing with increasing ANS concentration while at the same ANS concentrations the fluorescence of ANS–BSA complex in the solution reached a plateau which indicated the saturation of approximately four ANS binding sites in BSA, and (c) binding of ANS to the three different surface-adsorbed BSA layers are shown to be almost coincident at lower ANS solution concentrations but different at higher ligand concentrations.

In addition, a common isoemissive point was found at 416 nm in the case of the titration of solution BSA and at 406 nm in the case of the adsorbed BSA (2.1 mg m^{-2}, at $[ANS]<7\cdot10^{-5}\ M$), respectively (data not shown here). The

*The volume of the TIRF cell was approx. 3.5 cm^3 with 15 cm^2 surface available to BSA adsorption. In the case that $n=4$ and $[ANS]=1\cdot10^{-5}\ M$, the total concentration of ANS is depleted by 0.4% by 1.65 mg m^{-2} adsorbed BSA. The free ANS concentration would be $9.96\cdot10^{-6}\ M$.

existence of the isoemissivity indicates that the bound ANS molecules fluoresce with the same quantum yields as discussed earlier [14].

According to the present results (Fig. 2) the affinity of adsorbed BSA towards the first ANS molecules has decreased. It is assumed that the affinity decrease is due to a conformational change of the ANS binding sites in the adsorbed protein. This conformational change was inferred from the red-shift of fluorescence emission of adsorbed BSA–ANS complex [10]. As the free ANS concentration increases beyond the value of the saturation of ANS/BSA binding sites in solution, i.e. at $[ANS] > 1 \cdot 10^{-5}\ M$, the TIRF titration showed that additional ANS molecules bind to the adsorbed protein and that their fluorescence is enhanced. It has been found previously that eight to ten ANS molecules bind to one BSA molecule at $1 \cdot 10^{-3}\ M > [ANS] > 1 \cdot 10^{-4}\ M$ [20]. However, only four of the bound ANS molecules become strongly fluorescent upon binding to BSA in the solution while the other bound ANS molecules are "dark" emitters. It was suggested that the latter population of ANS molecules binds to the outer binding sites at the protein surface [20]. There, the bound ANS molecules are exposed to quenching by water molecules which act as a collisional quencher with a Stern–Volmer constant of $5\ M^{-1}$ [15]. The binding of ANS to BSA is shown schematically in Fig. 3. The present results show that the supramolecular organization of BSA molecules in the adsorbed layer effectively shields these outer site-bound ANS molecules from the quenching by water. The actual position of outer-site bound ANS molecules with respect to the surface of silica remains uncertain. It is uncertain whether the ANS molecules are shielded by two neighboring BSA molecules at the interface without contacting the solid surface (Fig. 3b), or are they sandwiched between the adsorbed BSA and the surface itself (Fig. 3c), or possibly both (Fig. 3d)? The first alternative alone (Fig. 3b) would imply that the BSA molecules at all three surface concentrations studied here are adsorbed in the form of densely populated protein "islands" on the silica surface which allow for a large number of lateral protein–protein contacts. It should be noted that the normalization of the surface fluorescence intensity with respect to the intrinsic BSA fluorescence is, effectively, also a normalization with respect to the amount of adsorbed protein. In this case the second alternative, i.e. that additional ANS molecules bind only between the protein and the surface (Fig. 3c), should bring to a full coincidence of the binding curves which should be independent on the BSA surface concentration. Such coincidence is found at $[ANS] < 4 \cdot 10^{-5}\ M$ for the two BSA surface concentrations; 1.32 and 2.1 mg m^{-2} (Fig. 2), respectively. The binding curve obtained at the BSA surface concentration of 1.64 mg m^{-2} differed slightly from the other two by showing a comparatively higher fluorescence intensity in the intermediate ANS concentration range. This probably reflects a low reproducibility of the supramolecular organization of BSA molecules in the adsorbed layer on the silica surface and cautions against oversimplification of the physical picture of an adsorbed protein layer. As shown

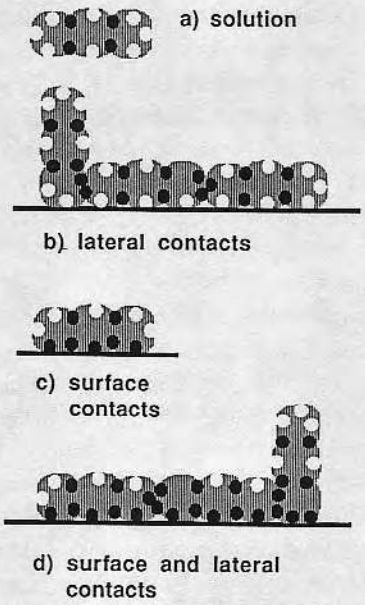

Fig. 3. Schematics of ANS binding to the dissolved and adsorbed BSA molecules at medium-to-high ANS solution concentrations: (a) only four ANS molecules emit fluorescence upon binding to the inner BSA binding sites in the solution (black circles), all other ANS molecules are bound to the outer binding sites at the BSA surface and their fluorescence is quenched by water (white circles), (b) lateral protein–protein contacts between the adsorbed protein molecules shield the ANS molecules bound to the outer protein binding sites from collisional water quenching, (c) adsorbed protein–surface contacts shield the ANS molecules bound to the outer protein binding sites from collisional water quenching, and (d) both the lateral protein–protein contacts and the adsorbed protein–surface contacts shield the outer site-bound ANS molecules.

in Fig. 2 the surface titration results become dependent on BSA surface concentration only at higher ANS concentration. The increase of fluorescence intensity followed the increase of the BSA surface concentrations at $[ANS] > 1 \cdot 10^{-4}$ *M*. Although the fluorescence quantum yield of bound ANS is not constant at these conditions as indicated by the lack of isoemissivity, this trend indicates the existence of ANS binding sites between the lateral BSA–BSA contacts and suggests that at higher BSA surface concentrations the protein molecules are organized in some sort of surface aggregates. The existence of two-dimensional aggregates of adsorbed BSA has been found by others [21]. Because the observed BSA layer was not in contact with protein in solution, any conclusion about the organization of the adsorbed layer may not be pertinent to a physical picture of the same layer during the adsorption process. Some artifacts can be also due to the extensive flush-out of nonadsorbed BSA from the TIRF cell which might cause desorption of less tightly adsorbed protein from the surface.

The excitation at 285 nm in the titration experiments caused an intrinsic BSA fluorescence emission which decreased as an increased number of ANS molecules was bound to the protein. This is due to the radiationless fluorescence energy heterotransfer from BSA tryptophan residues to bound ANS ligands. A necessary condition for this energy mechanism to be operative is extensive overlap between the emission band of the donor and the absorption band of the acceptor [8]. This condition is met by the ANS molecules bound to BSA: the ANS absorption band ($^{max}\lambda_{abs}=360$ nm) overlaps with the emission band of intrinsic protein fluorescence which is centered at $\lambda_{em}=342$ nm in the case of solution BSA, and at $\lambda_{em}=335$ nm in the case of surface-adsorbed BSA, respectively. The 285 nm excitation will excite tyrosinyl BSA residues as well. In order to avoid seeing a contribution from tyrosine fluorescence emission, the intrinsic BSA fluorescence emission decrease was monitored at 365 nm. Figure 4 shows the fractional decrease of intrinsic BSA fluorescence due to the ANS binding; the quenching of dissolved BSA and surface-adsorbed BSA fluorescence was quite different. In order to achieve the same quenching effect in the case of adsorbed BSA the concentration of ANS in solution needed to be increased almost 10-fold. Part of this effect is certainly due to the different spectral overlaps between the ANS absorption band and the BSA emission in the solution and at the surface, respectively. The characteristic distance for energy transfer between tryptophanyl BSA residues and bound ANS ligands in solution, $R_{o(solution)}$, equals 2.9 nm, as calculated from spectroscopic data according to the Förster mechanism of energy transfer [22]. The value of $R_{o(surface)}=2.7$ nm was estimated from $R_{o(solution)}$ by applying corrections for a different spectral overlap due to blue-shifted BSA fluorescence [10] and a 25% decrease in the fluorescence quantum yield of the adsorbed BSA [7]. The same average orientation of donor–acceptor pair in the solution and at the silica

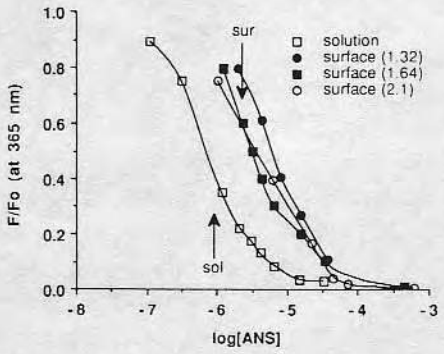

Fig. 4. The intrinsic BSA fluorescence intensity change upon the surface and the solution titrations of BSA with ANS as a function of ANS concentration in solution. The BSA concentration in the solution, $[BSA]=3\cdot10^{-6}$ M, the surface BSA concentrations at the interface as indicted (in mg m^{-2}). $\lambda_{ex}=285$ nm, $\lambda_{em}=365$ nm.

surface, and no change of the absorption spectrum of ANS when bound to adsorbed BSA were assumed, respectively. The average distance between donor and acceptor can be calculated from:

$$E = R_o^6/(R_o^6 + r^6)$$

where E equals $1 - F/F_o$ [8]. When the first ANS ligand binds to dissolved BSA, i.e. at $[ANS] = 9 \cdot 10^{-7}$ M (indicated by "sol" in Fig. 2), the average distance, $r_{(solution)}$, calculated from $F/F_o = 0.4$ (indicated by "sol" in Fig. 4), was found to be 2.7 nm. For the binding of the first ANS ligand to the surface adsorbed protein the ANS concentration has to be increased to approximately $[ANS] = 2.5 \cdot 10^{-6}$ M (indicated by "sur" in Fig. 2). In this case the F/F_o parameter amounted to approximately 0.7 (indicated by "sur" in Fig. 4) and the average distance was calculated to be, $r_{(surface)} = 3.0$ nm. As a rule, similar calculations performed at different levels of ANS fluorescence intensity always resulted in a $r_{(solution)} < r_{(surface)}$. This increase in distance between the donors and acceptors can be interpreted as due to conformational changes in BSA upon adsorption. Assuming that the four inner binding sites of BSA are occupied first in the surface titration as in the case of the solution titration, the present results point to the partial unfolding of adsorbed BSA; the average ANS binding site(s) distance from emitting tryptophan residue(s) has increased by 10% due to the adsorption of BSA.

Throughout this study the steady-state protein–ligand fluorescence was used in the analysis of particular characteristics of the adsorbed protein/dye layer. A more informative study of the adsorbed protein–ligand dynamics can be made by measuring the fluorescence lifetimes of BSA tryptophan residues and ANS ligands as a function of ANS binding. Such a study of adsorbed BSA-bound ANS fluorescence lifetime has been initiated at the Utah laboratory. The first results indicate that the overall ANS lifetime decreases at high ANS concentrations, possibly reflecting an increased fluorescence contribution from ANS molecules bound in the outer protein binding sites (P. Suci and V. Hlady, unpublished results).

CONCLUSIONS

It was found that the apparent binding affinity of surface-adsorbed BSA towards the ANS ligand is lower as compared with the solution protein (Fig. 1 and Table 1). However, only when properly corrected and normalized with respect to intrinsic protein fluorescence, the respective results of the protein fluorescence titrations in the solution and at the solid/liquid interface could be compared in a quantitative way (Fig. 2). This comparison revealed that at higher ANS concentrations the number of BSA-bound ANS ligands, as detected via their enhanced fluorescence, was considerably larger in the case of adsorbed protein than in the case of dissolved protein. In the latter case only

the four ANS molecules which bind to the inner BSA binding sites could be detected by fluorescence. According to the present results, the ANS molecules bound to the outer binding sites on protein surface were "dark" emitters in the solution but were effectively shielded from the quenching by water molecules in the case when the protein was adsorbed at the interface. The fact that this ligand population is bound on the protein surface can be used for a qualitative analysis of supramolecular organization in the adsorbed protein layer. The other difference between the protein–ligand interactions in the solution and at the solid/liquid interface was the weaker quenching of adsorbed BSA intrinsic fluorescence by the bound ANS ligands. The energy transfer calculations showed an increased distance between BSA tryptophan residues and bound ANS at the interface.

In conclusion, the new TIRF titration method showed a potential for the study of the conformational change of adsorbed proteins. The present availability of various fluorescent probes, by which one can probe many different properties of adsorbed proteins, warrants further use of this technique.

ACKNOWLEDGEMENTS

The financial help from the Center for Biopolymers at Interfaces, Department of Bioengineering, University of Utah, Utah, USA and the Selfmanagement Council for Scientific Research of Croatia, Yugoslavia is gratefully acknowledged.

REFERENCES

1 J.D. Andrade (Ed.), Surface and Interfacial Aspects of Biomedical Polymers, Vol. 2, Protein Adsorption, Plenum, New York, 1985.
2 W. Norde, Adv. Colloid Interface Sci., 25 (1986) 267.
3 S.L. Cooper and N.A. Peppas (Eds), Biomaterials: Interfacial Phenomena and Applications, American Chemical Society, Washington DC, 1982.
4 J.D. Andrade and V. Hlady, Adv. Polym. Sci., 79 (1986) 1.
5 N.J. Harrick, Internal Reflection Spectroscopy, Interscience, New York, 1967.
6 M.K. Debe, Prog. Surface Sci., 24 (1987) 1.
7 V. Hlady, D.R. Reinecke and J.D. Andrade, J. Colloid Interface Sci., 111 (1986) 555.
8 J.R. Lakowicz, Principles of Fluorescence Spectroscopy, Plenum, New York, 1983.
9 A.J. Pesce, C-G. Rosen and T.L. Pasby (Eds), Fluorescence Spectroscopy, Marcel Dekker, New York, 1971.
10 V. Hlady and J.D. Andrade, Colloids Surfaces, 32 (1988) 359.
11 L.S. Stryer, J. Mol. Biol., 13 (1965) 432.
12 S.D. Dowling and W.R. Seitz, Anal. Chem., 57 (1985) 602.
13 R. Gibrat, C. Romieu and C. Grignon, Biochim. Biophys. Acta, 736 (1983) 196.
14 E. Daniel and G. Weber, Biochemistry, 5 (1966) 1893.
15 D.A. Kolb and G. Weber, Biochemistry, 14 (1975) 4476.

16 V. Hlady, R.A. Van Wagenen and J.D. Andrade, in J.D. Andrade (Ed.), Surface and Interfacial Aspects of Biomedical Polymers, Vol. 2, Protein Adsorption, Plenum, New York, 1985, pp. 81–119.
17 R.A. Van Wagenen, S.A. Rockhold and J.D. Andrade, Advan. Chem. Ser., 199 (1982) 351.
18 C-G. Rosen and G. Weber, Biochemistry, 10 (1969) 3915.
19 D.V. Naik, W.L. Paul, R.M. Threatte and S.G. Schulman, Anal. Chem., 47 (1975) 267.
20 T.L. Pasby, Ph.D. Thesis, University of Illinois, 1969.
21 S.D. Riccitelli, F.H. Bilge and R.C. Eberhart, Trans. Am. Soc. Artif. Intern. Organs, 23 (1984) 420.
22 G. Weber and E. Daniel, Biochemistry, 5 (1966) 1900.

Biosensors & Bioelectronics 5 (1990) 291–301

Spatially Resolved Detection of Antibody–Antigen Reaction on Solid/Liquid Interface using Total Internal Reflection Excited Antigen Fluorescence and Charge-Coupled Device Detection

V. Hlady,* J. N. Lin & J. D. Andrade

Department of Bioengineering, University of Utah, Salt Lake City, Utah 84112, USA

(Received 21 July 1989; revised version received 13 November 1989; accepted 20 November 1989)

ABSTRACT

Spatially-resolved detection of antibody–antigen reactions at the solid/liquid interface was investigated by total internal reflection excited fluorescence from large area flat surfaces. Anti-HSA immunoglobulin G (IgG) antibody was immobilized at four spatially distinct spots. Binding of fluorescein-labeled human serum albumin (HSA) from the solution to immobilized antibody was detected by a cooled charge-coupled device (CCD) as a change in the fluorescence intensity. A two-dimensional representation of the fluorescence was obtained during the binding reaction time of 25 mins. The contributions from bound and free antigen to the total signal were evaluated. The influence of the scattered excitation light and the normalization of fluorescence signal with respect to the two-dimensional incident light intensity distribution are discussed.

Key words: antigen–antibody binding, evanescent surface wave, total internal reflection fluorescence (TIRF), charge-coupled device.

*On leave of absence from 'Ruder Boskovic' Institute, Zagreb, Yugoslavia.

Biosensors & Bioelectronics 0956-5663/90/$03.50

INTRODUCTION

There is a considerable interest in developing immunosensors (Turner *et al.*, 1987; Edmonds, 1988; Guilbault & Mascini, 1988). Such sensors can have excellent selectivity because of high antibody–antigen specificity (North, 1985; Bush & Reichnitz, 1987). A particularly attractive idea is to develop a multichannel immunosensor using different antibodies immobilized on a solid support. Such a device can be either engineered for simultaneous detection of different antigens or for an extended sensitivity range of a single antigen. Simultaneous detection of different antigens requires the immobilization of different antibodies, while the extended sensitivity range of a sensor can be achieved by using a set of antibodies with different association constants for a single antigen. In addition, one also needs a method for separating those sensor responses which originate from different sets of antibodies. Although the binding of a single antigen to antibodies which are characterized by different binding constants can be, in principle, resolved by numerical methods, it is possible to resolve different responses of a multichannel sensor by distinct spatial arrangements of antibodies on the sensor surface. In this case the problem of designing the multichannel immunosensor is transformed into the problem of simultaneous detection of spatially resolved sensor responses. The authors have previously reported the development of immunosensors based on the excitation of fluorescence by an electromagnetic surface wave created by total internal reflection (Andrade *et al.*, 1985, 1988). Such an approach is attractive because of the possibility of remote immunosensing using total internal reflection optics inside a single optical fiber (Andrade *et al.*, 1985; Wang *et al.*, 1989). Here, an initial study of spatially resolved detection of antibody–antigen reaction at the flat interface between fused silica and a buffer solution is reported.

EXPERIMENTAL

In this study a single type of antibody against human serum albumin (HSA) antigen was chosen in order to compare the spatially resolved fluorescence signals. Polyclonal anti-HSA IgG antibody was immobilized to four spatially distinct circular areas on the one side of the fused silica plate surface (2·5 cm × 7·5 cm). The immobilization procedure consisted of glutaraldehyde activation of the silica surface and chemical coupling of IgG as described elsewhere (Lin *et al.*, 1989). After the immobilization of antibody, bovine serum albumin (BSA) was adsorbed from concentrated solution (10 mg/ml) to the same surface to prevent any future nonspecific adsorption of fluorescein-labeled antigen. Antigen binding to immobilized antibody was detected by imaging the total internal reflection (TIR) excited fluorescence of fluorescein-5-isothiocyanate-HSA (FITC–HSA) to the face of the charge-coupled device (CCD). The CCD used in this work was a thermoelectrically-cooled Thompson TH7882 (384 by 576 pixels, CCD200, Photometrics, Tucson) operating at 227 k. Optical geometry of the experiment is shown schematically in Fig. 1. The excitation light beam, centered at 488 nm, was obtained from a xenon–mercury 75 W lamp after passing the beam

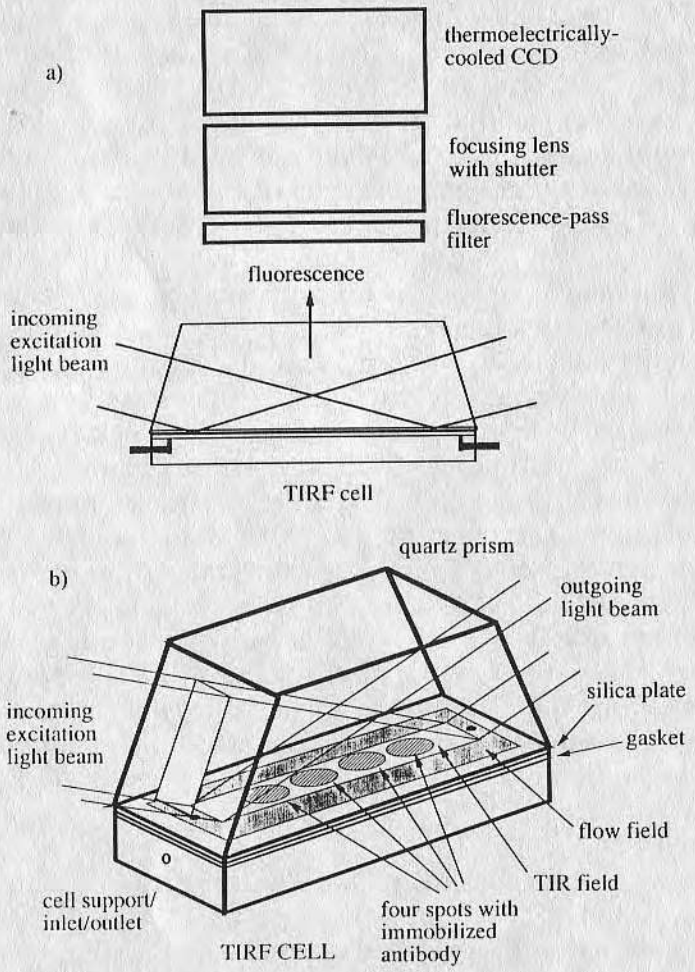

Fig. 1. Schematics of TIRF–CCD imaging of surface fluorescence: (a) optical arrangement of TIRF detection system, (b) the TIRF cell with four immobilized antibody spots and the outline of the excitation light path.

through the f/3·7, 0·10 m monochromator (H-10, ISA) equipped with two 2-mm slits (16 nm half bandwidth) and the collimating optics. The excitation light beam entered the large quartz dove-tail prism to which a fused silica plate was optically coupled with glycerol. The light impinged at the solid/liquid interface at the 70° angle and created an evanescent surface wave in the total internal reflection field (Fig. 1(a)). This wave had an optical depth of penetration, d_p = 180 nm for the 488 nm excitation (Hlady *et al.*, 1985). The excited fluorescence was collected through the quartz prism. A 520 nm long-pass filter was used to reject the excitation light. The TIR-excited fluorescence field was focused on the face of the CCD with a 50 mm f/4 lens equipped with an electronic shutter. The TIR excitation field covered nearly all four spots with immobilized antibodies. The whole TIR-excited fluorescence field (approx. 4 mm × 35 mm) fitted onto 38 × 345 wells of the CCD subarray. A CCD recording of fluorescence was followed by subtraction of background signal which was obtained previously with no antigen in the total internal reflection fluorescence (TIRF) cell, and by readout and storage of CCD data. In the present study the fluorescence images were obtained with 20 s CCD integration time. The length of the integration time was chosen in order to record fast binding changes after removal of unbound antigen from the TIRF cell. The 20 s integration resulted in a signal-to-noise ratio (S/N) between 3 and 10, depending on the extent of the antibody–antigen binding reaction. The fluorescence was collected 1, 10 and 25 mins after injection of 0·1 mg/ml of FITC–HSA in phosphate buffer (PBS, pH 7·4) into the TIRF cell. After 25 mins the unbound antigen was flushed out of the cell with PBS and after 1 min another 20 s integration was made to check for the contribution from free FITC–HSA to the overall fluorescence signal. A 20 s integration time of fluorescence from the bound FITC–HSA averaged to approximately 60 analog-to-digital units (ADU) per CCD well. This was equivalent to 900 photogenerated e^- at each well against an average of 9270 photogenerated e^- coming from the background signal plus the dark counts. No corrections of the fluorescence signal were made for the non-uniformity of light distribution of the excitation beam.

RESULTS AND DISCUSSION

Figures 2–4 show the images of total internal reflection fluorescence field obtained after 1, 10 and 25 mins binding of FITC–HSA to the surface immobilized antibody, respectively. In addition, three-dimensional profiles of fluorescence intensity of each TIRF image are also shown

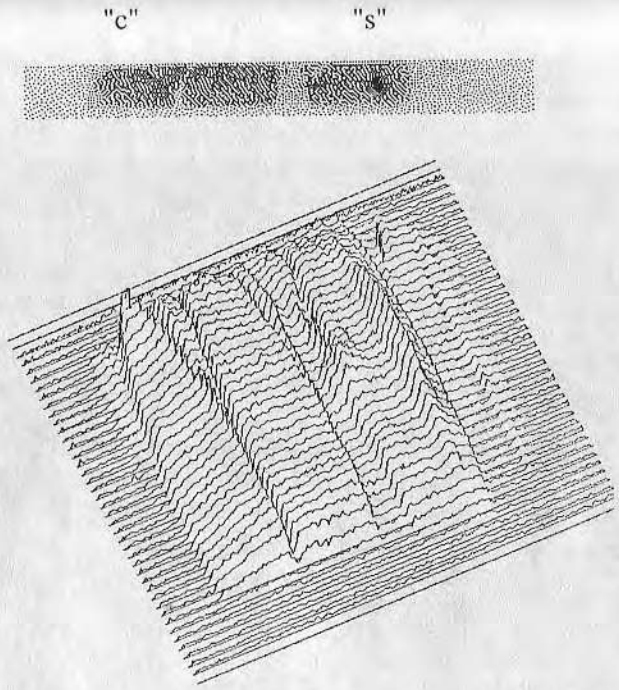

Fig. 2. The fluorescence image obtained 1 min after injection of FITC–HSA to surface-immobilized antibody (upper part, a dithered gray-scale image), and the three-dimensional fluorescence intensity profile (lower part, note that the 38 rows are shown expanded relative to 345 columns).

Figure 5 shows the fluorescence image and the 3-D intensity profile 1 min after the antigen solution was flushed out of the TIRF cell and replaced by the buffer. In Figs 2–5 the three different circular spots where immobilized antibody has bound antigens from adjacent solution are clearly seen. The TIR excitation field partly covered the fourth antibody spot which is barely seen at the far right of the images. A decrease of the light intensity at the edge of the field significantly decreased the fluorescence signal in this area. The fluorescence images were not corrected for non-uniform intensity of the excitation light across the total internal reflection excitation field. This normalization procedure, which is equivalent to image flat-fielding, is difficult to apply to the TIRF images obtained with the evanescent surface wave excitation. In principle, flat-fielding of TIRF images can be achieved by taking a TIRF image of a thin uniform layer of adsorbed or immobilized fluors at the interface and using it as the flat-field image. Since such an image contains the information about the distribution of the excitation light intensity in the TIR field, it can be used to correct other images obtained

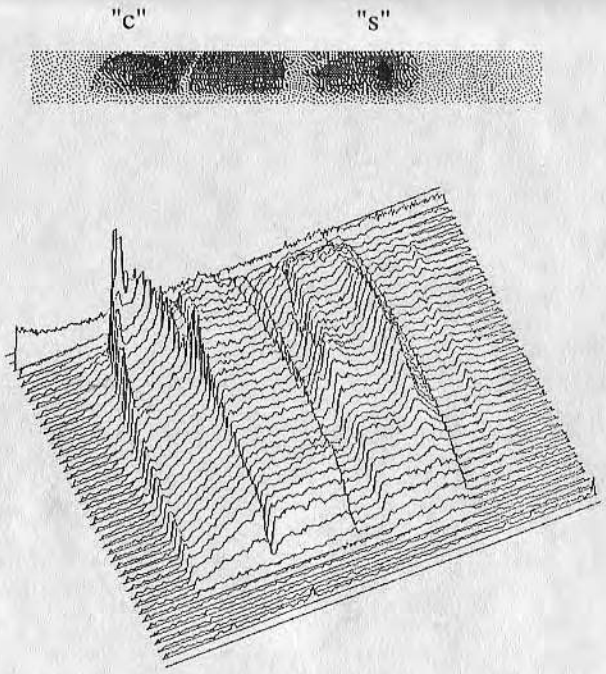

Fig. 3. The fluorescence image obtained 10 mins after injection of FITC–HSA to surface-immobilized antibody (upper part, a dithered gray-scale image), and the three-dimensional fluorescence intensity profile (lower part, note that the 38 rows are shown expanded relative to 345 columns).

with exactly the same optical arrangement. Ideally, a flat-field image can also be obtained by exciting the fluorescence from within the bulk fluorescent solution in the volume of the TIRF cell with the evanescent surface wave. In reality, however, this is hardly possible; the imperfections in the optical components in the TIRF cell usually become sources of scattering of excitation light. This scattered light propagates beyond the interfacial region and excites fluorescence in the whole volume of the TIRF cell, unlike the evanescent surface wave which is confined to the proximity of the interface (Hlady *et al.*, 1986). The difference between the two ways of excitation of fluorescence is exemplified here by a small denser area in the antibody spot on the right side of the image, which showed a higher fluorescence intensity (indicated by 's' in Figs 2–4). It was found that it originated from light scattering due to a small air bubble in the coupling glycerol layer. The air bubble served as a secondary source of light which did not arrive at the solid/liquid interface at 70° angle but at angles that are lower than the critical angle. Consequently, this so-called 'scatter' propagated beyond the range of

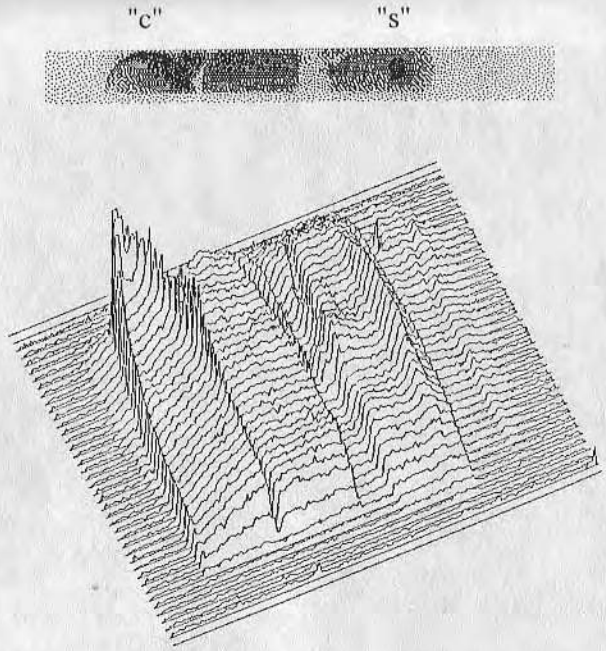

Fig. 4. The fluorescence image obtained 25 mins after injection of FITC–HSA to surface-immobilized antibody (upper part, a dithered gray-scale image), and the three-dimensional fluorescence intensity profile (lower part, note that the 38 rows are shown expanded relative to 345 columns).

penetration of the evanescent surface wave and produced a significant contribution of fluorescence from the bulk solution FITC–HSA.

Three-dimensional profiles of the fluorescence intensity can also be analyzed as a function of the binding time (Figs 2–5). Injection of antigen antigen into the TIRF cell resulted in a significant amount of bound antigen after 1 min of reaction time (Fig. 2). The fluorescence increased to the maximum during the next 9 mins (Fig. 3) and did not increase further with time (Fig. 4). At any reaction time the fluorescence signal was comprised of the signal from the antibody-bound antigen at the interface and the signal from the free antigen in the solution. The latter originated from free antigen in the solution adjacent to the surface inside the penetration depth of the evanescent surface wave, and from eventual scatter-excited fluorescence of bulk solution antigen.

The antibody-bound antigen contribution to the total fluorescence was obtained after the free antigen was flushed out of the TIRF cell with buffer solution (Fig. 5). The fluorescence intensity 3-D profile in Fig. 5 showed the absence of the fluorescence contribution due to the air bubble scatter. The light scattered from the air bubble in the glycerol

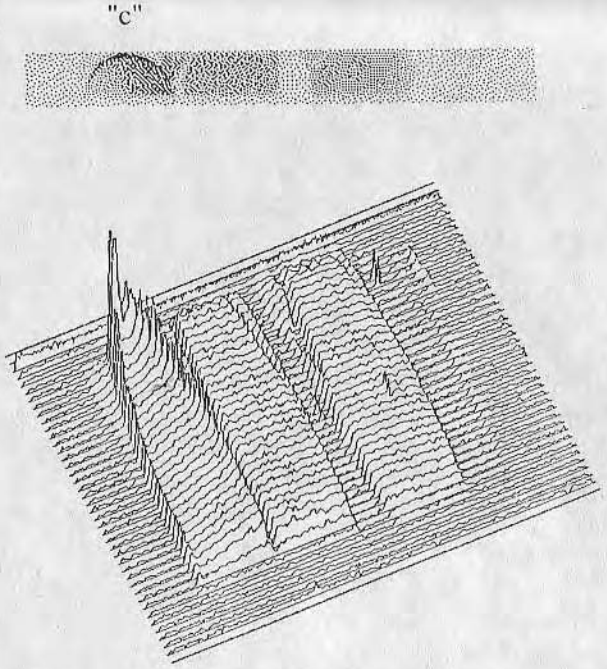

Fig. 5. The fluorescence image obtained 1 min after replacement of free FITC–HSA solution by buffer solution (upper part, a dithered gray-scale image), and the three-dimensional fluorescence intensity profile (lower part, note that the 38 rows are shown expanded relative to 345 columns).

layer excited predominantly the FITC–HSA fluorescence from the bulk solution ('s' in Figs 2–4), there was much less excitation of the bound antigen, as shown by the disappearance of the same fluorescence peak in Fig. 5. This result was expected since any propagating light will excite only a very weak fluorescence from a thin layer of fluorophores as compared with the excitation by an evanescent surface wave (Hlady *et al.*, 1985).

Another feature in Figs 2–5 requires additional comment: a crescent-shaped area on the antibody spot on the left side ('c' in Figs 2–5) with a larger fluorescence intensity than in the rest of the same antibody spot. In contrast to the scatter-excited fluorescence the intensity in this area remained high even after the free antigen in the TIRF cell was replaced with the buffer solution ('c' in Fig. 5). This indicated that the origin of this fluorescence contribution is not from the scatter of the excitation light but from an excess of antigen molecules bound by immobilized antibodies at the edge of the spot. The immobilization of antibody was done overnight from the droplet of IgG solution which was placed on the silica plate in saturated water atmosphere. It is possible that at this edge a part of the droplet dried out and thus a denser layer of antibodies, possibly a multilayer, was formed. This is worth further investigation since the signal from bound antigen was enhanced in this region.

The advantages of photon detection systems based on charge transfer devices over other types of photon detection systems are well documented in literature (Sweedler *et al.*, 1988). In the present study the S/N ratio could be significantly increased by increasing the integration time. Based on the full-well capacity of CCD ($\sim 2{\cdot}6 \times 10^5$ photogenerated e^-, which corresponds to 16 e^-/ADU for 14-bit analog-to-digital converter) the present integration time of 20 s could be increased at least 20 times before saturating the CCD. However, the increase of integration time would be at the expense of the resolution of the binding kinetics. One possibility to circumvent this problem is to use binning of the fluorescence signal along one of the dimensions of the CCD array (Epperson & Bonner Denton, 1989). Using binning one could obtain roughly the same S/N ratio using an integration time which is decreased proportionally to the number of binned rows (or columns). By assuming that the surface antibody–antigen binding constant was in the order of $10^7\ M^{-1}$, the binding of FITC–HSA from 0·1 mg/ml ($\sim 1{\cdot}5 \times 10^{-6}$ M) solution should result in 94% binding site occupation. Clearly, any useful sensor should have much lower limits of detection. As discussed above the detection of antigen from much less concentrated solution should be, in principle, possible either by increased integration time or by the binning of CCD elements. The problem of detection limits, although not studied here, is under current investigation.

CONCLUSIONS

Spatially resolved detection of an antigen–antibody reaction at the solid/liquid interface, a prerequisite for development of multichannel immunosensing devices has been demonstrated. The combination of TIR-excited fluorescence from a large surface area and the detection of antigen–antibody reaction via fluorescence by photon detection based on a charge-coupled device is one of the possible routes to multichannel immunosensors. The present results warrant future efforts in:

— lowering the detection limits by binning of CCD array and increasing the signal integration time,
— improvement of antibody surface-immobilization procedure

focused towards highly efficient and reversible binding of antigens, and
— implementation of 'on-line' optical signal processing, like adding a reference channel needed for flat-fielding and building-in a set of fluorescence standards to be used in sensor calibration.

ACKNOWLEDGEMENTS

One of us (V.H.) gratefully acknowledges leave of absence from 'Ruder Boskovic' Institute, Zagreb, Yugoslavia. This work was supported by NIH grant HL37046.

REFERENCES

Andrade, J. D., Herron, J., Kopecek, J., Lin, J. N., Yen, H. & Kopeckova, P. (1988). On-Line Sensors for Coagulation Proteins: Concept and Progress Report. *Biomaterials*, **9**, 76–9.

Andrade, J. D., VanWagenen, R. A., Gregonis, D. E., Newby, K. & Lin, J. N. (1985). Remote fiber-optics biosensors based on evanescent-excited fluoro-immunoassay: concept and progress. *IEEE Trans. Electr. Dev.*, **ED-22**, 1175–80.

Bush, D. L. & Reichnitz, G. A. (1987). Ab sensors for Ag monitoring. *Anal. Lett.*, **20**, 1781–90.

Edmonds, T. E. (Ed.) (1988). *Chemical Sensors*. Chapman and Hall, New York.

Epperson, P. M. & Bonner Denton, M. (1989). Binning spectral images in a charge-coupled device. *Anal. Chem.*, **61**, 1513–19.

Guilbault, G. G. & Mascini, M. (Eds) (1988). *Analytical Uses of Immobilized Biological Compounds for Detection, Medical and Industrial Uses*. D. Reidel Publ. Co., Dordrecht.

Hlady, V., VanWagenen, R. A. & Andrade, J. D. (1985). Total internal reflection intrinsic fluorescence spectroscopy applied to protein adsorption. In *Surface and Interfacial Aspects of Biomedical Polymers. Vol. 2. Protein Adsorption*, ed. J. D. Andrade. Plenum Press, New York, pp. 81–119.

Hlady, V., Reinecke, D. & Andrade, J. D. (1986). Fluorescence of adsorbed protein layers. I. Quantitation of total internal reflection fluorescence. *J. Colloid Interface Sci.*, **11**, 555–69.

Hlady, V., Reinecke, D. & Andrade, J. D. (1986). Fluorescence of adsorbed protein layers. I. Quantitation of total internal reflection fluorescence. *J. Colloid Interface Sci.*, **111**, 555–69.

Lin, J. N., Andrade, J. D. & Chang, I. N. (1989). The influence of adsorption of native and and modified antibodies on their activity. *J. Immunol. Methods*, **125**, 67–77.

North, J. R. (1985). Immunocensors: Ab-based biosensors. *Trends Biotech.*, **3**, 180–6.

Sweedler, J. V., Bilhorn, R. B., Epperson, P. M., Sims, G. R. & Bonner Denton, M. (1988). High performance charge transfer device detectors. *Anal. Chem.*, **60**, 282A–291A.

Turner, A. P. F., Karube, I. & Wilson, G. S. (Eds) (1987). *Biosensors: Fundamentals and Applications*. Oxford Univ. Press, Oxford.

Wang, J., Christensen, D., Brynda, E., Andrade, J., Ives, J. & Lin, J. (1989). Sensitivity analysis of evanescent fiber optics sensors. *Proc. Soc. Photoopt. Inst. Eng.*, SPIE (1067), 44–52.

Journal of Fluorescence, Vol. 1, No. 1, 1991

Adsorption of Firefly Luciferase at Interfaces Studied by Total Internal Reflection Fluorescence Spectroscopy

Vladimir Hlady,[1,3] Ping-Yang Yeh,[2] and J. D. Andrade[1,4]

Received December 6, 1990; revised December 20, 1990; accepted December 20, 1990

The adsorption of luciferase onto silica surfaces was studied by total internal reflection fluorescence (TIRF) spectroscopy. Two model surfaces were used: hydrophilic and hydrophobic silica. Luciferase adsorbed differently on these two surfaces. Initial kinetics of luciferase adsorption onto the hydrophilic surface showed that luciferase adsorbs over an adsorption energy barrier of ≈3 kT. The quantum yield of luciferase fluorescence decreased at the hydrophilic silica surface, which indicated that the protein conformation was altered during adsorption. Luciferase adsorption onto the hydrophobic silica surface proceeded with a small adsorption energy barrier and the fluorescence efficiency of adsorbed protein remained unchanged after adsorption. The affinity of luciferase for luciferin was measured using quenching of luciferase fluorescence with luciferin. The binding constant of the adsorbed luciferase–luciferin complex at the hydrophilic silica surface was two orders of magnitude smaller than the respective binding constant in the solution. Adsorbed luciferase showed an absence of ATP-dependent visible luminescence, indicating that the adsorbed enzyme was not active at either of the two silica surfaces.

KEY WORDS: Adsorption; luciferase; luciferin; fluorescence quenching.

INTRODUCTION

The immobilization of enzymes to solid carriers is important to biotechnology, diagnostics, and sensing[1]. An enzyme is "immobilized" when its release into the solution and its surface mobility are restricted or constrained by some physical or chemical means. While covalent binding of enzymes to solid carriers is the most common immobilization method, physical adsorption of enzyme to the solid surface often precedes the formation of the covalent bond. In pure adsorption, the enzyme molecule bonds to the surface by a variety of physical forces, some of which may influence its orientation, conformation, and biological activity. An adsorbed enzyme may be desorbed by a change in ionic concentration, pH, or temperature. Exposures of adsorbed protein to other solution proteins may replace it from the surface by the mechanism of preferential adsorption. Thus, control of adsorbed enzymes is rather difficult to achieve and involves the selection of proper surface and solution conditions. The change of protein conformation at interfaces is not limited only to physically adsorbed proteins. It is possible that a covalently bound molecule of enzyme also interacts with the underlying surface in an adsorption-like manner, a process which may result in a conformational change of the enzyme and its subsequent inactivation.

This study investigates the role of the surface in the adsorption of firefly luciferase, an enzyme which cata-

[1] Department of Bioengineering, University of Utah, Salt Lake City, Utah 84112.
[2] Department of Material Science and Engineering, University of Utah, Salt Lake City, Utah 84112.
[3] On leave of absence from "Ruder Boskovic" Institute, Zagreb, Yugoslavia.
[4] To whom correspondence should be addressed at Department of Bioengineering MEB 2480, University of Utah, Salt Lake City, Utah 84112.

1053-0509/91/0300-0047$06.50/0

lyzes the production of yellow-green light from firefly luciferin in the presence of adenosine triphosphate (ATP), Mg^{2+}, and O_2. There has been an increased interest in firefly luciferase bioluminescence [2–15]. It stems from the fact that the emitted luminescence intensity is proportional to the amount of ATP in the system (so-called ATP-dependent luminescence). The specificity of firefly luciferase for ATP in the conversion of luciferin into luciferyl adenylate has been used to develop many different assays, some of which involve a covalently bound enzyme [16–20]. Firefly luciferase was covalently bound to alkylamine glass beads by Lee *et al.* [16], but the bound enzyme had only 0.16–0.67% of the activity of the soluble enzyme. Ugarova *et al.* [17] studied the activity and stability of immobilized firefly luciferase using several different carrier surfaces. The most active form was found when luciferase was immobilized on the polysaccharide carrier surfaces, such as Ultradex and Sepharose, i.e., on the surfaces which are known to have very weak nonspecific interactions with the bound proteins.

There is very little experimental evidence describing the interfacial properties of firefly luciferase. The present study was undertaken to fill this void and to understand the functioning of the surface-bound enzyme. A surface-sensitive spectroscopic method, total internal reflection fluorescence (TIRF) [21], was used to measure the intrinsic fluorescence emitted by adsorbed luciferase. The fluorescence emission quantum yield of adsorbed protein can be determined by analysis of the fluorescence emission of adsorbed luciferase and an independent measurement of the amount of adsorbed protein [22]. Intrinsic protein fluorescence is a sensitive probe of protein conformation, so that a change of the fluorescence quantum yield of adsorbed luciferase can be used as an indicator of protein conformation as the molecule adapts to its new environment. The purpose of this study was to elucidate the extent of the conformational changes of adsorbed luciferase at model hydrophilic and hydrophobic silica surfaces.

MATERIALS AND METHODS

Radiolabeling of Luciferase

Crystallized and lyophilized powder firefly luciferase (*Photinus pyralis*), D-luciferin, ATP, and glycylglycine were purchased from Sigma; $MgSO_4$ was from Mallinckrodt. All other chemicals were analytical grade. Firefly luciferase was labeled with carrier-free $Na^{125}I$ (100 mCi/ml, Amersham) by chloramine-T as described by Chuang *et al.* [23]. The labeling procedure was as follows: 1 mg of firefly luciferase was dissolved into 1 ml of 0.45 *M* glycylglycine buffer. Three hundred micrograms of luciferase was added to glycylglycine buffer to make a total volume of 0.5 ml. A volume corresponding to 300 μCi of $Na^{125}I$ was added to the luciferase solution. Fifty microliters of freshly made chloramine-T solution (Kodak, 4 mg/ml in deionized water) was added to the luciferase solution and was gently mixed for 1 min. Fifty milliliters of sodium metabisulfite solution (Fisher Scientific Co., 4.8 mg/ml in deionized water) was then added and the resulting solution was mixed for 2 to 3 min in order to stop the oxidation reaction. The labeled luciferase was immediately separated from the free iodine by Sephadex G-25 column (Pharmacia) [24]. The degree of protein labeling (labeled protein/total protein) was 0.90 to 0.95.

Surface Preparation and Chemistry

Two types of surfaces were prepared for the adsorption experiments: a hydrophilic surface and a hydrophobic surface. Both surfaces were prepared by cutting a fused silica microscope quartz slide (CO grade, ESCO) into smaller (12 × 10 × 1 mm) pieces. These small slides were polished on the edges by an abrasive paper, cleaned by immersing in hot (90°C) chromic acid for 1 h, cooled to room temperature, rinsed thoroughly with purified water (Milli-Q), and dried under vacuum at 100°C for 2 h. The cleanliness of the slides was checked by the Wilhelmy plate water contact angle technique [25]. A clean fused silica slide was used as the hydrophilic surface. Hydrophobic surfaces were prepared by immersing the clean quartz slide into a solution of 10% (v/v) dimethyldichlorosilane (DDS) (Petrarch System Inc.) in dry toluene for 15 to 30 min at room temperature. After the incubation, the slides were rinsed with ethanol three to five times and then rinsed in purified water. The slides were desiccated under vacuum at 100°C for 2 h. All surfaces were used within 48 h.

Adsorption Experiments

Preferential adsorption of iodinated firefly luciferase was studied by preparing luciferase solutions of the same final concentration (0.13 mg/ml in 0.45 *M* glycylglycine buffer, pH 7.8) but with different ratios of unlabeled to labeled luciferase: 0, 1, 2, 5, and 11. Hydrophilic slides were exposed to the solution mixtures of luciferase for 14 h. After adsorption, the slides were removed and rinsed with buffer and the associated radioactivity was counted. The amount of protein on each

slide was determined from the corresponding radioactivity counts of stock luciferase solution. The adsorption isotherm was measured in a similar manner by exposing the silica slides to labeled luciferase solutions of different concentrations for 14 h at room temperature.

Adsorption Kinetics Measured by the Total Internal Reflection Fluorescence (TIRF) Spectroscopy

The firefly luciferase solution (0.2 mg/ml) was prepared in 0.45 *M* glycylglycine buffer (pH 7.8). The protein concentration was determined by UV absorbance (E_{1cm} = 0.75 ml mg^{-1} cm^{-1} at 280 nm [3]). The TIRF cell was assembled by using the hydrophilic or hydrophobic silica plate as the adsorbing surface [22]. The TIRF cell was positioned so that the collimated light struck the solid/liquid interface at a 70° angle from normal (Fig. 1). Total internal reflection of perpendicularly polarized light at the silica/buffer interface created an evanescent surface wave. The electric field amplitude of the surface wave, $E\perp$, decays exponentially with distance z normal to the interface into the buffer solution:

$$E_\perp = E_{o,\perp}\, e^{-z/d_p} \quad (1)$$

$$d_p = \lambda[2\pi(n_1^2 \sin^2\theta - n_2^2)^{1/2}] \quad (2)$$

where $E_{o,}\perp$ is the electric field amplitude right at the interface, d_p is the depth of penetration, λ is the wavelength of the light, θ is the incident angle, and n_1 and n_2 are the refractive indices of silica and buffer solution, repsectively. The depth of penetration for the present TIRF cell configuration was 119 nm. The excitation and emission slits were 1 mm (8-nm half-width) and 2 mm (16-nm half-width), respectively. The fluorescence emission was excited at 285 nm and collected at 340 nm. The TIRF setup was calibrated prior to the adsorption experiments by following the procedure described in Ref. 22. L-5-Hydroxytryptophan methyl ester HCl (TrpOH) was used as an external standard. Adsorption was started by injecting 1 ml of the 0.2 mg/ml luciferase solution into the TIRF cell. The fluorescence signal was observed at the initial adsorption time and at other desired times. A shutter was used to protect the luciferase molecules from overexposure to UV light during the adsorption process. After 14 h of adsorption, the fluorescence signal was measured as the cell was flushed with glycylglycine buffer to remove nonadsorbed luciferase. The intensity of fluorescence due to adsorption of luciferase was converted into adsorbed mass of protein per unit area using the standard TIRF quantitation method [22]. This procedure ignores eventual changes of protein fluorescence emission efficiency due to adsorption. The quantum yield of adsorbed luciferase was determined by combining the TIRF results with the measurement of adsorbed amount of ^{125}I-labeled luciferase.

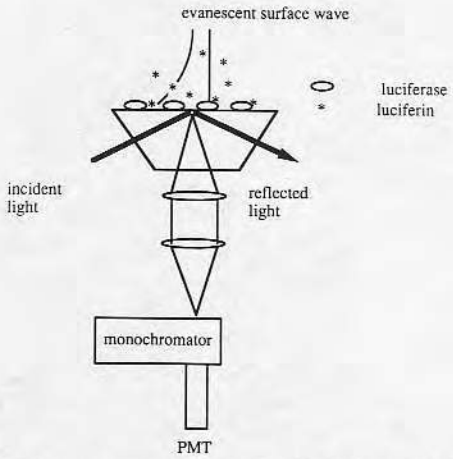

Fig. 1. A schematic picture of the TIRF cell and the optical geometry for the collection of surface fluorescence. The evanescent surface wave is not drawn to scale.

Quenching of Luciferase Fluorescence in Solution

Firefly luciferase solution was prepared in 0.45 *M* glycylglycine buffer (pH 7.8). The protein concentration was 0.2 mg/ml. This concentration was taken to be equal to 2.0 × 10^{-6} *M* by assuming that the molecular mass of protein is 100 kDa. Although this value differs from the molecular mass based on recent research on cDNA of luciferase (Mm ≈ 62 kDa [26]), it was chosen in order to compare the results of the present quenching experiments with published data [27]. Luciferin was used as a quencher. Aliquots of 10 μl of the luciferin solution (3.6 × 10^{-4} *M*) were introduced successively into a cuvette containing 1.0 ml of luciferase solution, and the intrinsic fluorescence spectra were obtained by a fluorometer operating in the photon counting mode (I.S.S., Inc., Greg 200; excitation, 285 nm; emission collected from 300 to 400 nm). A parallel quenching experiment was performed under the same conditions using the L-5-hydroxytryptophan methyl ester HCl (TrpOH) in the solution instead of luciferase. The TrpOH solution was prepared in 0.45 *M* glycylglycine buffer. The TrpOH concentration was adjusted so that the solution had the same UV absorbance (at 285 nm) as the 0.2 mg/ml luciferase solution. The quenching of TrpOH was used as correction for the inner filter effect, which occurs when the quencher absorbs at the same wavelengths as the protein and at the wavelengths of protein emission. The

fluorescence intensity was determined by integrating the background-corrected emission spectra. The fluorescence intensity of TrpOH was normalized to the fluorescence intensity of luciferase in order to correct for the difference in the emission quantum yields between TrpOH and luciferase. The quenched fluorescence of luciferase, F, was corrected in a subtractive manner, i.e., as $F = F_0 - (F_c - F_s)$, where F_0 is the fluorescence intensity of luciferase in the absence of the quencher, F_c is the normalized fluorescence intensity of TrpOH in the presence of the quencher, and F_s is the fluorescence intensity of luciferase in the presence of the quencher. One notes that, since both TrpOH and luciferase solution had the same UV absorbance, the subtractive manner of fluorescence correction also compensates for the dynamic quenching.

Quenching of Luciferase Fluorescence at the Solid/Liquid Interface

The procedure for luciferase adsorption was the same as described above. Luciferin solutions (6.0×10^{-3} M) were prepared in 0.45 M glycylglycine buffer (pH 7.8). This stock solution was then diluted with the glycylglycine buffer to produce quencher solutions with dilution factors of 0.50, 0.10, 0.05, 0.01, 0.005, and 0.001. After the nonadsorbed protein molecules were removed by the buffer and only luciferase was present at the solid/liquid interface, the luciferin solutions were introduced into the TIRF cell, starting with the least concentrated solution. The fluorescence was excited at 285 nm and emission recorded at 340 nm. After the quenching measurement with the most concentrated luciferin solution, 10 ml glycylglycine buffer solution was used to replace the quencher. This was done to determine if the intrinsic fluorescence signal will return to the original level, which was taken as a sign of no appreciable desorption of luciferase and no irreversible binding of luciferin to adsorbed luciferase. The increase in the evanescent surface wave intensity due to the increasing concentration of luciferin in the TIRF cell was very small (estimated <2%) and was neglected [22]. In the present TIRF experiment the fluorescence was collected normal to the surface, which is equivalent to the front-face geometry (Fig. 1), so that inner filter effects were absent.

Surface Tension of the Luciferase Solution

Kinetics of the surface tension of the luciferase solution (0.1 mg/ml in 0.45 M glycylglycine buffer, pH 7.8) were measured as a function of time using the Wilhelmy plate method, according to the procedure described by Wei [28].

RESULTS AND DISCUSSION

Adsorption Isotherms and Kinetics

When using iodine-labeled proteins in the adsorption experiments, one must ensure that there is no preferential interaction of either of the two protein populations with the surface. This was checked by repeating the same adsorption experiments with different ratios of unlabeled vs labeled luciferase, while keeping the total protein concentration constant. The expected surface radioactivity, calculated by assuming that the labeled luciferase adsorbs identically to the unlabeled luciferase, is given together with the experimental results in Fig. 2. The results suggested that neither labeled nor unlabeled luciferase preferentially adsorbs to the hydrophilic surface under given experimental conditions. However, in separate experiments it was found that the enzymatic activity of luciferase in solution was decreased after iodination; ^{125}I-labeled luciferase showed only about one-third the enzyme activity (measured as the intial peak of luminescence emission) of unlabeled luciferase.

The isotherms of luciferase adsorption at two different silica surfaces are given in Fig. 3. The equivalent Scatchard plots (not shown here) provided an estimate of the apparent binding constants and maximal surface coverages, Γ^{max}: in the case of the binding onto the

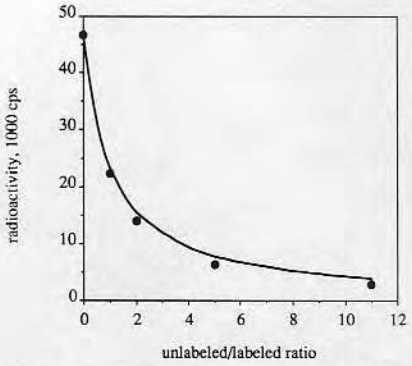

Fig. 2. Adsorbed amount of firefly luciferase as a function of the ratio of unlabeled versus labeled protein; the points are experimental results and the line is the adsorption calculated by assuming that unlabeled and labeled proteins adsorb identically. The total luciferase concentration (i.e., labeled + unlabeled protein) prior to adsorption was 0.13 mg/ml. Adsorption onto the hydrophilic silica surface was carried out for 14 h at room temperature.

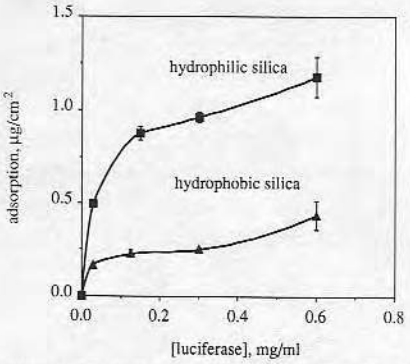

Fig. 3. The adsorbed amount of firefly luciferase on the two types of silica surfaces as a function of the solution concentration of protein. Each point represents the mean value of two separate experiments, while the error bars represent one standard deviation. Adsorption was carried out for 14 h from 0.45 *M*, pH 7.8, glycylglycine buffer at room temperature.

hydrophilic silica surface $K_{(hydrophilic)} = 0.0321$ L/g and $\Gamma^{max} = 1.062$ μg/cm², and for the binding to the hydrophobic silica surface $K_{(hydrophilic)} = 0.0151$ L/g and $\Gamma^{max} = 0.258$ μg/cm², respectively. The somewhat higher affinity in the case of the binding onto the hydrophobic surface was expected since firefly luciferase is a very hydrophobic protein: about 60% of the amino acids of luciferase are hydrophobic. It was found that the adsorbed amount of luciferase at the hydrophilic surface is much higher than at the hydrophobic surface. One hypothesis is that the high content of hydrophobic amino acids in luciferase causes an aggregation of protein at the hydrophilic surface. This hypothesis was supported by the observation that luciferase readily aggregates in the solution. Thus, if the adsorption of luciferase leads to the neutralization of electrical charges of protein and surface, lateral aggregation could be driven by the hydrophobic interactions between the adsorbed molecules. On the other hand, the adsorption of luciferase onto the hydrophobic surface may result in protein molecules at the surface which are charged so that the electrostatic repulsion opposes a dense surface packing. Accordingly, the different levels of the plateau of the adsorption isotherms (Fig. 3) may reflect a difference in the lateral interactions between adsorbed protein.

The amount of luciferase adsorbed for 14 h was calculated from the TIRF measurements using the calibration curves prepared by the extrinsic fluorescence standards. In this calculation the fluorescence emission quantum yield of adsorbed luciferase, $\phi_{surface}$, was assumed to be identical to the emission quantum yield of luciferase in the buffer solution, $\phi_{solution}$, i.e., that $\phi_{surface}/\phi_{solution} = 1$. The TIRF-measured adsorption of 0.25 μg/cm² on the hydrophobic silica surface was identical to the luciferase adsorption determined by the ^{125}I-labeled protein (0.25 μg/cm², Fig. 3), indicating that the assumption about the same fluorescence quantum yields was indeed true for this surface. In the case of the hydrophilic silica surface, the TIRF-measured adsorption amounted to 0.11 μg/cm², while the adsorption determined by the ^{125}I-labeled protein was 0.90 μg/cm² (Fig. 3). Accordingly, the emission quantum yield of adsorbed luciferase at the hydrophilic silica surface, $\phi_{surface}/\phi_{solution}$, was found to decrease to 0.12.

The fluorescence quantum yield of proteins with few tryptophanyl residues can often be used as a measure of local change in protein conformation [22]. In the case of multitryptophanyl proteins, the fluorescence intensity is often not proportional to the number or to the concentration of fluorophores. This is due to the excitation energy homotransfer, which has a higher probability when a large number of fluorophores or molecules are densely packed in a relatively small volume. Therefore, the decrease in luciferase fluorescence efficiency upon adsorption onto the hydrophilic surface could not be used to differentiate whether the observed effect is due to a conformational change in the adsorbed protein molecule, to its aggregation on the surface, or to some combination of both. The examination of the fluorescence emission spectra did not show any significant differences between protein on silica surfaces and protein in solution.

The adsorption of luciferase at the air/water interface, which may be considered as an ideal hydrophobic interface, causes the surface tension to decrease rapidly from approximately 73.0 dyne/cm ($t = 0$) to 48 dyne/cm ($t = 2$ h) (Fig. 4). This result supports the hypothesis that luciferase adsorption onto hydrophobic surfaces is

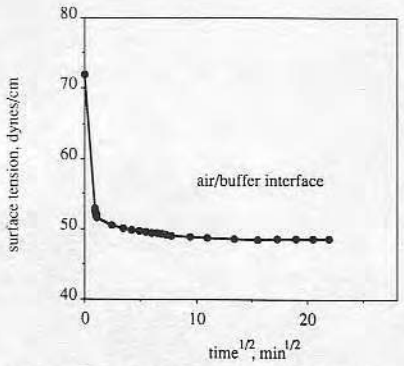

Fig. 4. Surface tension of 0.1 mg/ml firefly luciferase solution in 0.45 *M*, pH 7.8, glycylglycine buffer given as a function of time$^{1/2}$.

driven by the high effective hydrophobicity of the protein. It is instructive to compare the surface tension results with the surface tension of two other proteins, lysozyme and serum albumin [28], performed at comparable concentrations. Lysozyme lowers the surface tension of phosphate buffer solution from 73.0 to 63 dyne/cm, while serum albumin, which is known to be a very surface active protein [28], lowers the surface tension of water from 72.5 to 50 dyne/cm. The implications are that luciferase is also a protein of high surface activity.

The kinetics of luciferase adsorption on silica surfaces are similar to the kinetics of binding to the air/buffer interface. Figure 5 shows the adsorption of firefly luciferase (from solution of $c_p = 0.2$ mg/ml) as a function of (time)$^{1/2}$ onto hydrophilic and hydrophobic silica surfaces. The amount adsorbed was calculated from surface fluorescence intensities and corrected for the change in the $\phi_{surface}/\phi_{solution}$ ratio. Luciferase adsorbed onto the hydrophilic surface at a slow adsorption rate, while a rapid increase in luciferase surface concentration was observed in the case of the hydrophobic surface. Adsorption onto the hydrophobic surface was very similar to the fast binding of the same protein to the air/buffer interface (Fig. 4). The initial part of the adsorption kinetics onto the hydrophilic silica surface suggested that the rate-limiting step in luciferase adsorption was not the transport of the protein to the surface but, rather, its slow rate of binding to the surface binding sites. The slow increase in surface fluorescence indicated that the first

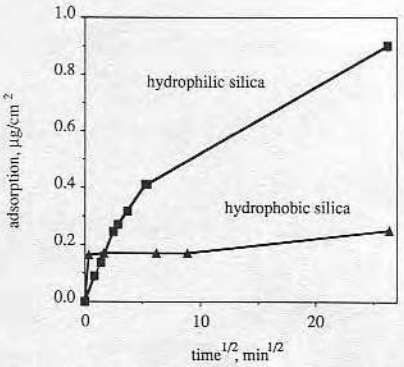

Fig. 5. Adsorption kinetics of firefly luciferase onto the two types of silica surfaces. The binding of luciferase, which was measured using the TIRF technique, is given as a function of time$^{1/2}$. The adsorbed amount was corrected for the fluorescence quantum yield decrease using the adsorption results obtained with ^{125}I-labeled luciferase. Adsorption was carried out from 0.2 mg/ml luciferase solution in 0.45 *M*, pH 7.8, glygylglycine buffer at room temperature from stagnant solution.

luciferase molecules bound to the surface already fluoresced with a decreased quantum yield; in other words, the conformational changes of the adsorbed protein molecules were immediate. In contrast, the much faster increase in luciferase surface concentration during adsorption onto the hydrophobic surface indicated efficient "sticking" of protein molecules, probably in their native form.

The adsorption kinetics results (Fig. 5) can be used to obtain an estimate of the energy barrier for the adsorption of luciferase. The adsorption energy barrier, E_a, can be found from the ratio of the experimentally measured initial adsorption rate, $k_{(exp)}$, and the maximally achievable adsorption rate, $k_{(max)}$:

$$\{k_{(exp)}/k_{(max)}\}_{t\to 0} = \exp(-E_a/kT) \qquad (3)$$

The maximum adsorption rate at the onset of adsorption is often limited by the transport of molecules from bulk solution to the surface. In the case of a surface which acts as a perfectly adsorbing barrier (i.e., an ideal adsorption sink), every protein molecule which is transported to the surface becomes adsorbed. If the solution is quiescent and diffusion is the only way by which the molecule can reach the surface, the interfacial concentration of protein per unit area is given by the classical formula [29]:

$$\Gamma_{(pot)}(t) = 2\, c_p\, (D/\pi)^{1/2} t^{1/2} \qquad (4)$$

where D is the protein diffusion coefficient (estimated as 5.0×10^{-7} cm^2/s for firefly luciferase), t is the adsorption time, and c_p is the concentration of protein in bulk solution. Using the results from Fig. 5 one can find the initial slope, $\Delta\Gamma_{(exp)}/\Delta(t^{1/2})_{t\to 0}$, and compare it with the slope from Eq. (4), which equals $c_p\,(D/\pi)^{1/2}$. Conditions under which Eq. (4) can be compared with the experiment exist only at the very beginning of the adsorption process. In such a case, the value of $[\Delta\Gamma_{(exp)}/\Delta(t^{1/2})_{t\to 0}]/[c_p\,(D/\pi)^{1/2}]$ can be used to replace $[k_{(exp)}/k_{(max)t\to 0}$ in Eq. (3) in order to estimate the value of E_a. This approximation is valid only at very low surface coverages. Once the surface is partly filled with the adsorbed protein, the assumption that the surface acts as an ideal sink fails to be correct and Eq. (4) can no longer be applied.

The energy barrier for luciferase adsorption onto the hydrophilic silica surface was $E_a \approx 3$ kT. Luciferase adsorption onto the hydrophobic surface proceeds with an apparent energy barrier of $E_a < 1$ kT. The estimates of E_a values follow the order of the apparent binding constants determined from the adsorption isotherms: the larger the apparent binding constants, the larger the energy barrier as observed from the initial kinetics measurements.

Fluorescence Quenching with Luciferin

The adsorption results from the previous section result in the following hypotheses: luciferase is a hydrophobic protein and easily undergoes aggregation in solution. When it adsorbs to the hydrophilic surface, it does so with a low "sticking" coefficient (high E_a); it becomes conformationally unstable (decrease in the $\phi_{surface}/\phi_{solution}$ ratio) and/or possibly aggregates at the interface (high Γ^{max}). When it adsorbs to the hydrophobic surface, it does so efficiently (low E_a) and probably retains at least parts of its native conformation (no change in the $\phi_{surface}/\phi_{solution}$ ratio). One way to test these hypotheses is to investigate the accessibility of luciferase binding sites to luciferin (LH_2) when the only protein present in the system is in the adsorbed state at the silica/buffer interface. It is known that the binding of luciferin quenches the intrinsic fluorescence of luciferase [27]. The quenching constant is expected to reflect the accessibility of the binding site and/or the binding affinity of luciferase toward luciferin and whether or not that has changed upon adsorption.

Figure 6 shows the modified Stern–Volmer plots for luciferase fluorescence quenching in the bulk solution. Figure 7 shows the same plot for quenching at the two types of silica/buffer interfaces. Several features of these plots deserve additional comments. Standard fluorescence quenching plots (F_o/F vs $[LH_2]$) showed an upward curvature which could not be corrected by replotting the data in the form which would allow differentiation between static and dynamic quenching, i.e., as $[(F_o/F) - 1)]/[LH_2]$ vs $1/[LH_2]$. Hence, modified Stern–Volmer plots were used in order to compare the results of the present study with the results from the literature [27]. The downward curvature of the modified Stern–Volmer plots implied that there were at least two different luciferin binding sites, each with a significantly different binding constant. This conclusion is consistent with the stoichiometric relation between luciferin and the luciferase used [30]. The quenching constants (K_{QS}) and accessible fractions of tryptophanyl residues (f_a) were determined from the slopes of the modified Stern–Volmer plots using only the high $1/[LH_2]$ region (i.e., data obtained at very low luciferin concentrations). It was assumed that in this quencher concentration range, the luciferase fluorescence was quenched entirely due to the binding of luciferin to the luciferase high-affinity binding site. In such a case the quenching constant is equivalent to the binding constant of quencher to the substrate [31, 32]. Calculation of the constants in the low $1/[LH_2]$ region was not attempted because of the possibility that dynamic quenching in solution at high luciferin concentrations was not entirely corrected by subtraction of the quenched TrpOH fluorescence. Dynamic quenching of surface-bound fluorophores is not expected to be the same as quenching of flurophores in solution. This is due to spatial restrictions between the quencher and the surface-

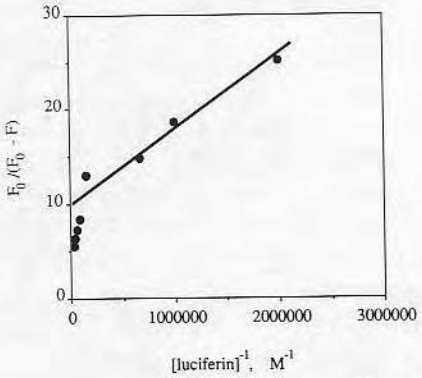

Fig. 6. Modified Stern–Volmer plot for the quenching of firefly luciferase fluorescence with luciferin in the bulk solution. The concentration of luciferase was 0.2 mg/ml (2.0×10^{-6} *M*) in 0.45 *M*, pH 7.8 glycylglycine buffer. The quenched fluorescence, *F*, was calculated as $F = F_0 - (F_c - F_s)$, where F_0 is the fluorescence intensity of luciferase in the absence of the quencher, F_c is the corrected fluorescence intensity of TrpOH in the presence of the quencher, and F_s is the fluorescence intensity of luciferase in the presence of the quencher.

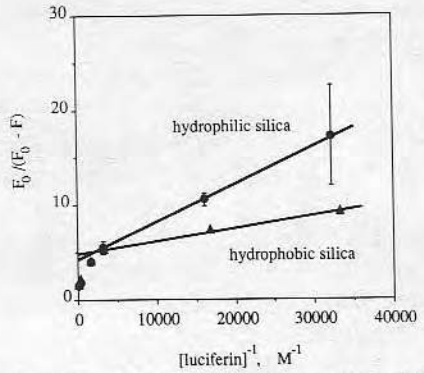

Fig. 7. Modified Stern–Volmer plot for the quenching of fluorescence of adsorbed firefly luciferase with luciferin. Luciferase was adsorbed onto the two types of silica surfaces from the 0.2 mg/ml solution prepared in 0.45 *M*, pH 7.8, glycylglycine buffer. Any nonadsorbed protein has been removed from the TIRF cell by the buffer flush. *F* is the quenched fluorescence and F_0 is the fluorescence intensity of adsorbed luciferase in the absence of the quencher, both measured in the TIRF optical geometry. No corrections for the inner filter effect have been applied. In the case of hydrophilic silica, each point represents the mean value of two separate experiments, while the error bars represent one standard deviation. Similar experimental errors are expected in the case of hydrophobic silica.

bound fluorophore molecules. Hence, it is questionable whether any accurate corrections for the dynamic quenching can be made in the case of adsorbed luciferase. No attempt was made to determine the dynamic portion of the observed quenching by fluorescence lifetime measurements. The Stern–Volmer quenching constants, K_{QS}, and accessible fluorophore fractions, f_a, are listed in Table I. One notes that K_{QS} changes by a factor of 100 upon adsorption of luciferase onto the hydrophilic silica surface. This dramatic difference between the solution and the surface quenching constants indicated that the binding affinity and/or the accessibility of the luciferin binding site had drastically changed upon adsorption. The changes are not so dramatic in the case of the hydrophobic silica surface: K_{QS} decreases by a factor of 26 from the respective solution value. Dement'eva *et al.* [27] investigated the binding of luciferin to firefly luciferase in solution using the same fluorescence quenching technique in the 0–20 μM luciferin concentration range. From the modified Stern–Volmer plot they reported an average binding constant, $K \approx 10^5\ M^{-1}$, for the range of solution pH values. However, they did not correct for dynamic quenching.

The differences between the two silica surfaces are not so illustrative in the case of the observed f_a values: f_a increases from 0.1 (solution) to 0.2 (hydrophobic silica) and to 0.24 (hydrophilic silica). It is uncertain, however, whether protein-bound luciferin quenches the same population of luciferase tryptophanyl residues at these two surfaces. The fluorescence quantum yield of luciferase was decreased upon adsorption at the hydrophobic silica surface. A possible conformational change of adsorbed protein at this surface might have changed the average distance between tryptophanyl residues and the bound quencher. Hence, the f_a values can not be interpreted unambiguously.

The luciferin quenching experiments were followed by the assay of light emission, in which luciferin was added together with ATP, Mg^{2+}, and O_2 to the adsorbed luciferase. No ATP-dependent visible luminescence was observed from the bound enzyme on either of the two surfaces, indicating that adsorption had resulted in inactivation of the enzyme.

Table I. Fluorescence Quenching Parameters for Firefly Luciferase in the Adsorbed State and in the Solution

System	f_a	K_{SQ}/M^{-1}
Luciferase in 0.45 *M* glycylglycine buffer solution	0.10	1.0×10^6
Luciferase adsorbed on hydrophobic silica surface	0.20	3.8×10^4
Luciferase adsorbed on hydrophilic silica surface	0.24	1.0×10^4

CONCLUSIONS

This study showed that the interfacial behavior of luciferase is determined largely by its hydrophobic nature. Luciferase adsorption onto hydrophobic silica surfaces and to air/buffer interfaces proceeds very fast as compared with its binding to hydrophilic silica. The initial slopes of the adsorption kinetics provided an estimate of the adsorption energy barrier, which was found to be larger for hydrophilic ($\approx$3 kT) than for hydrophobic (<1 kT) surfaces. The adsorption isotherm indicated that the enzyme, although it adsorbs relatively slowly, does aggregate on the hydrophilic silica surface. The plateau of the adsorption isotherm obtained on the hydrophilic silica surface was several times higher than the respective adsorption plateau found in the case of adsorption onto the hydrophobic surface. Comparison between the calibrated fluorescence intensity from adsorbed luciferase and the adsorbed amount as determined with ^{125}I-labeled luciferase showed that the fluorescence emission quantum yield of adsorbed protein is unchanged at the hydrophobic surface but decreased in the case of the hydrophilic surface. Further support for the change of enzyme conformation and/or aggregation at hydrophilic surfaces was found from fluorescence quenching of intrinsic luciferase fluorescence with luciferin. The luciferin binding constant to the high-affinity luciferase binding site decreased approximately 100 times upon protein adsorption to the hydrophilic silica surface, as compared with the respective binding affinity of the luciferase–luciferin complex in the solution. As judged from the absence of any ATP-dependent luminescence, luciferase was not enzymatically active upon adsorption at either of the two silica surfaces.

The luciferase used here was obtained from firefly lanterns using classical extraction, purification, and stabilization procedures (Sigma Chemical Co.). We are currently extending this study using pure firefly luciferase prepared by recombinant techniques (Amgen, Inc).

ACKNOWLEDGMENTS

The authors would like to acknowledge Protein Solutions, Inc., for support of the experimental work (P.-Y. Yeh). V. Hlady acknowledges financial assistance

from the Center for Biopolymers at Interfaces, University of Utah, a University–Industry–State consortium, and the Self-Management Council for Scientific Research of Croatia, Yugoslavia.

This paper was submitted by P.-Y.Y. in partial fulfillment of the M.S. degree, Department of Material Science and Engineering, University of Utah.

REFERENCES

1. K. Mosbach (Ed.) (1988) *Immobilized Enzymes and Cells, Methods in Enzymology, Vols. 135, 136, and 137*, Academic Press, New York.
2. M. DeLuca (Ed.) (1978) *Bioluminescence and Chemiluminescence, Methods in Enzymology, Vol. 57,* Academic Press, New York.
3. M. DeLuca (1969) *Biochemistry* **8,** 160–166.
4. M. DeLuca and M. Marsh (1967) *Arch. Biochem. Biophys.* **121,** 233–240.
5. M. DeLuca and W. D. McElroy (1974) *Biochemistry* **13,** 921–925.
6. W. D. McElroy and M. DeLuca (1981) in M. DeLuca and W. D. McElroy (Eds.), *Bioluminescence and Chemiluminescence*, Academic Press, New York, pp. 179–186.
7. W. D. McElroy and H. H. Seliger (1961) in W. D. McElroy and B. Glass (Eds.), *Light and Life*, Johns Hopkins Press, Baltimore, p. 219.
8. A. A. Green and W. D. McElroy (1956) *Biochim. Biophys Acta* **20,** 170–176.
9. W. C. Rhodes and W. D. McElroy (1958) *J. Biol. Chem.* **233,** 1528–1537.
10. M. DeLuca, G. W. Writz, and W. D. McElroy (1960) *Biochemistry* **3,** 935–939.
11. S. C. Alter and M. DeLuca (1986) *Biochemistry* **25,** 1599–1605.
12. J. L. Denburg, R. T. Lee, and W. D. McElroy (1970) *Arch. Biochem. Biophys.* **134,** 381–394.
13. J. Travis and W. D. McElroy (1966) *Biochemistry* **5,** 2170–2176.
14. F. Gorus and E. Schram (1979) *Clin. Chem.* **25,** 512–519.
15. T. P. Whitehead, L. J. Kricka, T. J. W. Carter, and G. H. G. Thorpe (1979) *Clin. Chem.* **25,** 1531–1546.
16. Y. Lee, I. Jablonsky, and M. DeLuca (1977) *Anal. Biochem.* **80,** 496–501.
17. N. N. Ugarova, Yu. L. Brovko, and N. V. Kost (1982) *Enzyme. Microb. Technol.* **4,** 224–228.
18. N. N. Ugarova, L. Yu. Brovko, and I. V. Berezin (1980) *Anal. Lett.* **13,** 881–892.
19. C. Carrea, R. Bovara, G. Mazzola, S. Girotti, A. Roda, and S. Ghini (1986) *Anal. Chem.* **58,** 331–333.
20. L J. Blum, P. R. Coulet, and D. C. Gautheron (1985) *Biotech. Bioeng.* **27,** 232–237.
21. V. Hlady, R. A. Van Wagenen, and J. D. Andrade (1985) in J. D. Andrade (Ed.), *Surface and Interfacial Aspects of Biomedical Polymers. Vol. 2. Protein Adsorption*, Plenum Press, New York, pp. 81–119.
22. V. Hlady, D. R. Reinecke, and J. D. Andrade (1986) *J. Colloid Interface Sci.* **111,** 555–569.
23. H. Y. K. Chuang, W. F. King, and R. G. Mason (1978) *J. Lab. Clin. Med.* **92,** 483–496.
24. G. P. Tuszynski, L. Knight, J. R. Piperno, and P. N. Walsh (1980) *Anal. Biochem.* **106,** 118–122.
25. J. D. Andrade, L. M. Smith, and D. E. Gregonis (1985) in J. D. Andrade (Ed.), *Surface and Interfacial Aspects of Biomedical Polymers. Vol. 1. Surface Chemistry and Physics*, Plenum Press, New York, pp. 249–292.
26. J. R. De Wet, K. Y. Wood, M. DeLuca, D. R. Helinski, and S. Subramani (1987) *Mol. Cell. Biol.* **7,** 725–737.
27. E. I. Dementéva, L. Yu. Brovko, E. N. Druzhinina, O. A. Gandelman, and N. N. Ugarova (1986) *Biokhimiya (Russ.)* **51,** 130–142.
28. A. P. Wei (1990) *M.Sc. thesis*, University of Utah, Salt Lake City.
29. A. F. H. Ward and L. Tordai (1946) *J. Chem. Phys.* **63,** 485–488.
30. W. D. McElroy and M. DeLuca (1985) in G. A. Kerkut and L. I. Gilbert (Eds.), *Comprehensive Insect Physiology Biochemistry and Pharmacology, Vol. 4*, Pergamon Press, New York, pp. 553–563.
31. J. R. Lakowicz (1983) *Principle of Fluorescence Spectroscopy*, Plenum, New York.
32. M. R. Eftink and C. A. Ghiron (1981) *Anal. Biochem.* **114,** 199–231.

Ab Hlad-5-1992
Surfaces in Biomaterials

PLASMA PROTEIN ADSORPTION ON MODEL AND BIOMATERIAL SURFACES

Vladimir Hlady, Joseph D. Andrade, Chih-Hu Ho,
Kevin Tingey, Yeong-Shang Lin and A. Scott Lea

University of Utah,
Department of Bioengineering,
Salt Lake City, UT 84112

Introduction

It is often stated that the first readily observable event at the interface between a material and a biological fluid is adsorption of macromolecular components from the fluid(1). Plasma contains over 200 proteins. Within seconds after initial contact of blood with an artificial surface the over 200 different blood proteins begin to collide with- and competitively adsorb onto the interface. Very few proteins have been studied with respect to interfacial activity and adsorption. The results obtained during the past five years of plasma protein adsorption research reflect the complexity of this problem (2,3,4). Recent recognition of a competitive plasma protein adsorption process (the "Vroman effect") has shown that plasma protein adsorption is a complex and highly interactive molecular process in which an interfacially active "trace" protein can dominate the adsorption process under certain conditions (5,6). Due to technique and resource constraints, competitive plasma protein adsorption studies are usually limited to a small number of plasma proteins (7,8,9). Studying the interfacial behavior of all 200 plasma proteins would be a stupendous task. A true understanding of the complex phenomena requires a combination of several experimental approaches.

We are addressing the problem of protein adsorption complexity at several levels by:

- studying adsorption of small, model protein adsorption at air/water (10) and model solid/water interface,
- studying adsorption of plasma proteins onto wettability "gradient" surfaces(11,12) and on surfaces of biomaterials, and
- observing the process of adsorption of large plasma proteins onto crystal surfaces by atomic force microscopy (13,14).

Adsorption from the complex protein mixtures or dilute plasma detected by a quantitative 2-D PAGE

One of the methods to study protein adsorption from dilute plasma onto the high surface area adsorbent is a quantitative, high resolution, two-dimensional polyacrylamide gel electrophoresis technique (2-D PAGE). Two main advantages of the 2-D PAGE technique as applied to protein adsorption are that it can identify the proteins removed from the protein mixture by a biomaterial surface, and that it can measure simultaneously and in a quantitative way the adsorbed amounts of tens of plasma proteins without any special labels. There are some disadvantages; the 2-D PAGE protein adsorption experiments are based on a depletion of proteins from solution rather than on direct analysis of the adsorbed layer. Hence, this approach requires a high surface area adsorbent and/or dilution of plasma. The solution concentration of some proteins will not be changed significantly enough to be detected by 2-D PAGE. In addition, some proteins may not be present in plasma in either sufficient quantities to be quantitatively detected in 2-D PAGE gels or, their positions in the 2-D PAGE gels have not been identified yet.

In this study we will report on protein adsorption onto three different types of biomaterials: a) calcium hydroxyapatite, b) low temperature isotropic carbon particles, and c) polyetherurethane particles.

Figure 1 show three-dimensional 2-D PAGE gel maps of the plasma solution (1/30 dilution) before (upper panel) and after contact with the CaHA surface (lower panel). The numbers associated with the "peaks" indicate individual proteins spots and are listed in the figure caption. Comparison of upper and lower panels shows that many proteins have been removed from the plasma solution by adsorption onto the surface of CaHA particles. By titrating the plasma solution with different amounts of CaHA particles one can construct how individual proteins distributed themselves between the surface of the adsorbent and the diluted plasma solution. This approach has been used with all three different biomaterials.

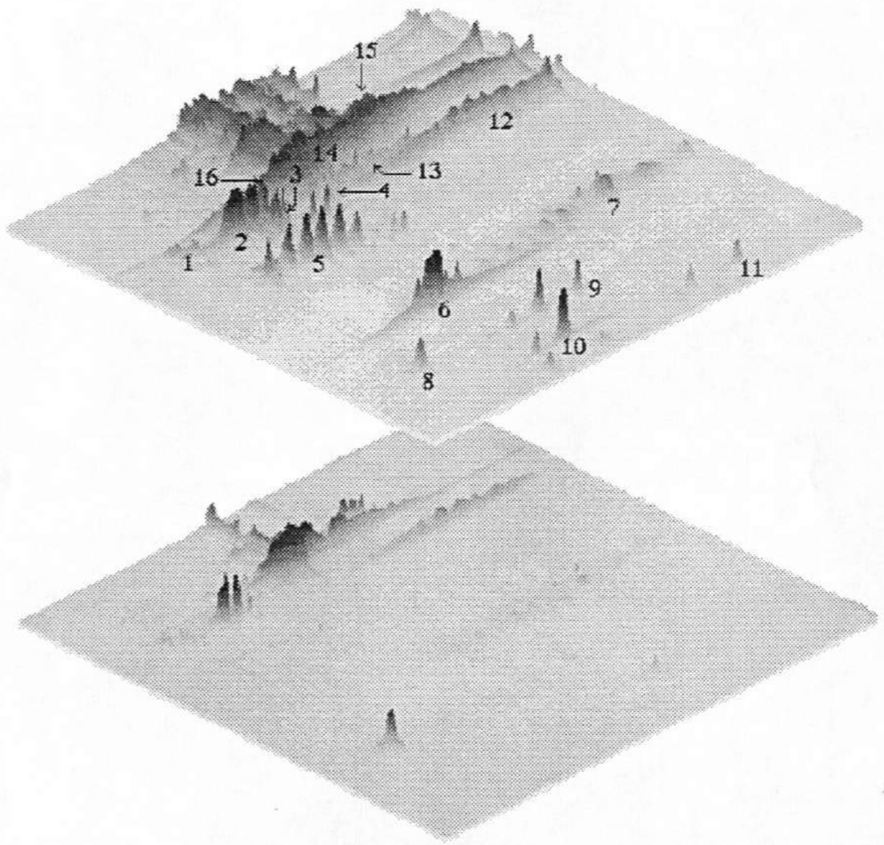

Figure 1. The 2-D PAGE map of plasma proteins (1/30 dilution) proteins before adsorption onto the CaHA surface (upper panel) and after adsorption onto the CaHA surface (lower panel, total surface area of CaHA was 3.81 m^2, total volume was 1.5 ml). Proteins: 1) α_1-antichymotrypsin, 2) α_1-antitrypsin, 3) Gc-globulin, 4) fibrinogen γ chain, 5) haptoglobin β chain, 6) apo A-I, 7) immunoglobulin λ and κ chains, 8) trypsin inhibitor (external standard), 9) haptoglobin α_2 chain, 10) prealbumin, 11) hemoglobin β chain, 12) immunoglobulin γ chain, 13) fibrinogen β chain, 14) albumin, 15) transferrin, 16) antithrombin III.

Adsorption of proteins from ternary mixture onto the gradient surfaces studied by spatially resolved total internal reflection fluorescence

Total internal reflection fluorescence (TIRF), has been successfully applied to the quantitative analysis of protein adsorption at solid surfaces (15,16). Using TIRF one can determine:

- the amount of adsorbed protein and protein adsorption kinetics,
- the conformational and orientational states of adsorbed protein, and
- the interaction of an adsorbed protein with ligand.

TIRF can be modified to provide for a spatial resolution of protein adsorption along one of the linear dimension of, so-called, wettability gradient surfaces (17). The novelty of the new TIRF technique is that it measures temporaly- and spatially-resolved binding of protein to surfaces. The temporal resolution of 1 sec and the spatial resolution of 50 μm were achieved using fluorescein-labeled protein and the spectroscopic imaging with the charge coupled device (CCD). Figure 2 shows the course of IgG adsorption of IgG the buffer solution which, in addition to FITC-IgG, contained unlabeled albumin (Alb) and fibrinogen (Fbn). The latter system, IgG + Alb + Fbn, is interesting because it can serve as a model system for studying interactions between the surfaces of biomaterials and plasma proteins. The transient adsorption of FITC-IgG in the intermediate surface wettability demonstrates the dynamic nature of the "Vroman-effect.

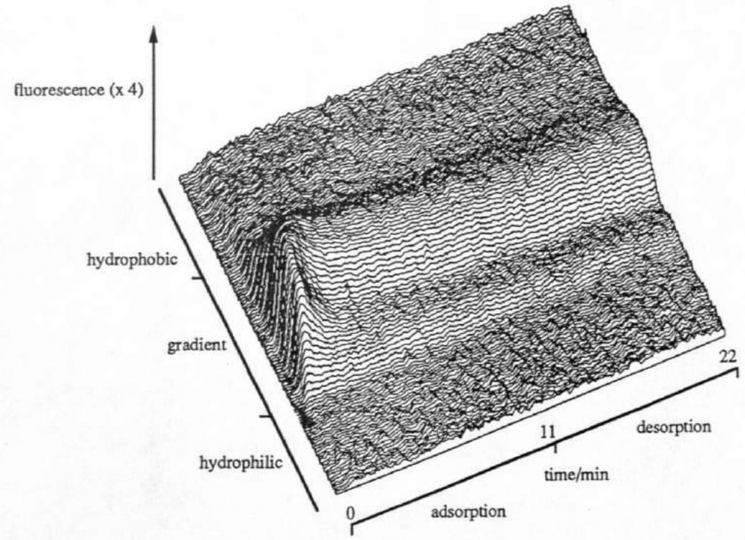

Figure 2. The three-dimensional presentation of the composite image obtained from the experiment of FITC-IgG adsorption/desorption kinetics from the buffer solution (cIgG = 0.013 mg/ml) which contained albumin and fibrinogen (cAlb = 0.041 mg/ml and cFbn = 0.003 mg/ml, respectively). The original image (1200 by 384 pixels, 14 bits/pixel) was compressed to a 394 by 122 pixels, 8 bits/pixel for sake of clarity, and smoothed by a Gaussian smoothing 7 x 7 kernel using image analysis software (Image 1.28c, W. Rasband, NIH). Three regions of the wettability gradient surface and adsorption/desorption times are indicated.

Atomic force microscopy of IgM adsorption on mica

The ability of the atomic force microscope (AFM) to image nonconductors in both air and aqueous environments has enabled it to be used as a research instrument for the biological community. To directly observe the dynamics of the protein adsorption processes, we followed the adsorption of an IgM on mica. IgM has a molecular weight of 900 kDa and its tertiary structure when viewed by electron microscopy resembles a five-pointed star. The IgM is a mouse monoclonal antifluorescyl antibody (clone 18-2-3). To conduct the IgM adsorption experiment, mica was first imaged under pH 8.0 phosphate buffer saline (PBS) in a fluid cell. The PBS was then exchanged for a 20 μg/mL IgM solution in pH 8.0 PBS. The experiment was performed at pH 8.0, the isoelectric point of the IgM clone, where adsorption of the protein would be maximum and the lateral interactions between the proteins would be the greatest, due to decreased electrostatic repulsion. A very small area was initially scanned in order to minimize the effect of the cantilever tip on the adsorbing protein while the applied force was being minimized. Once the force was minimized, the scan area was increased to 3000 nm by 3000 nm and the adsorption process was observed using constant force mode (4 nN).

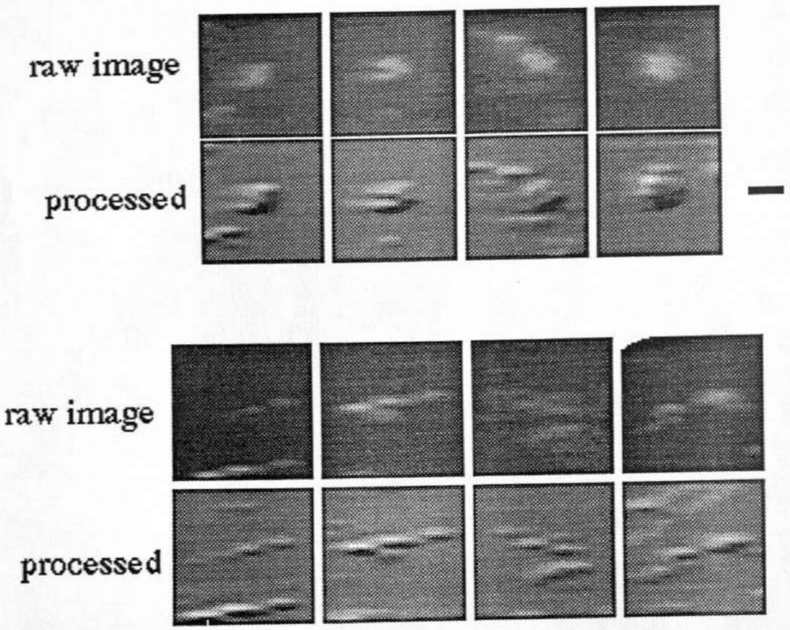

Figure 3 shows two distinct morphological features found by AFM during the first minute of the adsorption-scanning time. The bar on the right side is 60 nm long. As the raw images do not allow sufficient differentiation between the features, the image processing with a bar-relief algorithm was used. The upper two rows show the AFM images of surface-bound IgM in a presumably native state; the lower two rows present the AFM images of the denatured protein, presumably by the action of the scanning AFM tip.

References

1 J. D. Andrade and V. Hlady, Adv. Polym. Sci., **79** (1986) 1.

2 E.F. Leonard, V.T. Turrito and L. Vroman, Eds, "Blood in Contact with Natural and Artificial Surfaces", Ann. New York Acad. Sci., **516** (1987) entire volume.

3 J.D. Andrade, Ed., "Surface and Interfacial Aspects of Biomaterials, Vol. 2., Protein Adsorption", Plenum Press, 1985.

4 T. A. Horbett and J. L.Brash, Eds, "Proteins at Interfaces", ACS Symp. Ser. 1987, also J. Colloid and Interface Science, vol **111** (1986) entire volume.

5 L. Vroman and A.L. Adams, J. Biomed. Mat. Res., **3** (1969) 43.

6 L. Vroman, A.L. Adams, G.C. Fisher, P.C. Munoz and M. Stanford, Adv. Chem. Ser., **199** (1982) 264.

7 J. L.Brash and P. ten Hove, Thromb. Haemostas., **51** (1984) 326, also Macromol. Chem. Macro. Symp., **17** (1988) 441.

8 T. A. Horbett, Thromb. Haemostas., **51** (1984) 174.

9 S.M. Slack and T. A. Horbett, J. Colloid Interface Sci, **133** (1989)

10 A.-P.Wei M.Sc. Thesis, University of Utah, 1990.

11 C-G. Gölander, Y-S. Lin, V. Hlady and J. D. Andrade, Colloids and Surfaces **49** (1990) 289.

12 V. Hlady, Applied Spectroscopy, **45** (1991) 246.

13 J.-N. Lin, B. Drake, A. S. Lea, P. K. Hansma and J. D. Andrade, Langmuir, **6** (1991) 509.

14 A.S. Lea, A. Pungor, V. Hlady, J. D. Andrade, J. N. Herron and E. W. Voss Jr , in press, Langmuir, **8** (1992) 68.

15 V. Hlady, R. A. Van Wagenen and J. D. Andrade, in "Surface and Interfacial Aspects of Biomedical Polymers. Vol. 2. Protein Adsorption", (J. D. Andrade, Ed.), Plenum Press, N.Y. 1985. p 81.

16 V. Hlady, D. R. Reinecke and J. D. Andrade, J. Colloid Interface Sci. **111** (1986) 555.

17 H. Elwing, S. Welin, A. Askendahl, U. Nilsson and I. Lundström, J. Colloid Interface Sci. **119** (1987) 1.

Surfaces in *Biomaterials* Symposium

OCTOBER 14-16, 1992
Hyatt Regency Minneapolis Hotel
Minneapolis, MN

Sponsored by Surfaces in Biomaterials Foundation

Thursday, October 15, 1992

Nicollet Grand Ballroom A

SESSION III Surface Analysis II: Innovative Approaches

1:30 **Plasma Protein Adsorption on Model and Biomaterial Surfaces**
Invited Speaker: Vladimir Hlady
J D Andrade, C-H Ho, K Tingey, Y S Lin, A S Lea
Department of Bioengineering, University of Utah

2:10 **Force Measurements Between Diblock Copolymers Adsorbed on Mica in Aqueous Solutions**
M Tirrell, G-Z Mao, N Dan, C Amiel, P Guenoun, J Mays
Department of Chemical Engineering and Materials Science, University of Minnesota

2:30 **Contact and Non-Contact Atomic Force Microscopy of Type I Collagen**
D A Chernoff, E A G Chernoff, K Kioller
Advanced Surface Microscopy Inc

2:50 **NEXAFS and XPS Characterization of Self-Assembled Fluorocarbon Films**
D G Castner, K B Lewis, G R Llanos, B D Ratner
National ESCA and Surface Analysis Center for Biomedical Problems, University of Washington

3:10 **PM Break** Nicollet Grand Ballroom A3

3:30 **Characterization of Surfaces and Biomacromolecules Using Scanning Tunneling Microscopy (STM) and Atomic Force Microscopy (AFM)**
Invited Speaker: D Fennell Evans
S X Yang, Y Tsao
Center for Interfacial Engineering (CIE)
University of Minnesota

4:10 **Molecular Ion Imaging of Treated Human Hair at Sub-Micron Lateral Resolution Using TOF-SIMS**
F Reich, P M Lindley
Charles Evans and Associates

4:30 **End of Thursday Sessions**

5:00-6:30 **New Member Orientation** Suite 601

Representatives of corporations/institutions interested in Foundation membership are encouraged to attend this informal introduction. Member representatives will be available to answer questions and share their experiences.

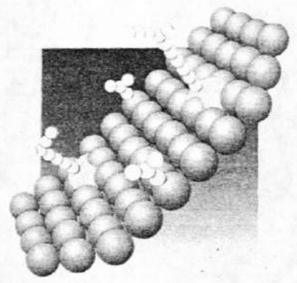

Clinical Materials **13** (1993) 85–93

Plasma Protein Adsorption on Model Biomaterial Surfaces*

V. Hlady‡

'Ruder Boskovic' Institute, 41000 Zagreb, Croatia

J. D. Andrade, C.-H. Ho, L. Feng & K. Tingey

The Center for Biopolymers at Interfaces, University of Utah, Salt Lake City, Utah 84112, USA

Abstract: The study of plasma protein adsorption onto biomaterial surfaces using a quantitative, high-resolution, two-dimensional polyacrylamide gel electrophoresis technique (2-D PAGE) is reported. Surfaces of three different types of biomaterial were examined: calcium hydroxyapatite, low-temperature isotropic carbon particles, and polyetherurethane particles. All three biomaterials were found to bind, simultaneously and in a kinetic dependent way, a number of plasma proteins. In the case of CaHA, the experimental titration of diluted plasma with the adsorbent allowed calculation of the adsorption isotherms and permitted estimation of the affinity of individual proteins for the surface. In the case of an LTI carbon surface, the kinetics of binding were different for different proteins; fibrinogen was completely removed in 10 min from diluted plasma, while the adsorption kinetics of other proteins were slower and resulted only in their partial removal from solution. The surface of carbon was also found to be morphologically heterogeneous due to the different orientation of carbon crystallites. This might have an effect on the binding of some larger plasma proteins, like fibrinogen. The polyurethane surface might also have been heterogeneous; it is thought to consist of separate microdomains of hard and soft segments. The present results indicated that some proteins, like hemopexin, might have an extraordinary affinity for PU surfaces. Advantages and disadvantages of the 2-D PAGE technique applied to the study of biomaterial–protein interactions are discussed.

INTRODUCTION

It is often stated that the first readily observable event at the interface between a material and a biological fluid is adsorption of macromolecular components from the fluid.[1] Plasma contains over 200 proteins. Within seconds after initial contact of blood with an artificial surface these different blood proteins begin to collide with, and competitively adsorb onto, the interface. Very few proteins have been studied with respect to interfacial activity and adsorption. The results obtained during the past five years of plasma-protein adsorption research reflect the complexity of this problem.[2,3,4] Recent recognition of a competitive plasma-protein adsorption process (the 'Vroman effect') has shown that plasma-protein adsorption is a complex and highly interactive molecular process in which an interfacially active 'trace' protein can dominate the adsorption process under certain conditions.[5,6] Due to technique and resource constraints, competitive plasma protein adsorption studies are usually limited to a small number of plasma proteins.[7,8,9]

Multiple protein–surface and adsorbed protein–protein interactions in blood and plasma can result in altered biochemical protein activity, covalent immobilization (complement C-3), increased proteolytic susceptibility, generation of new molecular species, and local depletion of active, soluble

* Presented at the Conference on Biomedical Polymers, 9–13 June 1991, Jerusalem, Israel.

‡ To whom correspondence should be addressed at: The Center for Biopolymers at Interfaces, University of Utah, Salt Lake City, Utah 84112, USA.

Clinical Materials 0267-6605/93/$6.00

factors. Interfacial protein effects may also promote adhesion or activation of platelets or white cells.

Studying the interfacial behavior of all 200 plasma proteins would be a stupendous task. A true understanding of the complex phenomena requires a combination of several experimental approaches.

We are addressing the problem of protein adsorption complexity at several levels by:

—studying the adsorption of small, model protein adsorption at air/water[10] and model solid/water interfaces;
—studying adsorption of plasma proteins onto wettability 'gradient' surfaces[11,12] and on surfaces of biomaterials;
—observing the process of adsorption of large plasma proteins onto crystal surfaces by atomic force microscopy.[13,14]

Here, we report on the study of plasma protein adsorption onto biomaterial surfaces using a quantitative, high-resolution, two-dimensional polyacrylamide gel electrophoresis technique (2-D PAGE). The application of the 2-D PAGE technique to the study of protein adsorption is based on the following experimental elements:

(a) a high-surface-area adsorbent is titrated with a diluted plasma solution;
(b) adsorbent with adsorbed proteins is separated from non-adsorbed proteins in solution;
(c) proteins present in the solution are analyzed before and after adsorption using 2-D PAGE;
(d) the amount of each protein in the 2-D PAGE gel is determined by quantitative densitometry.

The two main advantages of the 2-D PAGE technique as applied to protein adsorption are that it can identify the proteins removed from the protein mixture by a biomaterial surface, and that it can measure simultaneously and in a quantitative way the adsorbed amounts of tens of plasma proteins without any special labels. There are some disadvantages; the 2-D PAGE protein adsorption experiments are based on a depletion of proteins from solution rather than on direct analysis of the adsorbed layer. Hence, this approach requires a high-surface-area adsorbent and/or dilution of plasma. The solution concentration of some proteins will not be changed significantly enough to be detected by 2-D PAGE. In addition, some proteins may not be present in plasma in either sufficient quantities to be quantitatively detected in 2-D PAGE gels or, their positions in the 2-D PAGE gels have not been identified yet.

In this study we have selected three different types of biomaterial as the adsorbents: (a) calcium hydroxyapatite, (b) low temperature isotropic carbon particles, and (c) polyetherurethane particles, in order to examine the potential applications and limitations of the 2-D PAGE protein adsorption technique.

Calcium hydroxyapatite (CaHA) is a natural biomaterial. It is the inorganic constituent of bone and teeth. By composition, CaHA is $Ca_5(PO_4)_3(OH)$, the thermodynamically most stable calcium phosphate phase under physiological conditions. Small CaHA crystals with well-defined morphology and uniform size can be prepared directly by precipitation from supersaturated solution.[15] CaHA is used as a biomedical ceramic, as well as a coating of metallic and polymeric implants with the purpose of improving their ingrowth with bone.[16] As such, CaHA surfaces come into contact with body fluids containing plasma proteins. It has been long known that a CaHA surface adsorbs proteins; CaHA is often used in protein chromatography for separation purposes.[17,18]

Low-temperature isotropic (LTI) carbon is one of the few materials generally recognized as suitable for long-term blood contact applications.[19] LTI carbon is used in artificial heart-valve production[20] and as a thin film coating for other biomaterials.[21]

Polyetherurethanes (PU) have been used for decades as a material for biomedical applications: heart valves, vascular grafts, catheters, cardiac assist devices, and in the total artificial heart.[22] Polyurethanes are usually segmented copolymers made of hard and soft segments: the hard segment is often a diisocyanate chain extended with a low molecular weight diol or diamine and the soft segment is a moderately long-chain glycol, such as polytetramethyleneoxide, polyethyleneoxide or similar. The excellent mechanical properties of PU are attributed to the phase separation of hard and soft segments on a microscopic level. It has been shown that the surface of PU can respond to the polarity of the environment.[23]

MATERIALS AND METHODS

A detailed description of the protein adsorption protocols by the 2-D PAGE technique is given

Table 1. The composition of polyurethane particles

Name	*% Hard Segment*	*% Soft Segment*	*Soft Segment Mw*
PU-65-650	65	35	650
PU-65-1000	65	35	1000
PU-65-2000	65	35	2000
PU-65-2900	65	35	2900
PU-37-1000	37	63	1000
PU-37-2000	37	63	2000

elsewhere.[24,25] Briefly, a high-surface-area adsorbent is added to the solution containing a mixture of proteins. After a given adsorption time, the supernatant is separated from the adsorbent and a small volume of supernatant is taken for a quantitative analysis of protein content by 2-D PAGE. In this study we used diluted human plasma as an adsorbate–solvent mixture. Blood, drawn from several healthy human volunteers (50 ml blood/volunteer) was mixed with EDTA for anticoagulation; the plasma was then separated by centrifugation. One ml of plasma from each donor was pooled and the mixture aliquots were stored at −20 °C.

CaHA was prepared by a precipitation method as described elsewhere.[26] The precipitated crystals had average dimensions of 18 nm × 18 nm × 86 nm. Their crystal habit resembled the habit of the apatite crystals in human enamel. The specific surface area of the crystals was approximately 50 m^2/g. A volume of the CaHA suspension was added (0–1 ml, 0·1524 mg CaHA/ml) to 0·5 ml of diluted EDTA human plasma (1/10 dilution in TRIS buffer). The total volume of the system (1·5 ml) was made by adding TRIS buffer (0·1 M, pH = 7·4) and the final dilution of plasma was 1/30. The mixture was equilibrated overnight at room temperature and supernatant was separated by centrifugation.

LTI carbon was received as a gift from Sorin Biomedica (Sorin Biomedica, Saluggia, Italy). LTI carbon particles were crushed and sieved. The average size of LTI carbon particles was 1 μm. One gram of LTI carbon particles and TRIS buffer (0·1 M, pH = 7·4) were added to EDTA human plasma so that the final dilution of plasma was 1/30. The mixture was equilibrated at room temperature, and the supernatant samples were taken after 10 and 780 min for 2-D PAGE analysis. An LTI carbon heart-valve disk was imaged by scanning tunneling microscopy (Nanoscope II, Digital Instruments, CA).

PU particles were synthesized by emulsion polymerization.[27] Poly(tetramethyleneoxide) was used as the soft segment. The hard segment was a diol-chain extended urethane (butane diol + 4,4′-diphenylmethane diisocyanate). Table 1 lists the percentages of the hard and soft segments and the molecular weight of the soft segment. The average size of PU particles was 1 μm. PU particles (0·15 g) in TRIS buffer (0·1 M, pH = 7·4) were added to EDTA human plasma (final dilution of plasma was 1/30). The mixture was equilibrated for 4 h by rotation at room temperature. Supernatant samples were taken for 2-D PAGE analysis.

The 2-D PAGE was run on the ISODALT system (Hoefer Scientific Instruments, San Francisco, CA), developed by Anderson and coworkers.[28,29] All experiments were run in duplicate. Protein solution samples (25 μl) together with the 6 μl of external standard (soybean trypsin inhibitor, 0·2 mg/ml) were loaded in the first-dimension gels (isoelectro focusing, IEF, running for 22 000 V h). The IEF gels were placed on the second-dimension slab gels and electrophoresis was carried out at 50–60 mA for 9–12 h. The proteins in gels were silver stained.[30] The integrated optical density (IOD) of each protein spot was measured with a custom-built densitometer.[24] The integrated optical density of the protein spot consisted of background-subtracted optical densities measured at individual elements of the photodetector (CCD camera, Photometrics, Tucson, AZ) using the Beer–Lambert equation

$$OD_{prot} = \log(I/I_0)_{tot} - \log(I/I_0)_{back} \quad [1]$$

where I is the average intensity of the light transmitted through the gel to the individual elements of the photodetector in the area of the protein spot, I_0 is the intensity of the light source reaching the photodetector, and the subscripts $_{prot}$ and $_{back}$ represent the contribution from the protein and background, respectively. The integrated optical density of the external standard, soybean trypsin inhibitor, served to normalize results between different gels for any variation in the silver staining. The range of linearity between the integrated optical density and protein solution concentration was

verified with purified proteins in separate 2-D PAGE experiments.[24] After identifying protein in the gel, the fractional depletion of protein, F, was calculated from the ratio of integrated optical densities:

$$F = (\mathrm{IOD}_{\mathrm{control}} - \mathrm{IOD}_{\mathrm{sample}})/\mathrm{IOD}_{\mathrm{control}} \quad [2]$$

where subscripts 'sample' and 'control' represent results from the adsorption experiment and the control, respectively. The control 2-D PAGE gels were prepared by running 25 μl of non-depleted protein solution taken from the experimental system which did not contain adsorbent particles. Finally, the adsorbed amount was calculated by assuming that the protein depleted from the solution is present in the adsorbed state at the surface of the adsorbent particles.

RESULTS AND DISCUSSION

Plasma protein adsorption onto the CaHA surface

Figure 1(a) and (b) shows three-dimensional 2-D PAGE gel maps of the plasma solution (1/30 dilution) before and after contact with the CaHA surface, respectively. Total surface area in the experimental system shown in Fig. 1(b) was 3·81 m^2. The numbers associated with the 'peaks' indicate individual proteins spots and are listed in the figure caption. Comparison of Figs 1(a) and 1(b) shows that many proteins have been removed from the plasma solution by adsorption onto the surface of CaHA particles. By titrating the plasma solution with different amounts of CaHA particles, one can construct a plan of how individual proteins distributed themselves between the surface of the adsorbent and the diluted plasma solution. Adsorption isotherms for several plasma proteins are given in Fig. 2(a) and (b). The isotherms have been constructed using the experimentally determined fractional depletion of individual proteins, the literature data for the concentrations of protein in plasma,[31] and the surface area of CaHA available for protein adsorption in each system. Figure 2(a) shows the adsorption isotherms of three proteins which are present in relatively smaller amounts in undiluted plasma: prealbumin (mean plasma concentration, m.p.c. = 0·25 mg/ml), Gc-globulin (m.p.c. = 0·4 mg/ml) and antithrombin III (m.p.c. = 0·3 mg/ml). The molecular weights of these three proteins is between 50 and 65 kD and the adsorbed amounts are well below the usual 'monolayer' surface coverages for proteins of their size. It appears that their affinity for the CaHA surface ranks as antithrombin III > Gc-globulin > prealbumin.

Figure 2(b) shows how the proteins present in larger amounts in plasma distribute themselves between the CaHA surface and the solution: α_1-antitrypsin (m.p.c. = 2·6 mg/ml), apo A-I (m.p.c. = 1·5 mg/ml), haptoglobin (m.p.c. = 2 mg/ml) and fibrinogen (m.p.c. = 3 mg/ml). The same figure also illustrates how, in the case of multichain proteins like haptoglobin and fibrinogen, the adsorption can be detected by analyzing the optical density of different constituent protein chains in the 2-D PAGE gel map. The multichain protein is reduced to its constituent chains in the process of separation by the 2-D PAGE technique. By comparing the adsorption results obtained from the constituent chains of fibrinogen and haptoglobin, one can also estimate the precision of the 2-D PAGE protein adsorption technique. In Fig. 2(b), the symbols from the constituent chains of fibrinogen and haptoglobin are linked with dashed lines. The adsorbed amount differed as much as ±15% if determined from different constituent chains of fibrinogen and haptoglobin. The standard deviation of the measured fractional depletion from duplicate experiments in the case of single-chain proteins was on average ±5%.

The affinity of proteins for the CaHA surface (Fig. 2(b)) can be ranked as apo A-I > fibrinogen ≈ haptoglobin > α_1-antitrypsin. The highest affinity of apo A-I, a constituent protein of high-density lipoprotein (HDL), presented an interesting question: did binding of the whole HDL molecule take place or was the apo A-I molecule extracted from the HDL molecule by binding to the CaHA surface? No answer to this problem can be given at the present time. It is also interesting to note that the adsorption isotherm of α_1-antitrypsin displayed a plateau followed by an increase in the adsorbed amount at higher protein concentrations. This feature may be indicative of the formation of a second adsorbed layer: one protein may bind only weakly to the surface of the adsorbent but may have a higher affinity for binding to another, already adsorbed, protein. The Scatchard analysis of α_1-antitrypsin and haptoglobin adsorption does not yield a well-defined gradient and intercept, possibly indicating that the available number of binding sites is not constant during the experiments. Similar conclusions have been

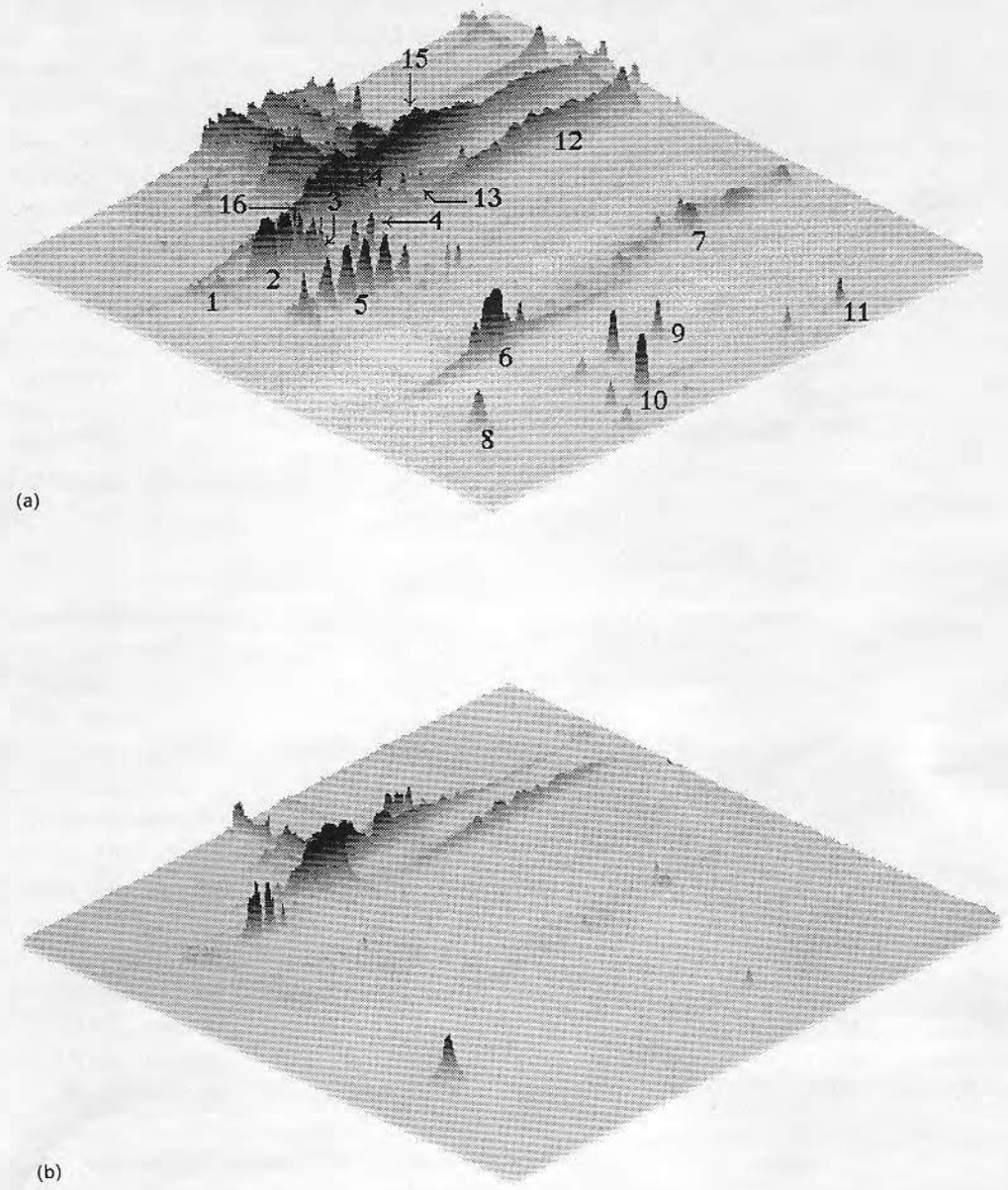

Fig. 1. The 2-D PAGE map of plasma proteins: (a) the plasma (1/30 dilution) proteins before adsorption onto the CaHA surface, (b) the plasma (1/30 dilution) proteins after adsorption onto the CaHA surface (total surface area of CaHA was 3·81 m^2, total volume was 1·5 ml). Proteins: (1) α_1-antichymotrypsin, (2) α_1-antitrypsin, (3) Gc-globulin, (4) fibrinogen γ chain, (5) haptoglobin β chain, (6) apo A-I, (7) immunoglobulin λ and κ chains, (8) trypsin inhibitor (external standard), (9) haptoglobin α_2 chain, (10) prealbumin, (11) hemoglobin β chain, (12) immunoglobulin γ chain, (13) fibrinogen β chain, (14) albumin, (15) transferrin, (16) antithrombin III.

inferred from plasma-protein adsorption experiments using different adsorbents.[24] The experimental confirmation of multilayer formation, however, was not accessible by the present technique.

One may ask the question: what about proteins that have not been analyzed for fractional depletion? From Fig. 1(a) and (b) one can see that the adsorption of albumin and immunoglobulins had taken place. However, the changes in their respective solution concentrations could not accurately be detected with the present technique. Detection of albumin depletion presents a particularly difficult problem: albumin is present in very high amounts in plasma and its spot in 2-D PAGE gel is often 'streaked', i.e. it extends from the top of the gel map down to the actual albumin position (spot #14, Fig. 1(a)). Moreover, when the 'streaking' is extensive, it also covers the spots from other

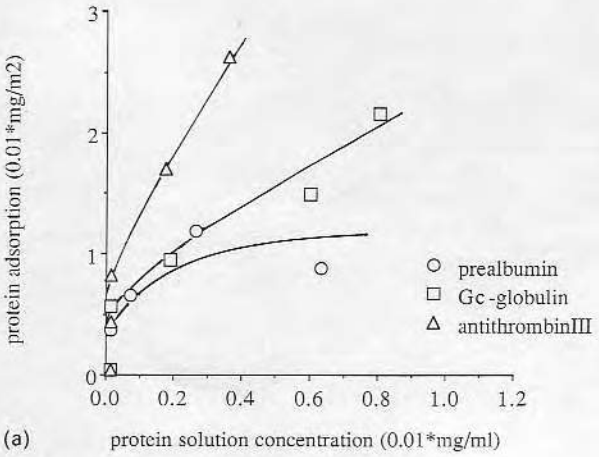

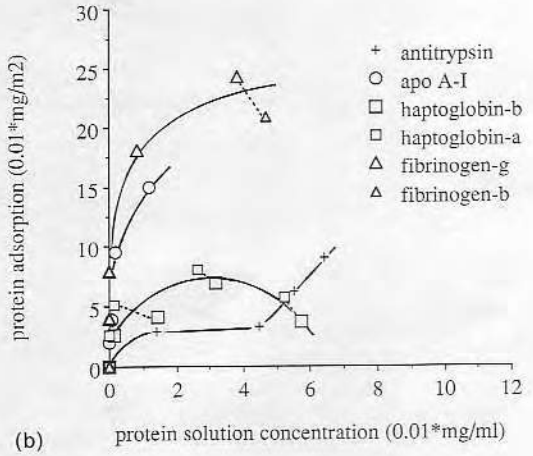

Fig. 2. The room temperature isotherms of plasma protein adsorption onto the CaHA surface: (a) prealbumin, Gc-globulin and antithrombin III, (b) α_1-antitrypsin, apo A-I, haptoglobin and fibrinogen. Dashed lines connect the results obtained by measuring optical density of constituent γ and β chains of haptoglobin (□) and γ and β chains of fibrinogen (△), respectively.

proteins, like prothrombin, α_2-macroglobulin and some others. Hence, the integrated optical density of albumin is often quite difficult to be determined accurately.

The problem with the immunoglobulins is their heterogeneity. The 2-D gel spots of immunoglobulins can be found mainly at two distinct regions since the γ and λ (or κ) chains have different molecular weights (spots #12 and #7, Fig. 1(a)). The two sets of spots are spread over a large horizontal range, indicating that the heterogeneity of the immunoglobulin chains shows largely as a difference of the charge of individual molecules.

Plasma protein adsorption onto the LTI carbon surface

Figure 3 shows a 5 nm by 5 nm scanning tunneling image of an LTI carbon surface from a heart-valve disk. The atomic carbon structure of the surface is easily recognized, as well as several microcrystalline regions. Different orientations of crystallites are exposed; a graphite-like structure, for example, is evident in the upper part of the STM image indicating that, in this region, the graphitic plane lies parallel with the surface plane. Figure 4 shows the results of the plasma-protein adsorption experiments onto the surface of LTI carbon particles. The plasma solution was sampled 10 min and 780 min after the initial contact. The available surface area in each experimental system was relatively low in comparison with the CaHA; based on the geometrical consideration it amounted to approximately 0·12 m^2. Because the actual surface area available for the protein adsorption was not known, the experi-

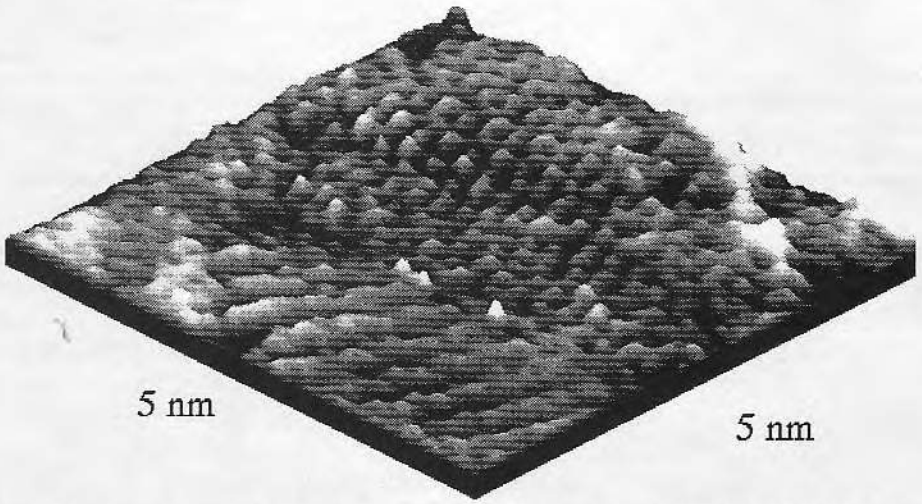

Fig. 3. The scanning tunneling microscopy image of LTI carbon surface from a heart valve disk. The STM probe was mechanically sharpened Pt/Ir wire, the bias tip voltage was 0·1 V and tunneling current was 1·0 nA. The surface was imaged in air.

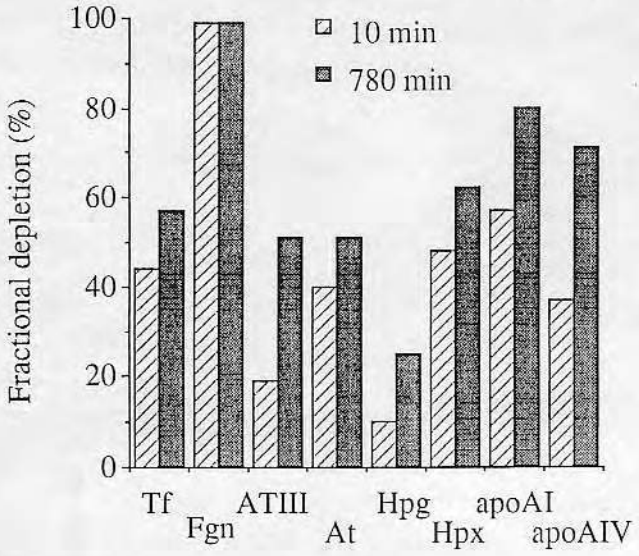

Fig. 4. The fractional depletion of plasma proteins after adsorption onto LTI carbon surface. Proteins: transferrin (Tf), fibronogen (Fgn), antithrombin III (ATIII), α_1-antitrypsin (At), haptoglobin (Hpg), hemopexin (Hpx), apo A-I and apo A-IV. The sampling times were 10 and 780 min.

mental results are presented as the fractional depletion of individual proteins. In the first 10 min of adsorption fibrinogen (Fgn) was almost completely depleted from the diluted plasma solution. At the same time transferrin (Tf), hemopexin (Hpx), α_1-antitrypsin (At), apo A-I and apo A-IV were depleted by approximately 50%. Haptoglobin (Hpg) and anti-thrombin III were depleted by 10 and 20%, respectively. After overnight equilibration, the fractional depletion of all proteins (except Fgn) had further increased. Figure 4 shows that the biggest increase in the adsorbed amount in the 10–780 min period was in the case of ATIII, Hpg, and apo A-IV, i.e. those proteins that showed low initial adsorption. The replacement of surface-bound fibrinogen with another protein from solution, the so-called 'Vroman effect'[5,6] which was often found in adsorption of plasma proteins,[7] had not been found in the 10–780 min period.

It is illustrative to compare the size of the microcrystalline regions of the carbon surface with the size of some plasma proteins. From Fig. 3 and from other STM images of carbon surfaces[32] it can be concluded that a plasma protein of average size will have a chance to interact with more than one microcrystalline region at the carbon surface. Due to the different orientation of carbon microcrystallites, the carbon surface will consist of the surface domains with different surface energies. One can speculate that the high affinity of fibrinogen for carbon might result from some unknown match or complementarity between the surface of protein and the carbon surface microdomains. It has been suggested by others that the good biocompatibility of carbon surfaces is related to a lack in conformational changes in the adsorbed protein.[33] This may be contradicted by the finding that the pyrolitic carbon coating in Dacron-based vascular grafts did not prevent thrombosis.[34]

Plasma-protein adsorption onto the PU surface

If the surface of a relatively simple material, like carbon, is heterogeneous on scales smaller or equal to that of the protein, what will one protein 'see' when it approaches the surface of polyurethane? It is thought that polyurethanes expose their microscopic hard and soft segments on their surfaces. Recent studies showed that high-voltage transmission electron microscopy and low-voltage, high-resolution scanning electron microscopy can resolve the size and distribution of these microdomains on polyurethanes.[35] Yet these observations have been made *in vacuo* and may not represent the PU surface under physiological conditions. It is known that the surface of PU can respond to the polarity of the environment.[23] If so, one can assume that the PU surface microdomains will also respond to the polarity of individual proteins once they adsorb to the PU biomaterials. There is a considerable effort to apply novel scanning probe techniques, like atomic force microscopy (AFM), in imaging the surface of polyurethane in an aqueous environment.[36] However, the PU surface may be too soft for the proximity probe technique like AFM. We are currently using the modulation atomic-force microscopy technique to probe for the polymer surface regions of different elasticities.[37] Possibly, with the same approach we will be able to distinguish the domains on the surface of PU materials.

Without knowing what the surface of PU 'looks like' on the scale of the protein molecule, the discussion of plasma protein adsorption results will remain largely phenomenological. Table 2 shows the fractional depletion of several plasma proteins after the contact with the PU materials. The total depleted protein, which is calculated from the total integrated optical density of the 2-D PAGE sample gel *versus* the same parameter from the control gels, is the smallest for the PU-65-1000. In the case of this polyurethane, barely 15% of the total 2-D PAGE-measured proteins have been removed; in contrast, the PU-65-650 materials removed 65% of the total 2-D PAGE-measured

Table 2. The fractional depletion of plasma proteins after adsorption onto the surface of different polyetherurethane particles.

Plasma Proteins	*Polyurethanes*					
	PU-65-650	*PU-65-1000*	*PU-65-2000*	*PU-65-2900*	*PU-37-1000*	*PU-37-2000*
Immunoglobulin G	60	20	0	20	70	0
Apo A-IV	100	60	70	70	90	40
Fibrinogen	100	80	80	80	100	40
Complement C3	70	30	60	40	60	20
Hemopexin	100	100	100	100	100	90
Prealbumin	70	20	10	40	60	0
Total depleted protein (%)	65	15	25	40	60	20

Total depleted protein fraction was calculated from total integrated optical densities of sample and control 2-D PAGE gels

proteins. Apparently, the surface composition of these two PUs were different enough to cause different plasma protein adsorption. Is the reason for the difference due to the molecular weight of the soft segment or to the packing of soft and hard segments on the particle surface? In answering this question, one has to keep in mind that although the geometrical area of the PU particles was similar in each experiment, the actual surface area available for the adsorption was not known. A more porous PU particle could cause removal of a larger fraction of the plasma proteins from solution, decreasing the concentration of proteins in supernatant and in this way influence the composition of the adsorbed layer.

It is interesting to note that the removal of some proteins by the polyurethane surface is quite efficient: all PU samples removed hemopexin, a protein which scavenges heme from the circulation, almost completely from solution. Why? The hemopexin amino acid sequence is homologous to vitronectin, a protein which displays a high adsorption affinity for many solid surfaces, including polyurethanes.[38]

We also noted that apo A-IV is removed from the solution, an indication that lipids from lipoproteins might have been adsorbed by the PU surface. Complement C3 was also adsorbed, suggesting that the complement system would possibly be affected in the case of actual PU implants. The adsorption of fibrinogen was also quite extensive, indicating that platelet adherence and activation might follow.

CONCLUSIONS

The importance of interactions between proteins and surfaces of implanted biomaterials is widely recognized. All surfaces, if exposed to biological fluids like blood, will bind proteins from the surrounding fluid. Protein–surface interactions can influence biocompatibility of a given material by several different mechanisms:

—by direct activation of the intrinsic pathway of the blood coagulation via contact activation;
—by direct activation of the alternative complement pathway;
—by creating local depletion of proteins which act as regulators or inhibitors of the naturally occuring processes in hemostasis and thrombosis;
—by covering the surface with a 'non-specifically' bound protein layer in which protein conformation may be sufficiently altered so that the overall effect will be as in the creation of a new surface.

The present study demonstrated that the 2-D PAGE technique can be used to examine protein adsorption from a multicomponent mixture onto high-surface-area materials. All three biomaterials studied here: calcium hydroxyapatite, low-temperature isotropic carbon, and polyurethane were found to bind, simultaneously and in a kinetic dependent way, a number of plasma proteins. In the case of CaHA, the experimental titration of diluted plasma with the adsorbent allowed calculation of the adsorption isotherms and permitted us to estimate the affinity of individual proteins for the surface. In the case of an LTI carbon surface, the kinetics of binding were different for different proteins; fibrinogen was completely removed in 10 min from diluted plasma, while the adsorption kinetics of other proteins were slower and resulted only in their partial removal from diluted plasma. The surface of carbon was found to be morphologically heterogeneous due to the different orientation of carbon crystallites. This may have an effect on the binding of some larger plasma proteins like fibrinogen. The polyurethane surface may also be heterogeneous; it is thought to consist of separate microdomains of hard and soft segments. The pre-

sent results indicate that some proteins, like hemopexin, may have an extraordinary affinity for PU surfaces.

The main disadvantage of the 2-D PAGE protein adsorption technique is that it is a solution depletion technique: mass balance of proteins is determined in solution rather than directly on the biomaterial surface. Hence, this approach required a high-surface-area adsorbent and/or dilution of plasma and it is limited to detectable changes of protein concentration in solution. The advantages of the 2-D PAGE technique as applied to protein adsorption are substantial: one can identify the proteins removed from the protein mixture by a biomaterial surface and one can measure quantitatively the adsorbed amounts and binding kinetics of tens of plasma proteins without any special labels. The 2-D PAGE technique should preferably be used for initial screening of plasma protein–surface interactions. In such cases, results obtained with the 2-D PAGE technique will permit the formulation of a set of hypotheses which can be tested and used to design more definitive experiments. In conclusion, the 2-D PAGE technique is a powerful method for determining and screening competitive protein adsorption from complex solutions.

ACKNOWLEDGEMENTS

The experimental work presented in this paper has been funded by the research grants from the Center for Biopolymers at Interfaces, University of Utah, Salt Lake City. One of us (V. H.) acknowledges the supports from the European Community Programme for International Cooperation (Grant #CII*/0345) and from the Ministry of Science and Technology of The Republic of Croatia (Grant #1-07-189). We thank Sorin Biomedica for the carbon samples and Becton Dickinson Corp. for the polyetherurethane samples.

REFERENCES

1. Andrade, J. D. & Hlady, V. *Adv. Polym. Sci.*, **79** (1986) 1.
2. Leonard, E. F., Turrito, V. T. & Vroman, L. (eds), Blood in contact with natural and artificial surfaces. *Ann. New York Acad. Sci.*, **516** (1987) entire issue.
3. Andrade, J. D. (ed.), *Surface and Interfacial Aspects of Biomaterials*, Vol. 2, *Protein Adsorption*. Plenum Press, New York, 1985.
4. Horbett, T. A. & Brash, J. L. (eds), *Proteins at Interfaces*, ACS Symp. Ser., 1987; also *J. Colloid Interface Sci.*, **111** (1986) entire issue.
5. Vroman, L. & Adams, A. L., *J. Biomed. Mater. Res.*, **3** (1969) 43.
6. Vroman, L., Adams, A. L., Fisher, G. C., Munoz, P. C. & Stanford, M., *Adv. Chem. Ser.*, **199** (1982) 264.
7. Brash, J. L. & ten Hove, P., *Thromb. Haemostas.*, **51** (1984) 326; also *Macromol. Chem. Macro. Symp.*, **17** (1988) 441.
8. Horbett, T. A., *Thromb. Haemostas.*, **51** (1984) 174.
9. Slack, S. M. & Horbett, T. A., *J. Colloid Interface Sci.*, **133** (1989) 148.
10. Wei, A. -P., MSc Thesis, University of Utah, USA 1990.
11. Gölander, C-G., Lin, Y-S., Hlady, V. & Andrade, J. D., *Coll. & Surf.*, **49** (1990) 289.
12. Hlady, V., *Appl. Spectrosc.*, **45** (1991) 246.
13. Lin, J. -N., Drake, B., Lea, A. S., Hansma, P. K., & Andrade, J. D., *Langmuir*, **6** (1991) 509.
14. Lea, A. S., Pungor, A., Hlady, V., Andrade, J. D., Herron, J. N. & Voss, E. W. Jr., *Langmuir* **8** (1992) 68.
15. Bett, J. A. S., Christner, L. G. & Hall, W. K., *J. Amer. Chem. Soc.*, **89** (1967) 5535.
16. de Groot, K., In *Biocompatibility of Clinical Implant Materials*, Vol 1 ed. D. F. Williams. CRC Press, Boca Raton, FL, 1981, p. 199.
17. Tiselius, A., Hertjen, A. & Levin, O., *Arch. Biochem. Biophys.*, **65** (1956) 132.
18. Makino, K. & Kim, B. -K., *J. Chromatog. Sci.*, **27** (1989) 659.
19. Haubold, A. D., Shim, H. S. & Bokros, J. C., In *Clinical Implant Materials*, Vol II, ed. D. F. Williams. CRC Press, Boca Raton, FL, 1981, p. 4–42.
20. Haubold, A., *Ann. N.Y. Acad. Sci.*, **283** (1977) 383.
21. Paccagnella, A., Majni, G., Ottaviani, G., Arru, P., Santi, M. & Vallana, F., *Int. J. Art. Org.*, **9** (1986) 127.
22. Lelah, M. D. & Cooper, S. L., In *Polyurethanes in Medicine*. CRC Press, Boca Raton, FL, 1986.
23. Chen, J. -H. & Ruckenstein, E., *J. Colloid & Interface Sci.*, **135** (1990) 496.
24. Ho, C. -H., MSc Thesis, University of Utah, USA 1990.
25. Ho, C. -H., Hlady, V., Nyquist, G., Andrade J. D. & Caldwell, K. D., *J. Biomed. Mater. Res.*, **25** (1991) 423.
26. Hlady, V. & Furedi-Milhofer, H., *J. Colloid Interface Sci.*, **69** (1979) 460.
27. Lambert, J. M., *Polym Prep.*, **30** (1989) 583.
28. Anderson, N. L. & Anderson, N. G., *Proc. Nat. Acad. Sci. USA*, **74** (1977) 5421.
29. Anderson, N. L., Tracey, R. P. & Anderson, N. G. In *The Plasma Proteins*, 2nd edn, ed. H. Neurath. Plenum Press, **4** (1985) 221.
30. Switzer, R. C., Merril, C. R. & Shifrin, S., *Anal. Biochem.*, **98** (1979) 231.
31. *Table of Human Blood Plasma Proteins*. Diagnostica, Behringwerke AG, Marburg, Germany.
32. Feng, L. & Andrade, J. D., *J. Biomed. Mater. Res.*, (in press).
33. Bockor, J. C., LaGrange, L. D. & Schoen, F. J., In *Chemistry and Physics of Carbon*, Vol. 9, ed. P. L. Walker. Marcel Dekker, New York, 1972, p. 103.
34. Scott, S. M., Gaddy, L. R. & Parra, S., *J.Surg. Res.*, **29** (1990) 395.
35. Goodman, S. L., Li, C., Pawley, J. B., Cooper, S. L. & Albrecht, R. M., In *Surface Characterization of Biomaterials*, ed. B. D. Ratner. Elsevier, Amsterdam, 1988.
36. Orang, F., Zenhausern, F., Emch, R. & Descouts, P., In *Book of Abstracts*, Vol III, 7th ICSCS, 7–13 July 1991, Compiegne, France, p. 365.
37. Stroup, E. W., Lea, A. S., Pungor, A., Hlady, V. & Andrade, J. D., In *Book of Abstracts*, Int. Conf. on STM, 12–16 August 1991, Interlaken, Switzerland, p. 238.
38. Fabricius-Homan, D. J. & Cooper, S. L., *J. Biomed. Mater. Res.*, **25** (1991) 953.

Protein Interactions with Model Heterogeneous Surfaces

Vladimir Hlady, Joseph D. Andrade, Chih-Hu Ho,
David W. Britt and Yeong-Shang Lin

Departments of Bioengineering
and Materials Science and Engineering
University of Utah
Salt Lake City, UT 84112

Introduction

Proteins concentrate at interfaces; they are surface-active (1). This general observation is in contrast with the weak, non-specific interactions between soluble plasma proteins and blood cells, which are either minimal or absent. Cell-protein interactions proceed primarily via specific molecular recognition mechanisms. Interactions between protein and man-made materials are different: so called "non-specific" plasma protein interactions with the surfaces of artificial materials is a principal means by which an inert material surface can become thrombogenic (2).

Our understanding of proteins has greatly improved in the last decade due to the increasing number of protein structures solved by X-ray crystallography and/or NMR-spectroscopy (3). Extensive homology between proteins has enabled reliable extrapolations of structural and functional predictions from known to unknown proteins. The same molecular level understanding of biomaterial surfaces has been less forthcoming. The concepts of solid state (4) and polymer surface physics (5) are only beginning to be applied to interfaces between complex biological systems and biomaterials. Biomaterials surfaces are often heterogeneous, rarely clean and always dynamic. As a result experimental observations in this area remain largely unsupported by a rigorous physical theory.

We are addressing the role of surface heterogeneity in protein adsorption:

- by preparing and characterizing so-called "gradient surfaces" using different silane chemistries,
- by studying adsorption kinetics of one or more plasma proteins onto these "gradient" surfaces, and
- by comparing the experiments with the predictions of relatively simple adsorption models.

The aim of this study was to find the underlying mechanisms of low density lipoprotein (LDL) adsorption onto silica - octadecyldimethylsilyl-silica (C18-silica) gradient surfaces, and to determine the effect of human serum albumin (HSA) and immunoglobulin G (IgG) on the LDL adsorption process.

What are the C18-silica gradient surface like on a molecular scale?

The gradient surface prepared on flat silica is a convenient tool for studying protein surface adsorption. Here, we have used a surface density gradient of octadecyldimethylsilyl groups which had a several millimeter long gradient region of increasing surface density of octadecyldimethylsilyl groups between a clean silica end and a self-assembled C18 monolayer end (6). While the macroscopic characterization techniques such as contact angle measurements indicate a smooth, almost linear increase of C18 surface density in the gradient region, the atomic force microscope images of C18 sub-monolayers on Si/SiO_2 (and on mica) surfaces show a surface morphology dominated bu fractal-like islands of C18 (7). Even the full coverage self-assembled C18 monolayer displays a number of "pinholes". As a first approximation in protein adsorption analysis we decide to assume that any protein adsorbing to such a surface will be faced with a choice of finding either a C18 binding site or a plain silica binding site.

Adsorption of LDL onto the silica - C18-silica gradient surface

Adsorption kinetics of LDL onto a silica - C18-silica gradient surface was studied by using Total Internal Reflection Fluorescence (TIRF) (8). The adsorption from the LDL buffer solution (1/100 of LDL plasma concentration) was quantified using autoradiography (9). The FITC-LDL adsorption results are shown in Fig 1. While the initial fluorescence increase was linear and fast in the region of the hydrophilic silica surface, it increased much more slowly in the C18-gradient region and at the C18 end of the gradient. As a first step in the protein adsorption analysis, the LDL adsorption at either end of the gradient (i.e. at the silica and the C18 end of the gradient) was fit to a simple adsorption model comprised of two opposing processes: adsorption and desorption

$$d\Gamma(t)/dt = k_{on} \bullet (1 - \Gamma(t)/\Gamma_{max}) \bullet c(0,t) - k_{off} \bullet (\Gamma(t)/\Gamma_{max}) \qquad [1]$$

where Γ_{max} is the maximum adsorption, $\Gamma(t)$ is the adsorbed amount per unit surface at time t, $(1 - \Gamma(t)/\Gamma_{max})$ is the fraction of unoccupied adsorption sites and c(0,t) is the protein concentration right next to the adsorbing surface. The fit provided the values for the intrinsic adsorption and desorption rate constants, the k_{on} and k_{off}, respectively.

Table 1. The LDL adsorption parameters obtained by fitting the experimental results to the model given by Eq. 1.

	hydrophilic silica	hydrophobic C18-silica
θ_{adv}	0°	104°
$\Theta/\Theta_{max(C18)}$	0	0.9
Γ_{max} ($\mu g\ cm^{-2}$)	0.4	0.3
$k_1 (cm^3 \mu g^{-1}\ s^{-1})$	$7.5 \bullet 10^{-4}$	$4.5 \bullet 10^{-5}$
k_{-1} (s^{-1})	$2.9 \bullet 10^{-4}$	$2.3 \bullet 10^{-4}$
K (M^{-1})	$6.5 \bullet 10^{9}$	$4.9 \bullet 10^{8}$

Does the LDL adsorption on a mixed silica - C18 silica gradient surface region behave as a simple addition of two independent adsorption processes, one occurring on silica and the other on C18-silica? To answer this question, the experimental LDL kinetics measured in the C18 gradient region were fitted to an "adsorption sum" model:

$$d\Gamma(t)/dt = \{1 - \Theta/\Theta_{max(C18)}\} \bullet \{d\Gamma_{sil}(t)/dt\} + \{\Theta/\Theta_{max(C18)}\} \bullet \{d\Gamma_{C18}(t)/dt\} \qquad [2]$$

which simply adds the adsorption on the C18 and silica surface binding sites, respectively, and weights each adsorption process according to the probability of finding a given adsorption site. Interestingly, the "adsorption sum" model given by Eq. 2. fitted the experimental results very well (Figure 2), indicating that the initial assumption of two independent adsorption processes may indeed be correct.

The effect of HSA and of IgG on LDL adsorption

The binary mixtures of LDL and HSA or LDL and IgG (all protein were present in concentrations equal to 1/100 of their respective plasma concentrations), were used to examine the effect of the second protein on LDL adsorption. The effects were very subtle on the silica end of the gradient: the adsorption kinetics fitted quite well to a simple "two proteins" adsorption model:

$$d\Gamma_{tot}(t)/dt = d\Gamma_{LDL}(t)/dt + d\Gamma_{HSA}(t)/dt \qquad [3]$$

using the previously determined LDL adsorption parameters (Table 1). However the "two proteins" adsorption model failed to predict the adsorption behavior of two proteins in the gradient and C18 surface regions indicating that two proteins "feel" each other during the adsorption process. In separate experiments, preadsorbed HSA (or IgG) on partial and full C18 monolayers had a dramatic effect on LDL adsorption.

Acknowledgments

The authors are indebted to Dr. Lilly Wu (University of Utah) for teaching them how to isolate human lipoproteins. We thank all blood donors for providing us with their low density lipoproteins and H. P. Jennissen for helpful discussions. This work was financially supported by the Whitaker Foundation, NIH grant (R01 NIH-44538) and the Center for Biopolymers at Interfaces, University of Utah.

References

1. Andrade, J. D. 1985. Surface and Interfacial Aspects of Biomaterials, Vol. 2., Protein Adsorption. Plenum Press, New York. 1 - 346.

2. Horbett, T. A. 1993. Principles underlying the role of adsorbed plasma proteins in blood interactions with foreign materials. *Cardiovascular Pathology.* 2:137S - 148S.

3. Hendrickson, W. A., and K. Wuthrich. 1991 - 1994. Macromolecular Structures. Current Biology, London.

4. Luth, H. 1993. Surfaces and Interfaces of Solids. Springer-Verlag, Berlin. 1 - 487 pp.

5. Sanchez, I. C. 1992. Physics of Polymer Surfaces and Interfaces. Butterworth-Heinemann, Boston. 1 - 336.

6. Lin, Y.-S., and V. Hlady. 1994. Human serum albumin adsorption onto octadecyldimethylsilyl-silica gradient surface. *Colloids and Surfaces B: Biointerfaces.* 2:481-91.

7. Britt, D. W., and V. Hlady. 1995. Influence of temperature, surface hydration and annealing time on octadecyltrichlorosilane self-assembly on mica. J. Colloid Interface Sci. submitted.

8. Hlady, V. 1991. Spatially-resolved adsorption kinetics of immunoglobulin G onto the wettability gradient surface. *Applied Spectroscopy.* 45:246 - 252.

9. Ho, C.-H. 1995. Adsorption of plasma lipoproteins onto model hydrophobic-hydrophilic gradient surfaces. Ph.D. Thesis, University of Utah, Salt Lake City.

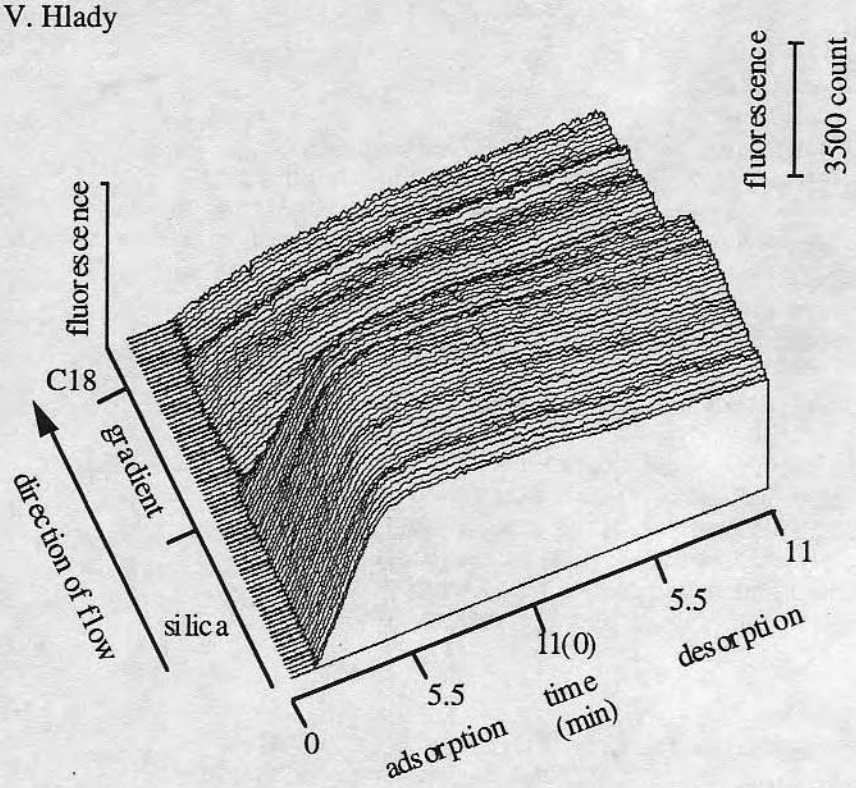

Figure 1. Kinetics of FITC-LDL adsorption onto the silica - C18 gradient surface.

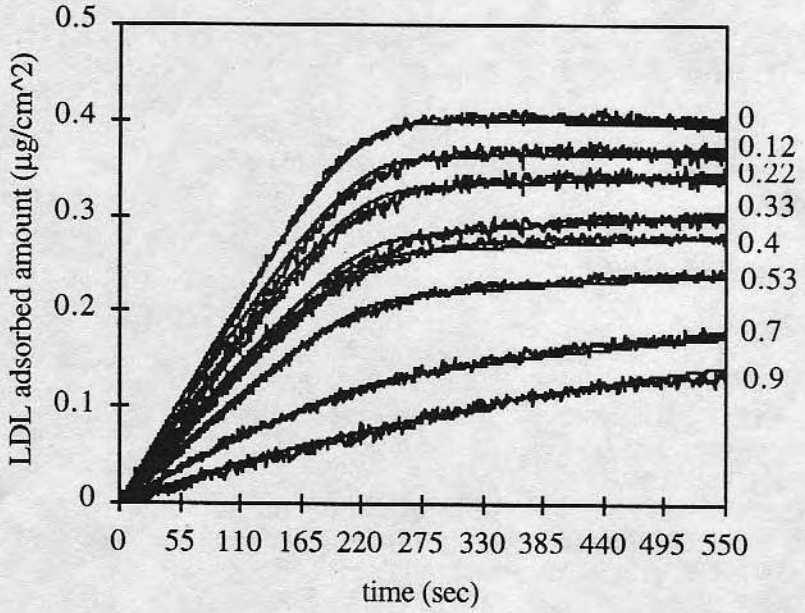

Figure 2. The fit between the experimental LDL adsorption and that predicted by the model (Eq.2). The fractional C18 surface coverage is given on the right.

SPEAKER BIOGRAPHICAL OUTLINE

Vladimir Hlady
Associate Professor of Bioengineering
Department of Bioengineering, University of Utah
MEB 2480
Salt Lake City, UT 84112
801-581-5042

FUNCTION OF COMPANY/INSTITUTION	Education and research
BRIEF PERSONAL HISTORY	Born 1949 in Zagreb, Croatia (formerly Yugoslavia); Research Assistant/Associate Professor, R. Boskovic Institute, Zagreb, Croatia, 1981-1988; moved to the U.S. in 1988
CURRENT RESPONSIBILITIES	Teach graduate courses in surface chemistry, polymer surface characterization and protein-interface interactions; research supervision of several Ph.D. and M.S. students
HIGHER EDUCATION/TRAINING	B.Sc., Chemistry, 1972; M.Sc., Chemistry, 1975; D.Sc., Chemistry, 1981; all degrees at the University of Zagreb, Croatia
PROFESSIONAL AFFILIATIONS	Faculty member of the Center for Biopolymers at Interfaces, University of Utah; American Chemical Society, Croatian Chemical Society, International Association of Colloid and Interface Scientists
AWARDS/PATENTS/PUBLICATIONS	Fulbright Fellow and Senior Exchange Scholar, 1983-1985; 50+ refereed publications, several book chapters and reviews

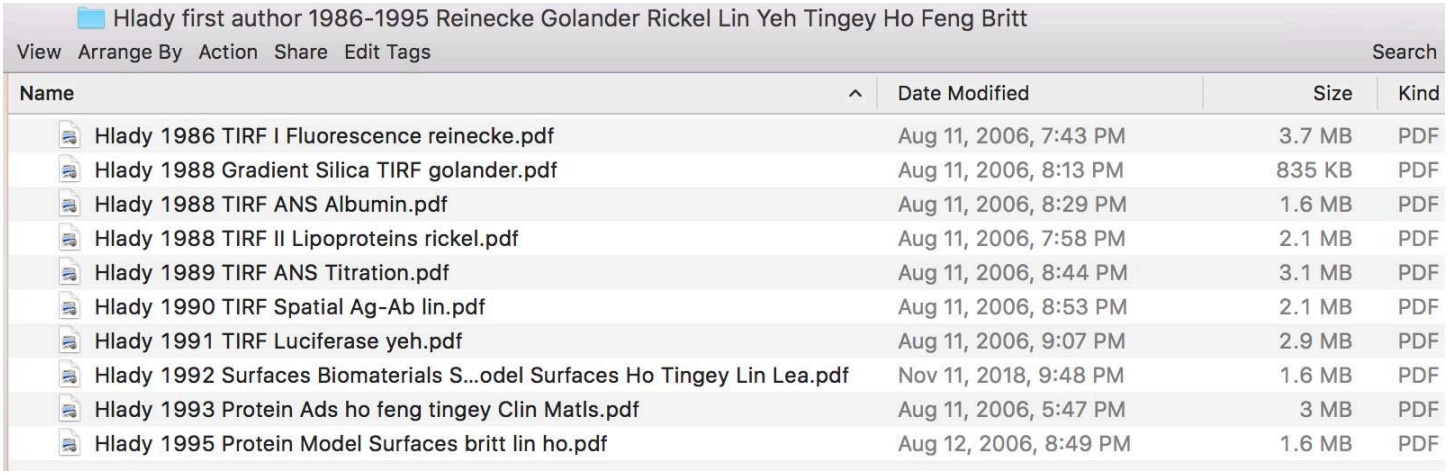
Hlady first author 1986-1995 Reinecke Golander Rickel Lin Yeh Tingey Ho Feng Britt
View Arrange By Action Share Edit Tags
Search
Name
Date Modified
Size
Kind
Hlady 1986 TIRF I Fluorescence reinecke.pdf
Aug 11, 2006, 7:43 PM
3.7 MB
PDF
Hlady 1988 Gradient Silica TIRF golander.pdf
Aug 11, 2006, 8:13 PM
835 KB
PDF
Hlady 1988 TIRF ANS Albumin.pdf
Aug 11, 2006, 8:29 PM
1.6 MB
PDF
Hlady 1988 TIRF II Lipoproteins rickel.pdf
Aug 11, 2006, 7:58 PM
2.1 MB
PDF
Hlady 1989 TIRF ANS Titration.pdf
Aug 11, 2006, 8:44 PM
3.1 MB
PDF
Hlady 1990 TIRF Spatial Ag-Ab lin.pdf
Aug 11, 2006, 8:53 PM
2.1 MB
PDF
Hlady 1991 TIRF Luciferase yeh.pdf
Aug 11, 2006, 9:07 PM
2.9 MB
PDF
Hlady 1992 Surfaces Biomaterials S...odel Surfaces Ho Tingey Lin Lea.pdf
Nov 11, 2018, 9:48 PM
1.6 MB
PDF
Hlady 1993 Protein Ads ho feng tingey Clin Matls.pdf
Aug 11, 2006, 5:47 PM
3 MB
PDF
Hlady 1995 Protein Model Surfaces britt lin ho.pdf
Aug 12, 2006, 8:49 PM
1.6 MB
PDF